École polytechnique de Louvain

Communications over doubly dispersive channels : transceiver design and performance analysis

Author: **Félix Willaumez**
Supervisors: **Claude Oestges, Luc Vandendorpe**
Readers: **Jérome Louveaux, Baptiste Sambon**
Academic year 2024–2025
Master [120] in Electrical Engineering

Acknowledgments

I would like to thank everyone who has dedicated their time answering questions and guiding me throughout this work.

Among those people, I would like to particularly express my gratitude to Prof. Claude Oestges, Baptiste Sambon and Prof. Luc Vandendorpe who have been of great help both on the technical and social aspects of this thesis.

Thank you also Prof. Louveaux for your interest in this work and the time dedicated to assess it.

Finally, thank you to my family and friends for their support and encouragements that I have received all this year through.

Abstract

The objective of this thesis is to provide the reader with a comprehensive description of one of the main limitations of the fifth generation of mobile networks. Especially, scenarios in which the geometry around the user is quickly evolving over time are described. A mathematical model of these channel scenarios is provided along with its implication on the OFDM modulation which is used in 5G. To overcome the limitations of OFDM, a new modulation technique called OTFS has been recently proposed in the literature. A framework in which both OFDM and OTFS are easily described with well-know telecommunication tools is presented. In this framework, the equations of this new modulation are derived from scratch. Then, a new equalization technique for OTFS is provided. Finally, OTFS performance in terms of bit error rate is assessed and compared with OFDM and its variant, the CP-SC modulation.

Contents

Acronyms

4G Fourth generation of cellular networks technology.

5G Fifth generation of cellular networks technology.

AWGN Additive white Gaussian noise.

BER Bit error rate.

BPSK Binary phase shift keying.

CFO Carrier frequency offset.

CP Cyclic prefix.

CP-SC Cyclic prefix - single carrier.

dD delay-Doppler.

DFT Discrete Fourier transform.

dT delay-Time.

DZT Discrete Zak transform.

EVA Extended Vehicular A.

FFT Fast Fourier transform.

i.i.d. Independent and identically distributed.

IDFT Inverse discrete Fourier transform.

IDZT Inverse discrete Zak transform.

IFFT Inverse fast Fourier transform.

ISI Inter-symbol interferences.

LTI Linear time invariant.

M2M Machine to machine.

MAP Maximum a posteriori.

MF Matched filter.

ML Maximum likelihood.

MMSE Minimum mean square error.

MRC Maximum-ratio combining.

OFDM Orthogonal frequency division multiplexing.

OTFS Orthogonal time frequency space.

PAPR Peak to average power ratio.

PDP Power delay profile.

RRC Root raised cosine.

SINR Signal to interferences and noise ratio.

SNR Signal to noise ratio.

V2V Vehicle to vehicle.

ZF Zero forcing.

Symbols

Symbol	**definition**
j	Imaginary unit
$\lvert . \rvert$	Absolute value operator
$\angle$	Phase of a complex number
$*$	Convolution operator
$\ast$	Convolution operator between continuous and discrete time quantities
$\circledast$	Circular convolution operator
$\mathcal{F}_t\{.\}(w)$	Fourier transform from variable t to variable w
$\mathcal{Z}_t\{.\}(\tau, \nu)$	Zak transform from variable t to variables τ and ν.
$\delta(t)$	Dirac delta function
$\mathbb{R}^+$	Set of real positive numbers
$\mathbb{Z}$	Set of integer numbers
$\mathbb{E}\{.\}$	Ensemble average operator
$Q(.)$	Q function defined as $Q(x) = \frac{1}{\sqrt{2\pi}} \int_x^\infty e^{-\frac{u^2}{2}} du$
$\exists!$	There exists a unique
$\triangleq$	Is defined as
$\lfloor . \rfloor$	Floor operator
$[.]_N$	Modulo N operator
$\lvert\lvert . \rvert\rvert$	l^2 vector norm
A^H	Hermitian of A
$\Re\{.\}$	Real part
$\Im\{.\}$	Imaginary part
$\boldsymbol{W}$	Unitary DFT matrix
$\sim$	Distributed as
$\mathcal{U}_{[a,b]}$	Uniform distribution on the interval $[a, b]$
$\mathcal{CN}(\mu, \sigma^2)$	Complex normal distribution with mean μ and variance σ^2

Notations

Throughout this thesis, the quantities used frequently switch between continuous time signals and discrete time sequences. A continuous time signal is denoted by a lowercase letter and the variable is enclosed in parentheses. For example, a time continuous quantity named y is written $y(t)$, where t denotes time. On the other hand, for a discrete time sequence, the discrete step variable is written inside brackets, e.g., a sequence named x indexed with the variable n is written $x[n]$. In this work, a discrete sequence is always assumed to have a sampling period associated with it, whether explicitly or implicitly defined. Since a sampling period denoted T_s is associated to every sequence, this work makes no distinction between the quantity $x(t) = \sum_l x[l]\delta(t - lT_s)$ and $x[n]$ itself, despite them being two different mathematical objects. This enables a very concise notation of the convolution operator between a sequence and a continuous time signal. Indeed, every time a convolution product is written between a discrete sequence and a continuous time signal, the author refers to the following mathematical operation

$$\begin{aligned}(x \boldsymbol{*} y)(t) &\triangleq \int_{-\infty}^{\infty} y(t-\tau) \sum_l x[l]\delta(\tau - lT_s) d\tau, \\ &= \sum_l x[l] y(t - lT_s),\end{aligned}$$

where the asterisk symbol is written in bold to highlight the fact that one of the quantity is a sequence.
Following this idea of implicitly defined sampling period, no distinction in the notation is made between the Fourier transform of a continuous signal and a discrete time sequence. The continuous time Fourier transform from variable t to the output variable w is defined as

$$\mathcal{F}_t\{x(t)\}(w) \triangleq \int_{-\infty}^{\infty} x(t) e^{-jwt} dt.$$

The exact same notation is used for the discrete time Fourier transform from the discrete variable n to the continuous variable w

$$
\begin{aligned}
\mathcal{F}_n\{x[n]\}(w) &\triangleq \sum_{n=-\infty}^{\infty} x[n]e^{-jwnT_s} \\
&= \int_{-\infty}^{\infty} \underbrace{\sum_{n=-\infty}^{\infty} x[n]\delta(t-nT_s)}_{x(t)} e^{-jwt}dt \\
&= \mathcal{F}_t\{x(t)\}(w)
\end{aligned}
$$

Vectors and matrices are written with bold lowercase and uppercase letter respectively.

Chapter 1

Introduction

With the fast development of electronic devices, we are heading toward a society of highly connected systems. In some applications, the reliability of the communication between those systems is critical. In this context, the role of the telecommunication engineer is twofold. First, he has the responsibility to understand the intrinsic limitations and restrictions of the current communication systems. Then, in light of these limitations, novel techniques and systems can be developed to improve the quality of service. A deep understanding of the phenomena involved in the already deployed systems is crucial to the successful development and release of new standards. One of the limitations of the fifth generation of mobile networks (5G) lies in the way signals are treated in scenarios where the geometry around the user is quickly changing over time. In a world where the immediateness of information has become the norm, this limitation is quite restrictive in many applications. Moreover, this bottleneck may raise issues in applications such as vehicle to vehicle (V2V) or machine to machine (M2M) communications. Indeed, for example, the increasing demand and interest around autonomous vehicles requires strongly reliable communications between the vehicles and sensors, especially in high speed scenarios. This context has pushed researchers to develop alternative architectures more robust to those highly mobile scenarios. The goal of this thesis lies at the intersection of the two aforementioned roles of the telecommunication engineer. First, the framework and context of the current 5G system is presented and the limitations are clearly highlighted. Then, a recently proposed novel system architecture is presented. Finally, a comparison of the two systems is provided to assess the relevance of this new architecture.

The basic scheme of a wireless telecommunication system can be broken down into three main steps. The first one, called the **modulation** step, is the process of transforming the information that one wishes to transmit into a signal with desired properties. The properties and shape of this transmitted signal dictate the overall performance of the system. This transmitted signal then undergoes a **wireless channel** where it is distorted. Finally, the whole point of such a system is to recover, at the receiving side, the transmitted information from this distorted signal. This final step is called the **demodulation** step.

In 4G and 5G, a new modulation scheme known as *orthogonal division multiplexing* (OFDM) was introduced to mitigate the effect of multipath propagation in the wireless channel [1]. This modulation relies on multiple subcarriers to carry information thus enabling very efficient resource allocation between users. However, in presence of a high Doppler effect which arises in high mobility scenarios, the orthogonality of those subcarriers breaks. This orthogonality property is central to this OFDM modulation and the bit error rate (BER) of the system therefore drops drastically when orthogonality is lost. Hadani et al. proposed in 2017 [2] a new modulation technique called OTFS. Since then, OTFS has become very popular and drew a lot of attention from the telecommunication field. This new modulation is more robust to Doppler effect and is one of the main candidates envisioned for 6G. However, if OTFS is to be the chosen modulation scheme for 6G, a deep comparison with the signal structure and architecture of OFDM is essential.

Contributions

This thesis provides a common framework to OFDM and OTFS where the doubly dispersive characteristic of high mobility channels is introduced. This framework is illustrated in Figure 1.1 and described as follows. First, the information bits that one wishes to send are mapped to symbols belonging to a given constellation. Then those symbols are digitally transformed to produce a sequence that is then brought to continuous time thanks to a pulse shaping filter. This continuous time signal is then sent through the wireless channel before being filtered at the reception. The output of this filtered signal is then sampled and digitally demodulated. Finally, the constellation symbols are estimated based on those demodulated samples. Please note that the name given to the different signals in Figure 1.1 does not make sense at this stage of the thesis but they follow the convention used throughout the entire thesis. Therefore, the reader is encouraged to come back to this illustration if needed.

This framework differs from the analog scheme usually used in the literature to derive the OTFS equations.

In this framework, a fair comparison between OFDM, its variant called *cyclic prefix single carrier* modulation (CP-SC) and OTFS is provided. Multiple figure of merits can be attributed to a communication system, however, this work mainly focuses on the bit error rate (BER). The comparison not only provides simulation results but also explores the fundamental differences between the structure of the signals involved in the different modulations scheme.

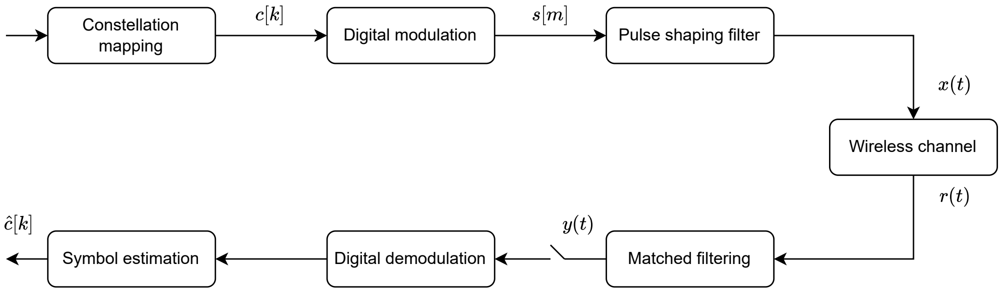

Figure 1.1: Considered framework of a telecommunication chain.

Report structure

In the first chapter of this thesis, the phenomena involved in highly mobile wireless channels are presented. A discrete time model is then developed. This model is used in chapter 3 and chapter 4. In chapter 3, the equations of OFDM are reminded. The heart of this thesis lies in chapter 4 where the equations of OTFS are derived in discrete time from basic principles. Chapter 5 provides a comprehensive comparison of the signal structure between OFDM and OTFS. Finally, before concluding in chapter 7 simulation results are provided in chapter 6 to confirm the results predicted in the previous chapters.

Chapter 2

Doubly dispersive channels

The ultimate goal of a telecommunication system is to transmit information between two places, usually geographically spread apart. In a wireless system, this information is imprinted onto electromagnetic waves, radiated by a transmitting antenna and then captured by a receiving antenna. During the transmission, the electromagnetic waves suffer from many distortions due to obstacles along the path. The study of those distortions is of primary importance for building a reliable telecommunication system and relies primarily on the theory of electromagnetic wave propagation. However, in order to have a general yet simple description of the communication channel a common approach is to take a step back from this electromagnetic point of view. Therefore, the wireless channel between the transmitting and receiving side is modeled here as a combination of multiple propagating paths each described with simple associated physical phenomena. This representation enables a somehow complete description of the physical channel while keeping the complexity of the representation relatively low. Nonetheless, the digital communication system design itself impacts the characterization of the channel due to its intrinsic resolution.

The goal of this section is threefold. First a mathematical description of the physical channel is proposed in section 2.1. This description is carried out with a particular attention to the impact of the user's mobility on the channel properties. Then, in section 2.2, the physical model is adapted to take into consideration the resolution of the discrete time system. Finally, alternative representations of the channel are presented in section 2.3 and in section 2.4.

2.1 Physics of the wireless channel

The physical channel is modeled here as a set of several propagating paths. Each path is characterized by three parameters called delay, gain and Doppler frequency. These parameters describe the physical channel between the transmitter and receiver while putting aside the complexity of having to solve Maxwell's equations each time we wish to characterize a system. Another important aspect is that typically, in a

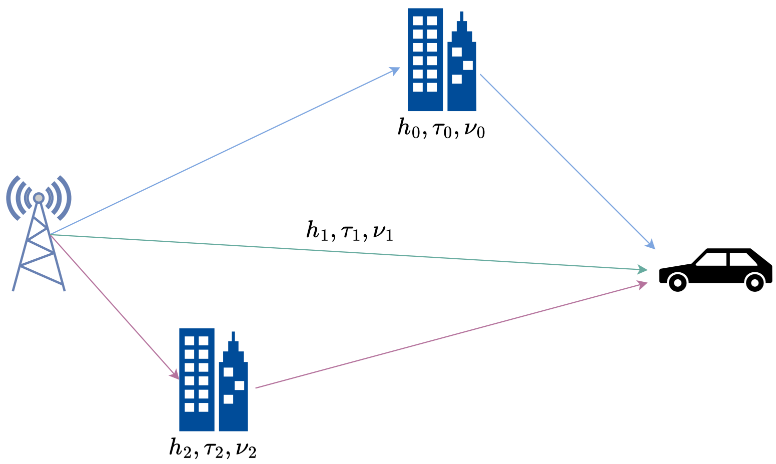

Figure 2.1: Example of a communication channel made of three propagating paths.

telecommunication system, the transmitted signals are band limited and centered around a carrier frequency. Without any loss of generality, the channel can be characterized as an equivalent baseband channel which is applied on the complex envelope of the transmitted signal[3]. A band limited signal rigorously spans an infinite time range. However, throughout this work the bandwidth and time span of a signal are considered in an essential sense as in [4] such that the signals can still be reasonably considered as limited in time and frequency [5]. Due to the band limited characteristic of the signals, the frequency dependence of the considered physical phenomena is not discussed here. The situation is presented in Figure 2.1 and the three parameters characterizing the propagating paths are detailed in the following.

Delay Due to the physical speed limit of any particle, the signal sent at one place inevitably reaches the receiver with a certain delay denoted τ_i for the i-th path.

Gain It is also clear that the power density caught at the receiving side is smaller than at the transmission side due to free-space propagation losses and obstacles absorbing power along the path. This effect is here taken into account by introducing a multiplicative factor h_i. Since the channel is described as a baseband equivalent, h_i can have an imaginary part. The amplitude $|h_i|$ is linked to the power density decay while the phase $\underline{/h_i}$ shifts the phase of the signal.

At this point, by considering a completely static scenario where the delays τ_i and gains h_i are constant over time, the channel can be represented as a linear time invariant (LTI) system whose impulse response $h(t)$ is given by result 2.1.1.

Result 2.1.1: LTI channel model

The channel impulse response of an LTI channel model is given by

$$h(t) = \sum_{i=0}^{P-1} h_i \delta(t - \tau_i), \tag{2.1}$$

where P is the number of propagating paths considered in the channel. The output of the system or equivalently the received signal writes

$$\begin{aligned} r(t) &= (h * x)(t) + n(t), &\quad (2.2)\\ &= \sum_{i=0}^{P-1} h_i x(t - \tau_i) + n(t), &\quad (2.3) \end{aligned}$$

where $x(t)$ and $r(t)$ are the sent and received signals respectively and $n(t)$ is an additive noise signal corrupting the system. This noise is often considered as additive, white and Gaussian distributed (AWGN).

Discussion 2.1: The convolution operator in (2.2) can be developed to highlight an interesting observation

$$r(t) = \int_{-\infty}^{\infty} h(t - \tau) x(\tau) d\tau + n(t). \tag{2.4}$$

Notice how the convolution operator introduces a temporary variable τ. This variable physically refers to the time at the input of the system. Since the system is invariant, the channel only cares about the difference of time between the output observation and input time $t - \tau$. These are well-known LTI system properties.

Doppler frequency In a mobile scenario, the delays τ_i might slowly change over time. Indeed, let us consider an emitter moving at speed v towards a receiver. The distance and consequently delay between the emitter and receiver are expressed as

$$\begin{aligned} d(t) &= d(t = 0) - vt, &\quad (2.5)\\ \tau(t) &= \tau(t = 0) - \frac{vt}{c}, &\quad (2.6) \end{aligned}$$

where c is the propagating speed of the signal (often associated to the speed of light in vacuum). As a consequence of this time-varying delay, the frequency of the received signal is modified. This effect is known as the Doppler effect and translates in baseband as a multiplicative factor $e^{j2\pi f_c \frac{vt}{c}}$ where f_c is the reference frequency chosen for the complex envelope representation. For ease of notation, the symbol ν

is introduced: $\nu \triangleq f_c \frac{v}{c}$. To take into account this Doppler effect, (2.3) is modified as such

$$r(t) = \sum_{i=0}^{P-1} h_i e^{j2\pi\nu_i t} x(t - \tau_i(t)) + n(t), \tag{2.7}$$

where ν_i is used to denote the Doppler frequency associated to the i-th path.

We realize that the effect of the channel is made up of two very different effects. On one hand, the signal is delayed which mathematically translates in a convolution between Dirac delta functions and the input signal. On the other hand, the Doppler effect leads to a multiplicative effect between the delayed signal and $e^{j2\pi\nu_i t}$. Due to this dual effect, a natural mathematical representation is to describe the channel as a quantity living in a two-dimensional space. The first dimension is nothing else than the temporary variable used for the convolution operator as in (2.4). The second dimension on the other hand, encapsulates the multiplicative effect. The two-dimensional channel and the output signal are given by result 2.1.2.

Result 2.1.2: Physical channel model with Doppler effect

When the Doppler effect is introduced into the model, the wireless channel can no longer be represented as an LTI model. Therefore, the channel is modeled as a two-dimensional quantity $h(\tau, t)$ given by

$$h(\tau, t) = \sum_{i=0}^{P-1} h_i e^{j2\pi\nu_i t} \delta(\tau - \tau_i(t)). \tag{2.8}$$

The output of the system is written as

$$\begin{aligned} r(t) &= (h *^{\tau} x)(t) + n(t), && (2.9) \\ &= \int_{-\infty}^{\infty} h(\tau, t) x(t - \tau) d\tau + n(t), && (2.10) \\ &= \sum_{i=0}^{P-1} h_i e^{j2\pi\nu_i t} x(t - \tau_i(t)) + n(t). && (2.11) \end{aligned}$$

The operator $*^{\tau}$ is introduced to represent a convolution along the first dimension of $h(\tau, t)$. It should be emphasized that the channel representation $h(\tau, t)$ is two-dimensional so that mathematically the convolutive effect is isolated from the multiplicative one. However, both quantities τ and t are manifestations of the same physical quantity which is time. Therefore, the two-dimensions collapse through the convolution operator so that the output quantity $r(t)$ is as expected a time signal which is only one dimensional.

As we have seen, with mobility, the channel deviates more and more from the LTI model. A simple way of dealing with time varying systems is to subdivide time into small blocks over which the system can reasonably be approximated as time invariant. The size of the subdivisions inherently depends on the rate of the time variations of the channel and subsequently on mobility inside the channel (i.e, the Doppler frequencies). One quantity that encapsulates the information about the rate of the variations is the coherence time denoted T_c. The coherence time is defined in order of magnitude as the time over which one can write

$$h(\tau, t_0 + \Delta t) \approx h(\tau, t_0) \quad \forall \Delta t \in [0, T_c]. \tag{2.12}$$

Based on this definition, one clearly sees that T_c refers to the second dimension of $h(\tau, t)$ but brings no information on the structure along the delay dimension τ. Therefore, another important metric in the characterization of the channel is the (root mean squared) delay spread denoted τ_{RMS} which writes

$$\tau_{RMS} = \sqrt{\frac{\int_0^\infty (\tau - \tau_M)^2 P(\tau)}{\int_0^\infty P(\tau) d\tau}}, \tag{2.13}$$

where τ_{RMS} is the delay spread and $P(\tau) = \mathbb{E}\left\{|h(\tau, t)|^2\right\}$ is the power delay profile (PDP). Note that the ergodicity and stationarity properties on $|h(\tau, t)|^2$ are implicitly assumed so that the PDP does not depend on time and the ensemble average is equivalent to a time averaging. Finally, τ_M is defined as

$$\tau_M = \frac{\int_{-\infty}^{\infty} P(\tau) \tau d\tau}{\int_{-\infty}^{\infty} P(\tau) d\tau}. \tag{2.14}$$

With these definitions, it is clear that the delay spread refers to the delay dimension of the channel. This delay spread is useful to justify a commonly used approximation of the channel representation.

Indeed, the time varying nature of the delays is often omitted in the convolutive dimension of the channel. Let us denote by T_b the time required for the transmission of a block of data. The change in delay after a time T_b is (considering only a line-of-sight path), for a user having a speed of 50m/s (180 km/h), $\Delta\tau = \frac{50}{3\times10^8} T_b$. In 5G, T_b is some hundreds of micro-seconds [6]. The order of magnitude of $\Delta\tau$ is then 10^{-13} which is small compared to typical outdoor delay spread which are around $100ns$ in urban scenarios[7]. Consequently, in the following of the thesis the time dependence in $\tau_i(t)$ is omitted.

2.2 The discrete time channel

The channel representation can be further developed to take into consideration the intrinsic resolution and digital characteristic of the system. In digital communications, prior to the continuous signal $x(t)$ is a discrete time sequence[1] $s[n]$. This digital sequence is then brought to continuous time thanks to a pulse shaping filter $g^{tx}(t)$ as such

$$x(t) = (s * g^{tx})(t) = \sum_{l} s[l] g^{tx}(t - lT_s), \tag{2.15}$$

where T_s denotes the sampling period that is chosen during the design of the system based on the desired system performance.

At the reception, the system performs matched filtering followed by a sampling operation. The continuous signal prior to this sampling operation writes

$$\begin{aligned} y(t) &= (g^{rx} * (h *^{\tau} (g^{tx} * s)))(t) + (g^{rx} * n)(t), & (2.16)\\ &= (g^{rx} * r)(t) + (g^{rx} * n)(t), & (2.17) \end{aligned}$$

where $g^{rx}(t)$ is the filter used at the reception.

Inserting the expression of $r(t)$ (2.11) in (2.17) and putting aside the noisy term for now the following development is made

$$\begin{aligned} y(t) &= \int_{-\infty}^{\infty} g^{rx}(t-\tau) r(\tau) d\tau, & (2.18)\\ &= \sum_{i=0}^{P-1} h_i \int_{-\infty}^{\infty} g^{rx}(t-\tau) e^{j2\pi\nu_i\tau} x(\tau - \tau_i) d\tau, & (2.19)\\ &\overset{(a)}{=} \sum_{i=0}^{P-1} \sum_{l=-\infty}^{\infty} h_i s[l] \int_{-\infty}^{\infty} e^{j2\pi\nu_i\tau} g^{tx,*}(\tau - t) g^{tx}(\tau - lT_s - \tau_i) d\tau, & (2.20) \end{aligned}$$

where step (a) comes from (2.15) and the architectural assumption that the receiving filter is matched to the transmitting one, i.e. $g^{rx}(t) = g^{tx,*}(-t)$. This last expression highlights that the receiving filter should not be matched to the transmitting one but rather to the product of the Doppler impairment and the transmitting pulse shaping filter. However, if the Doppler frequency ν_i is small compared to the bandwidth of the pulse shaping filter, the assumption $e^{j2\pi\nu_i t} g_{tx}(t) \approx g_{tx}(t)$ becomes

[1] In a real digital system the values of $s[n]$ are quantized. However, this characteristic is not discussed here

reasonable and things simplify[1]. Here is the simplification it leads to

$$\begin{aligned} y(t) &= \sum_{i=0}^{P-1}\sum_{l=-\infty}^{\infty} h_i s[l] e^{j2\pi\nu_i(lT_s+\tau_i)} \int_{-\infty}^{\infty} e^{j2\pi\nu_i(\tau-lT_s-\tau_i)} g^{tx,*}(\tau-t) g^{tx}(\tau-lT_s-\tau_i) d\tau, \\ &\approx \sum_{i=0}^{P-1}\sum_{l=-\infty}^{\infty} h_i s[l] e^{j2\pi\nu_i(lT_s+\tau_i)} \int_{-\infty}^{\infty} g^{tx,*}(\tau-t) g^{tx}(\tau-lT_s-\tau_i) d\tau, && (2.21) \\ &= \sum_{i=0}^{P-1}\sum_{l=-\infty}^{\infty} h_i s[l] e^{j2\pi\nu_i(lT_s+\tau_i)} C_{g^{tx}}(t-lT_s-\tau_i). && (2.22) \end{aligned}$$

In the previous expression, $C_{g^{tx}}(t)$ is the correlation function of g^{tx} defined as

$$C_{g^{tx}}(t) = \int_{-\infty}^{\infty} g^{tx}(\tau) g^{tx,*}(\tau-t) d\tau. \tag{2.23}$$

After the sampling operation we are left with the following sequence (the noisy term is reintroduced)

$$\begin{aligned} y[n] &= \sum_{i=0}^{P-1} h_i \sum_{l=-\infty}^{\infty} s[l] e^{j2\pi\nu_i(lT_s+\tau_i)} C_{g^{tx}}(nT_s-lT_s-\tau_i) + (g^{rx} * n)(nT_s), && (2.24) \\ &\overset{m=n-l}{=} \sum_{m} s[n-m] \sum_{i=0}^{P-1} h_i e^{j2\pi\nu_i nT_s} e^{j2\pi\nu_i(\tau_i-mT_s)} C_{g^{tx}}(mT_s-\tau_i) + w[n], && (2.25) \end{aligned}$$

where $w[n]$ is defined as the filtered noise $w[n] \triangleq (g^{rx} * n)(nT_s)$. It should be emphasized that in all generality, τ_i is not an integer multiple of T_s and the usual Nyquist criterion given as

$$C_{g^{tx}}(nT_s) = \delta(nT_s) \quad \forall n \in \mathbb{Z}, \tag{2.26}$$

cannot be used in (2.25).

Result 2.2.1: Discrete time equivalent channel model

The equivalent discrete time channel is identified from (2.25) as

$$h[m,n] = \sum_{i=0}^{P-1} h_i e^{j2\pi\nu_i nT_s} e^{j2\pi\nu_i(\tau_i-mT_s)} C_{g^{tx}}(mT_s-\tau_i) \tag{2.27}$$

[1]For typical system parameters in 5G such as the one used in chapter 6, i.e., $f_c = 4GHz$ and $\frac{1}{T_s} = 2MHz$, a user moving at speed $1000km/h$ towards the receiver leads to $\nu \approx 4kHz$. The bandwidth of $g_{tx}(t)$ being roughly equal to $\frac{1}{T_s}$ for common pulse shaping filter, the approximation is reasonable.

The first difference between expressions (2.8) and (2.27) is the Dirac delta function that turns into $C_{g^{tx}}(t)$. Consequently, a single delay impacts multiple output samples. Another difference is the manifestation of the Doppler effect. In the continuous channel (2.11), the Doppler shift is proportional to the output observation variable t, i.e. $e^{j2\pi\nu_i t}$. On the other hand, for the discrete time signal in (2.24), the effect of the Doppler is proportional to the variable $lT_s + \tau_i$ which is not necessarily equal to the output observation time nT_s. Indeed, due to the Nyquist criteria, $lT_s + \tau_i = nT_s$ only if τ_i is an integer multiple of T_s. This translates in the discrete time channel expression (2.27) in an additional factor $e^{j2\pi\nu_i(\tau_i - mT_s)}$. This change in the Doppler effect manifestation is due to the approximation introduced in (2.21) where the Doppler effect is fixed to a certain value for each $x[l]$.

Discussion 2.2: A common choice for g^{tx} and its associated matched filter g^{rx} is the root raised cosine filter (RRC). This leads to a correlation function and output signals $r(t)$ presented in Figure 2.2 (assuming $s[n] = [1, 1]$). In this figure, one clearly sees the impact of delays that are not an integer multiple of T_s and the resulting spreading of the input sample across multiple output samples due to the shape of $C_{g^{tx}}(t)$. Notice how the discrete system cannot make the difference between a fractional delay and a set of multiple paths each with an integer delay, specific gain and Doppler frequency, this phenomenon is referred to as the resolution of the system. Therefore, in the following of this thesis, the discrete channel is considered, with an abuse of notation as having a form given by

$$h[m, n] = \sum_{i=0}^{P-1} h_i e^{j2\pi\nu_i nT_s} \delta[m - r_i], \tag{2.28}$$

where $r_i \in \mathbb{Z}$ and P no longer refers to a physical number of paths but rather to a number of paths seen by the system. The quantity $h[m, n]$ is now called the *channel taps*. The extra terms between (2.27) and (2.28) are absorbed in the h_i. Note that this representation (as the previous ones) does not exclude redundancy in the sets r_i and ν_i. Consequently, it is not forbidden to have different Doppler frequencies associated to a same delay, i.e $\nu_i \neq \nu_{i' \neq i}$ while $r_i = r_{i' \neq i}$ and vice versa.

2.3 Other equivalent channel representations

The representation of the channel described up to now is called the delay-Time representation. The name refers to the two dimensions of the representation. The first dimension is used to represent the convolutive effect of the channel and is therefore called the delay dimension. The second dimension is named time as it encapsulates the time varying nature of the channel. This representation appears quite naturally as it directly links the time signal at the input and output of the

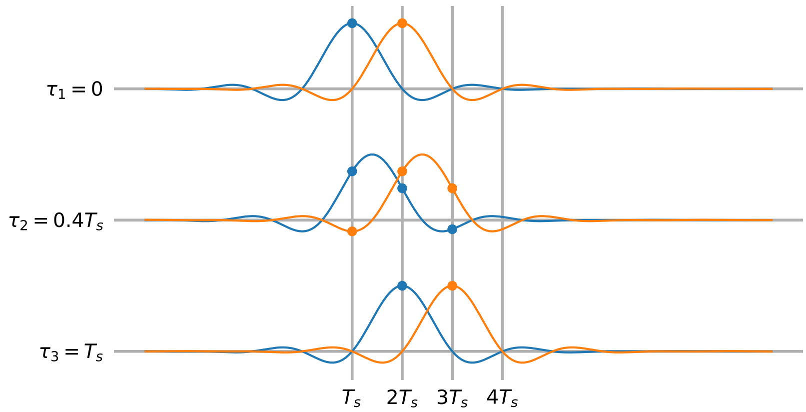

Figure 2.2: Impact of the correlation function and delay in the channel on the received signal. The received signal $y(t)$ (in this case $s[n]$ is made of only 2 elements) is presented in 3 situations. For each situation, the sampling instants of the system are represented with dots. The three situations correspond to a channel with only one path and an associated delay of 0, $0.4T_s$ and T_s by going from top to bottom. The Doppler frequency and gain of each scenario are zero and one respectively.

system. Still, other representations of the channel are also possible. Just as the Fourier transform provides another equivalent representation of any signal, the channel can be characterized by specifying the gains associated with each pair of delay and Doppler frequency. For example, the scenario in Figure 2.1 is completely characterized with the three triplets of information (τ_0, ν_0, h_0), (τ_1, ν_1, h_1) and (τ_2, ν_2, h_2). This representation is called the delay-Doppler representation and is linked to the delay-Time representation through a Fourier transform. To ease the reading, the subscripts dT and dD are introduced. The quantity previously defined in (2.8) is renamed $h_{dT}(\tau, t)$ to highlight the delay-Time representation and $h_{dD}(\tau, \nu)$ is the delay-Doppler representation defined as

$$h_{dD}(\tau, \nu) = \mathcal{F}_t\{h_{dT}(\tau, t)\}(\nu), \tag{2.29}$$

$$= \int_{-\infty}^{\infty} h_{dT}(\tau, t) e^{-j2\pi\nu t} dt. \tag{2.30}$$

Applied to (2.8) (still neglecting the time dependence in τ_i) this gives

$$h_{dD}(\tau, \nu) = \sum_{i=0}^{P-1} h_i \delta(\tau - \tau_i) \delta(\nu - \nu_i). \tag{2.31}$$

This last expression highlights a really important property of the delay-Doppler representation which is the sparsity. Figure 2.3 illustrates this sparsity characteristic for a simple channel with five paths. The stationary time of the delay-Doppler representation is also much higher than the coherence time of the delay-time representation. Indeed, the stationarity of the delay-Doppler representation depends exclusively on the different accelerations in the channel and no more on the speeds. Note also that, since a multiplication between two signals in time domain is equivalently represented as a convolution between the Fourier transform of the signals, the delay-Doppler channel effect is now represented as a 2D convolution with the delay-Doppler representation of the input signal. Of course, the notion of the delay-Doppler representation of a single dimensional signal is still to be defined which is precisely one of the goals of chapter 4.

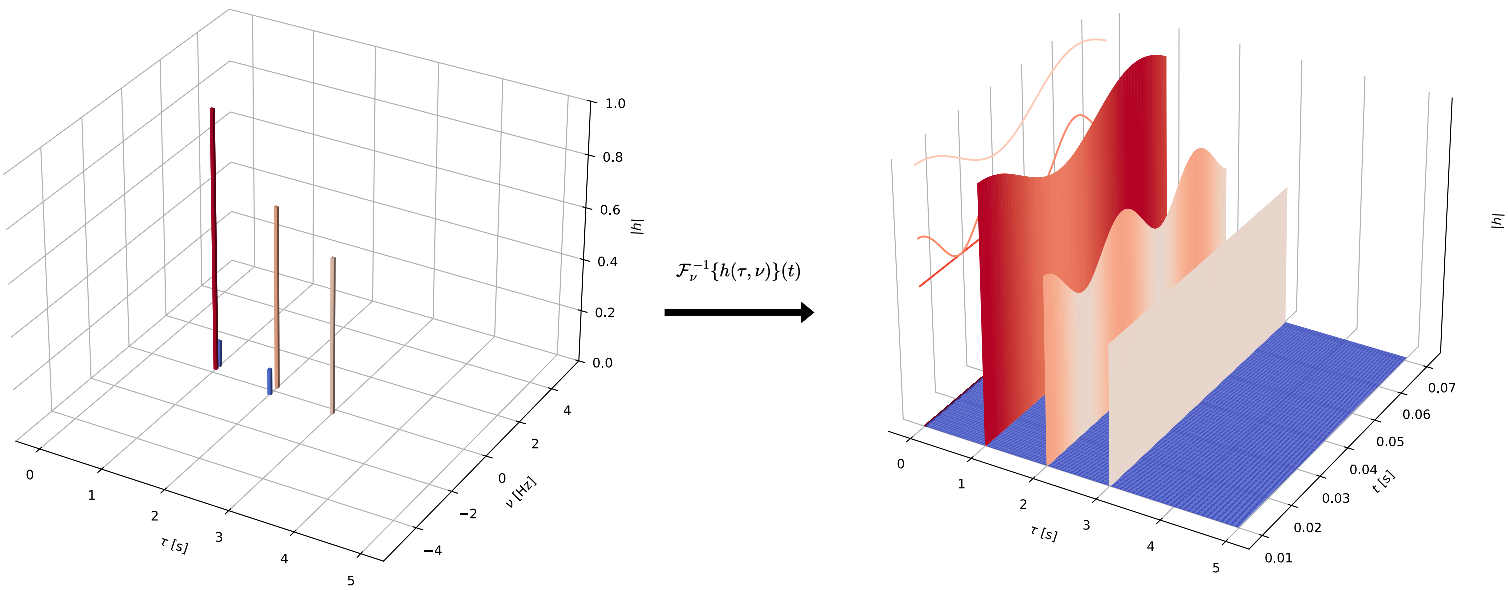

Figure 2.3: Illustration of a channel with five paths in the delay-Doppler domain on the left and in delay-Time on the right. When multiple paths with the same delays but different Doppler frequencies exist in the channel, we clearly see on the right graph the time varying nature of the channel. This time varying nature is also referred to as the fading of the channel

2.4 Statistical channels

As seen in (2.28), the channel taps are made of P artificial paths that interfere one with another. Depending on the coherence time of the channel, the mobility inside the channel might cause a *fading* of those channel taps over time due to coherent and destructive interferences of the Doppler frequencies[1]. To have a characterization

[1]This effect is observed on the continuous time channel model in Figure 2.3

of those channel taps valid on a certain range of time without actually referring to the physical continuous channel and its associated set of parameters τ_i,ν_i,h_i, the channel taps are often modeled as a stochastic quantity. In those statistical models, each tap $h[m, n]$ is a random variable for which the distribution can depend on the delay m but not on the time n. Indeed, the whole point of the statistical philosophy is to somehow simplify the representation of the channel by putting aside the true physics inside it. Consequently, there is little point in creating a statistical model that depends on time.

Frequently used models are the Rayleigh and Rician model. The Rayleigh model assumes many independent paths with uniformly distributed phase shifts [3]. This enables the modelization of $|h(m, n)|$ as a Rayleigh distribution

$$|h(m,n)| \sim \frac{x}{\sigma_m^2} e^{\frac{-x^2}{2\sigma_m^2}}, \quad x \in \mathbb{R}^+ \tag{2.32}$$

where σ_m^2 is the variance of the distribution which can depend on the delay m and x is the free variable of the distribution. The Rician model on the other hand accounts for a line-of-sight path (or equivalently any path with a much higher gain than the others) and writes

$$|h(m,n)| \sim \frac{x}{\sigma^2} e^{-\frac{x^2+|\bar{h}|^2}{2\sigma^2}} I_0\left(\frac{r|\bar{h}|^2}{\sigma^2}\right) \tag{2.33}$$

where again x is the free variable, $|\bar{h}|$ is the amplitude of the gain associated to the line-of-sight path, $2\sigma^2$ is the power in the diffuse components and finally I_0 is the 0th order modified Bessel function of the first kind. Two interpretations of the Rayleigh and Rician distributions are presented in Figure 2.4 and Figure 2.5.

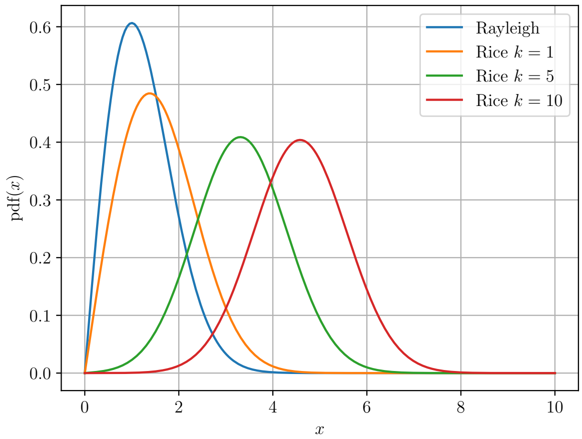

Figure 2.4: Rayleigh and Rician distributions for different value $k = \frac{|\bar{h}|^2}{2\sigma^2}$ with a fixed variance $\sigma^2 = 1$. When k approaches zero, the Rician distribution tends to the Rayleigh distribution. On the other hand, when k becomes larger, the Rician distribution approximates a Gaussian centered around $|\bar{h}|$.

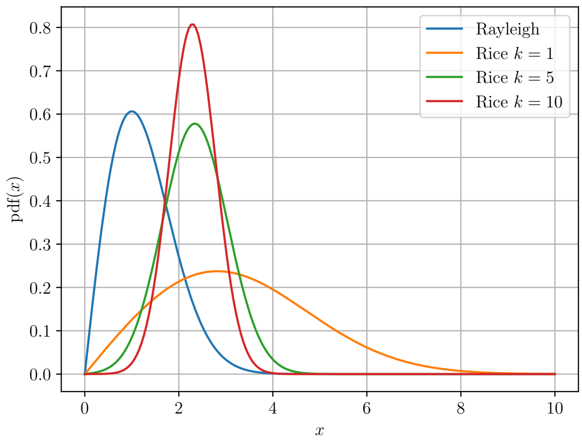

Figure 2.5: Rayleigh and Rician distributions for different value $k = \frac{|\bar{h}|^2}{2\sigma^2}$ with a fixed $|\bar{h}|^2 = 5$. The distributions tend to concentrate around $\sqrt{5}$ as k becomes larger (the channel becomes more and more deterministic).

We emphasize that with the Rayleigh and Rician model, the geometry of the physical channel is fixed and a system with an infinite resolution can perfectly describe the value of $h[m, n]$ for each m and n without relying on any notion of randomness. In an LTI scenario where there is no mobility inside the channel those two models do not even make sense anymore since there is no variation of $h[m, n]$ across the time n. It is in this context of statistical model that the notion of *diversity* is introduced. A very basic example of diversity is now given to fix the ideas. Let us consider a simplified version of the channel tap model made of a single delay as

$$h[m,n] = \sum_{i=0}^{P-1} h_i e^{j2\pi\nu_i n T_s}\delta[m]. \tag{2.34}$$

Any information transmitted at a time n where $h[m,n]$ is in deep fade is prone to decoding errors at the reception. Now if this same information is transmitted at two distinct instants n and n' and by assuming that $h[m,n']$ and $h[m,n]$ are uncorrelated, the odds that $h[m,n']$ and $h[m,n]$ are both in deep fade compare to the odd that only $h[m,n]$ is in deep fade is much lower. Transmitting an information at two instants in time when the channel taps are uncorrelated therefore improves the detection capability at the reception. This notion of diversity is often derived mathematically based on the statistical distribution of the channel tap model and breaks if the channel taps are correlated [3], [8].

Another source of randomness in the characterization of a channel is the incertitude on the geometry around the user. Indeed, the user might find itself in a rural environment or more in the countryside and moving at different speeds leading to different structures of the physical channel. Therefore, the physical channel and its geometry can also be considered random. It is critical for the following of this thesis to understand that this is a completely different source of randomness than the one leading to the Rayleigh or Rician fading where the physical channel was determined and fixed.

In the context of OFDM the point of view associated to the Rayleigh and Rician model is often used. On the other hand, in the context of delay-Doppler modulations where the channel is characterized through an image of the true physical parameters τ_i and ν_i it makes less sense to consider the Rayleigh and Rician point of view. However, even in delay-Doppler modulations the channel taps $h[m,n]$ fades over time in mobile scenarios. Therefore, the notion of diversity still applies in the context of delay-Doppler modulations even if the channel, once the geometry of the channel is fixed, is modeled as deterministic.

Key take-away messages of chapter 2:

- The physical channel is made up of many propagating paths each described with a gain h_i, delay τ_i and a Doppler frequency ν_i.

- When there is mobility inside the channel, the system is no longer LTI and the delay-Time continuous channel model writes:

$$h_{dT}(\tau, t) = \sum_{i=0}^{P-1} h_i e^{j2\pi\nu_i t}\delta(\tau - \tau_i)$$

- The channel can be described in the delay-Doppler world where it is much more sparse:

$$h_{dD}(\tau, \nu) = \sum_{i=0}^{P-1} h_i \delta(\tau - \tau_i)\delta(\nu - \nu_i)$$

- The coherence time is the time over which the channel can still be approximated as time invariant. This coherence time is intrinsically linked with the values of the Doppler frequencies inside the channel.

- The channel can equivalently be described in discrete time with a number of paths P, delays $r_i \in \mathbb{Z}$ and gains h_i that do not have a physical meaning anymore but rather describe the channel as seen by the system:

$$h[m, n] = \sum_{i=0}^{P-1} h_i e^{j2\pi\nu_i n T_s}\delta[m - r_i]$$

- Stepping away from the physical model, the channel can be characterized as a statistical quantity. Two frequently used model are the Rayleigh and Rician distribution. The Rician distribution can take into account a path with a much higher gain than the others. This statistical distribution only makes sense in mobile channel scenarios where the channel taps fade over time.

Chapter 3

Frequency equalization techniques

The physical distortion encountered by the transmitted signal in the wireless channel has been derived in chapter 2. However, it remains to investigate the structure of the transmitted signal $x(t)$. A widely used modulation technique is the orthogonal frequency division multiplexing technique (OFDM). Its genesis comes back to the 60's and has been widely used in different communication standards since then. It was introduced in 4G and is still the chosen modulation technique in 5G. This modulation technique ingeniously relies on the Fourier transform theory and enables a very low complexity equalization of the channel in low mobility scenarios where the coherence time of the channel is sufficiently high.

A first introduction of the working principle of OFDM is given in subsection 3.1.1. Then, the mathematical framework of OFDM is presented. It is used to derive the input/output relationship of the system and its frequency equalization technique. The important parameters of the modulation are discussed. Afterward, a system analogous to OFDM called *cyclic prefix single carrier* (CP-SC), is presented. The comprehension of this CP-SC scheme is fundamental for the comparison between OFDM and the delay-Doppler modulations. Finally, simulation results are shown to highlight the differences between OFDM and CP-SC.

3.1 OFDM

This section provides a quick overview of the basic discrete time OFDM system in order to fairly assess its performance against delay-Doppler modulations. Challenges such as PAPR, sensitivity to CFO, etc., are not discussed here. However, detailed discussion of those issues can be found in [9] and [10].

3.1.1 Principle description

The OFDM modulation is a particularization of a broader class of modulation techniques called multi-carrier modulations. In those modulations, the constellation symbols that one wishes to transmit are first assigned to a particular subcarrier before being transmitted. In an OFDM system, the subcarriers are orthogonal, overlapping and limited in time. The first step in a digital implementation of OFDM is to create blocks consisting of N symbols from the stream of constellation symbols, where N is the number of subcarriers available in the system. Those blocks are naturally called *OFDM blocks*. The whole chain that experiences such a block is presented in Figure 3.1 and the details about the different steps are presented in the next paragraph.

Each symbol inside an OFDM block is assigned to a specific subcarrier. This subcarrier assignment step is realized through an inverse discrete Fourier transform (IDFT). Therefore, the constellation symbols that one wishes to transmit are said to live in the frequency domain.
Before applying the pulse shaping filter and sending the signal over the wireless channel, the different OFDM blocks have to be concatenated. Let us first assume an LTI representation of the channel as in (2.2) (thus putting aside the mobility inside the channel for now). If the blocks are simply put one after another, the delay dispersive characteristic of the channel will induce interferences between the blocks. This prevents the reception side from working block by block. To avoid inter-block interferences, one can put guard samples in between the blocks so that two distinct blocks do not overlap at the output of the channel. The key characteristic of OFDM that made it so popular is the shape chosen for those guard samples. At this point, one can wonder why the Fourier basis has been chosen for our system. Indeed, other waveforms could have been chosen. This Fourier basis is justified with regard to the following objective *"The structure of $x(t)$ should provide a low complexity channel equalizer at the reception"*. The convolution operator in the channel representation (2.2) along with the IDFT suggest a simple equalization in the frequency domain. Indeed, a convolution between two continuous time signals is equivalently represented as a product of their Fourier transform [11]. For this property to translate with discrete time convolution and the DFT operator, the convolution in the channel should appear as a (block-)circular convolution [12]. The physics inside the channel being as it is, the only way to transform the convolution of the channel into a (block-)circular one is to play with the structure of the input signal. It is with that objective in mind that a copy of the end of each OFDM block is prepended at its beginning. By doing so, the samples at the beginning of each block are convoluted with the samples at the end of their own block, mimicking a circular convolution. This operation is known as the cyclic prefix (CP) addition step. At the reception, this CP is discarded and of no use. This CP addition thus induces a small degradation of the datarate of the system but the channel equalization at the receiving side is much easier since the channel effect is simply represented as a product between the DFT of the channel and the input symbols. The whole discussion is illustrated in Figure 3.2 and Figure 3.3.

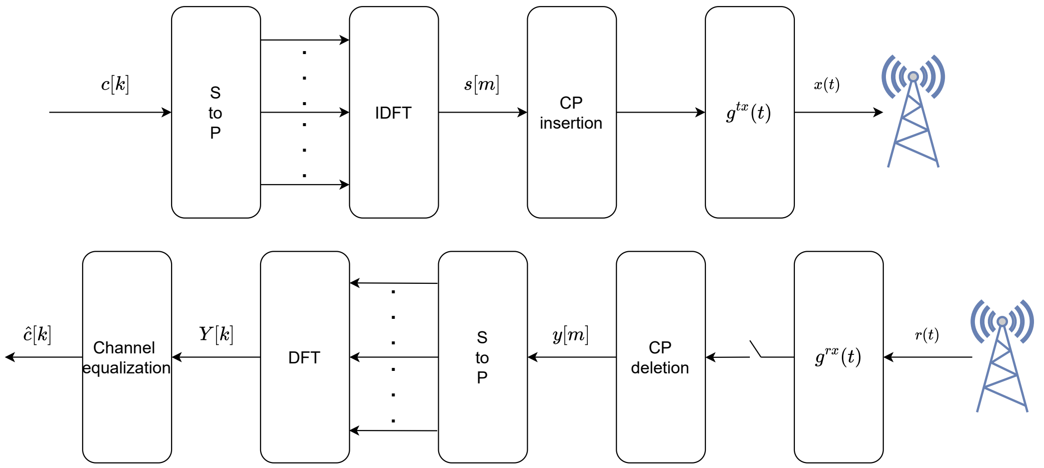

Figure 3.1: Transmission chain of an OFDM system. The blocks serial to parallel (S to P) symbolize the fact that the DFT and IDFT blocks take as an input a whole block of N samples at once.

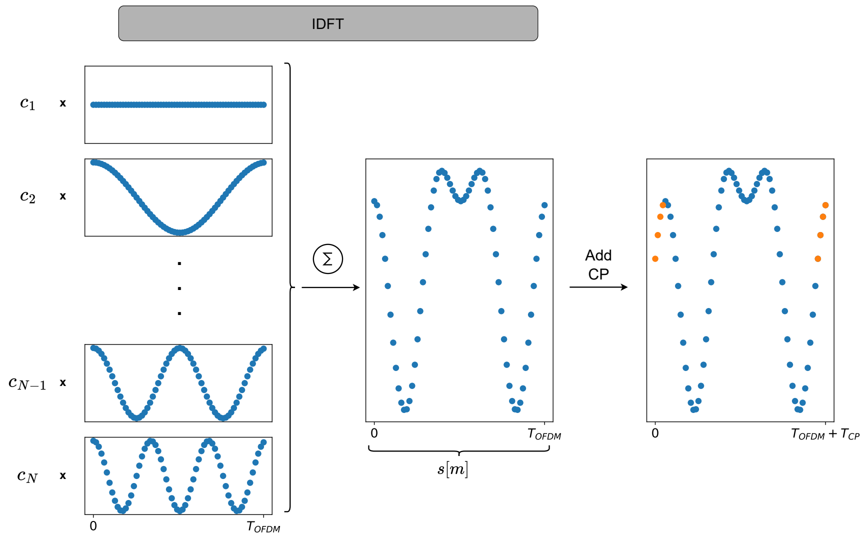

Figure 3.2: Real part of the transmitted signal for one block of an OFDM system. c_k is the k-th constellation symbol of the block and is considered as one for every $k \in \{1, 2, N-1, N\}$ and zero otherwise. Each constellation symbol is assigned to a basis function of the N points DFT, then the CP is added. The cyclic prefix is composed here of 4 samples.

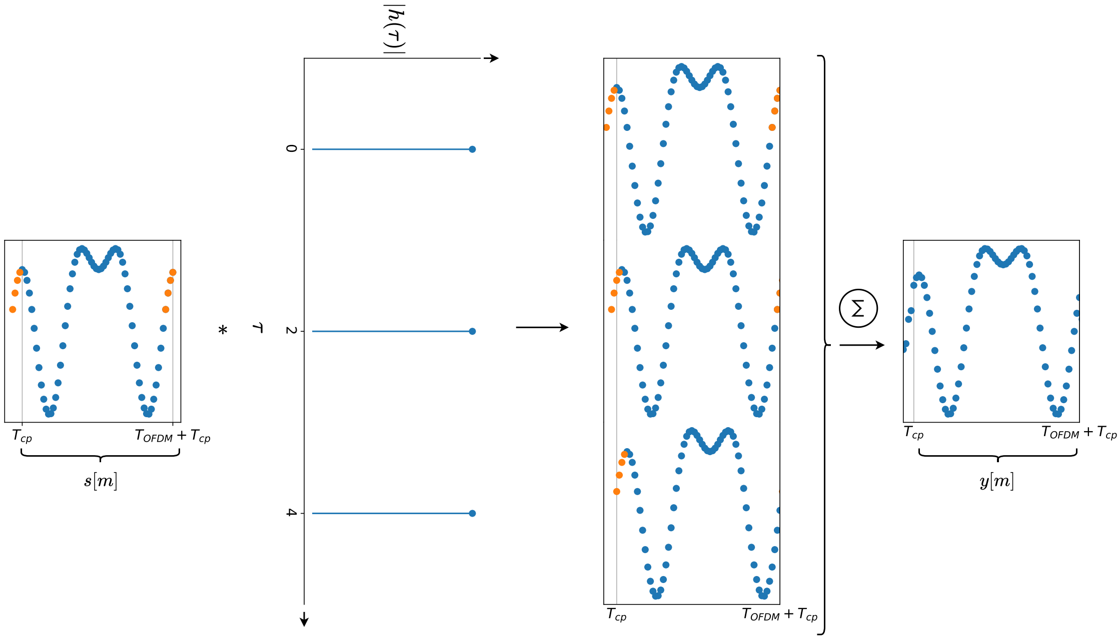

Figure 3.3: Illustration of the impact of a static channel made of three paths each with a unitary gain on the received signal. The convolution is explicitly developed into three delayed versions of the input signal that are summed together. Notice how the length of the cyclic prefix has to be carefully chosen based on the length of the channel impulse response in order to avoid inter-block interferences. (The noise is not represented in the illustration)

3.1.2 Mathematical description. Input/output relationship and channel equalization

The mathematical description of an OFDM system is now described. Thanks to the CP insertion, the analysis is presented only for one block. Indeed, if the size of the length of the CP is well-chosen in regard to the impulse response of the channel, restricting the analysis to only one block presents no loss of generality. The discrete time sequence after the IDFT operator is written as

$$s_n[m] = \frac{1}{\sqrt{N}} \sum_{k=0}^{N-1} c_n[k] e^{j2\pi \frac{mk}{N}} \tag{3.1}$$

where the subscript n indicates the index of the block and $c_n[k]$ is the sequence of constellation symbols inside block n. Then, using the discrete time representation of the channel (2.28) developed in chapter 2, the received samples with the CP discarded are written as given in result 3.1.1 (the index of the block is omitted).

Result 3.1.1: Received time signal of an OFDM system

The received signal corresponding to one block of an OFDM system with the CP discarded is given by

$$y[m] = \sum_{i=0}^{P-1} h_i e^{j2\pi\nu_i m T_s} s\Big[[m - r_i]_N\Big] + w[m], \tag{3.2}$$

where the modulo N operator comes from the effect of the CP and $w[m]$ is the AWGN term.

At the reception, the first step is a DFT leading to the following expression[1] (the noise is omitted)

$$\begin{aligned}
Y[k] &= \frac{1}{\sqrt{N}} \sum_{m=0}^{N-1} y[m] e^{-j2\pi\frac{mk}{N}}, &(3.3)\\
&= \frac{1}{N} \sum_{m=0}^{N-1}\sum_{i=0}^{P-1} h_i e^{j2\pi\nu_i m T_s} \sum_{k'=0}^{N-1} c[k'] e^{j2\pi\frac{(m-r_i)k'}{N}} e^{-j2\pi\frac{mk}{N}}, &(3.4)\\
&= \frac{1}{N} \sum_{k'=0}^{N-1}\sum_{i=0}^{P-1} h_i c[k'] e^{-j2\pi\frac{r_i k'}{N}} \sum_{m=0}^{N-1} e^{j2\pi\frac{mk'}{N}} e^{-j2\pi\frac{mk}{N}} e^{j2\pi\nu_i m T_s}, &(3.5)\\
&= \frac{1}{N} \sum_{k'=0}^{N-1}\sum_{i=0}^{P-1} h_i c[k'] e^{-j2\pi\frac{r_i k'}{N}} \sum_{m=0}^{N-1} e^{j2\pi m(\frac{k'}{N}-\frac{k}{N}+\nu_i T_s)}, &(3.6)\\
&= \frac{1}{N} \sum_{k'=0}^{N-1}\sum_{i=0}^{P-1} h_i c[k'] e^{-j2\pi\frac{r_i k'}{N}} e^{j\pi\frac{N-1}{N}(k'-k+\nu_i T_s N)} \frac{\sin\left(\pi(k'-k+\nu_i T_s N)\right)}{\sin\left(\frac{\pi}{N}(k'-k+\nu_i T_s N)\right)}. &(3.7)
\end{aligned}$$

The advantage of OFDM is highlighted when the variations of the terms $e^{j2\pi\nu_i m T_s}$ are neglected. Indeed, freezing those terms to a certain value leads to (the periodic sinc function degenerates into $N\delta[k-k']$)

$$Y[k] = c[k] \sum_{i=0}^{P-1} h'_i e^{-j2\pi\frac{r_i k}{N}}, \tag{3.8}$$

where $h'_i = h_i e^{j2\pi\nu_i m_{freeze} T_s}$ and m_{freeze} is the chosen reference time instant for the Doppler effect. Without loss of generality, $m_{freeze} = 0$ is chosen here for simplicity. In this last expression, one identifies up to a factor $\frac{1}{\sqrt{N}}$ the DFT of the channel impulse response at time $n = 0$. Indeed, the DFT of the channel impulse response

[1]The CP is used to go from (3.3) to (3.4). Indeed, if the channel effect is not represented as a circular convolution, the values of $s[m-r_i]$ when $m - r_i < 0$ are not equal to $\sum_{k'=0}^{N-1} c[k'] e^{j2\pi\frac{(m-r_i)k'}{N}}$.

is expressed as

$$\lambda[k] = \frac{1}{\sqrt{N}} \sum_{m=0}^{N-1} \sum_{i=0}^{P-1} h_i \delta[m - r_i] e^{-j2\pi \frac{km}{N}}, \tag{3.9}$$

$$= \frac{1}{\sqrt{N}} \sum_{i=0}^{P-1} h_i e^{-j2\pi \frac{kr_i}{N}}. \tag{3.10}$$

Finally, we conclude as expected. When the mobility inside the channel is neglected, i.e., when the time duration of a whole OFDM block is shorter than the coherence time, the DFT of the sampled output of the matched filter is given by the product of the transmitted symbols and the DFT of the channel impulse response. However, when the mobility is high, orthogonality between the different subcarriers is lost due to the periodic sinc, $\frac{\sin(x)}{\sin(\frac{x}{N})}$, function in (3.7).

The last block that remains to be defined in Figure 3.1 is the channel equalization step. To that aim, we still neglect the mobility inside the channel and thus assume an input/output relationship given by[1]

$$Y[k] = \lambda[k]c[k] + \nu[k], \tag{3.11}$$

where $\nu[k]$ is the DFT evaluated at frequency k of the AWGN noise. The maximum likelihood (ML) detection for (3.11) is equivalent to taking the symbol by symbol detection on the following equalized signal [13]

$$\widehat{c}[k] = \frac{Y[k]}{\lambda[k]}, \tag{3.12}$$

$$= c[k] + \frac{\nu[k]}{\lambda[k]}. \tag{3.13}$$

One clearly sees that every symbol $c[k]$ is transmitted through a flat fading channel with an associated channel gain given by $\lambda[k]$. For a BPSK constellation, if γ is defined as the inverse of the noise variance $\gamma = \frac{1}{\sigma_n^2}$ and the constellation variance is assumed to be normalized, the BER of a single subcarrier with a given $\lambda[k]$ is expressed as $BER_k^{OFDM} = Q\left(\sqrt{2\gamma|\lambda[k]|^2}\right)$. The mean BER of the whole system is consequently given in result 3.1.2.

[1]A slight abuse of notation is done here. Indeed, this relationship is only valid if the DFT of the impulse response of the channel is defined without the $\frac{1}{\sqrt{N}}$ factor, i.e., $\lambda[k] = \sum_{i=0}^{P-1} h_i e^{-j2\pi \frac{kr_i}{N}}$.

Result 3.1.2: BPSK BER of OFDM on a given static channel realization

For a given channel scenario without any mobility, the overall BER of a BPSK OFDM system is given by

$$BER^{OFDM}(\gamma) = \frac{1}{N}\sum_{k=0}^{N} Q\left(\sqrt{2\gamma|\lambda[k]|^2}\right), \tag{3.14}$$

with $Q(x)$ the Q function as defined in chapter *Symbols* and $\gamma = \frac{1}{\sigma_n^2}$.

Note that in this basic OFDM structure, the global BER of the system is given by the mean BER of every individual branch. Therefore, the branches with low gain are really detrimental to the global performance. This issue is partially fixed with the CP-SC transceiver scheme.

Discussion 3.1: Please note that in (3.7), the number of terms interfering together is P if $\nu_i = \frac{k''}{NT_s}$ with $k'' \in \mathbb{Z}$ and NP otherwise. This is an important result to be compared with delay-Doppler modulations (chapter 4).

3.2 Impact of parameters

The two parameters introduced up to now are the number of subcarriers N and the implicit sampling period of $s[m]$, T_s. Based on the DFT properties, the duration of the OFDM block without CP is $T_{OFDM} = NT_S$ and the spacing between two subcarriers along the frequency axis is given by $\Delta_f = \frac{1}{NT_s}$. The bandwidth occupied by the system is, by neglecting the leakage due to the chosen pulse shaping filter, given by $B = \frac{1}{T_s}$.

The performance of the presented frequency equalization depends on whether the Doppler effect can be neglected on the duration of an OFDM block T_{OFDM}. Mathematically, we require

$$2\pi\nu_i m T_s \approx 2\pi\nu_i m_{freeze} T_s \quad \forall m \in \{0, 1, ..., N-1\} \quad \text{and} \quad \forall i \in \{0, 1, ..., P-1\} \tag{3.15}$$

with the same meaning attributed to m_{freeze} as in (3.8). It is clear that choosing $m_{freeze} = \frac{N}{2}$ and decreasing T_{OFDM} leads to better performance. However, by decreasing T_{OFDM}, the overhead induced by the CP is increased. Consequently, in an OFDM system, limiting both the effect of mobility and the delay dispersive characteristic of the channel are two conflicting objectives.

3.3 Single carrier with frequency equalization

The single carrier with frequency domain equalization transceiver is a scheme that relies on the cyclic-prefix concept just as in OFDM but with only one carrier in the whole system. Therefore, the acronym for this single carrier modulation is CP-SC. The whole chain of a CP-SC system and the denomination of its associated signals are given in Figure 3.4. One clearly sees that compared to the OFDM system, the IDFT step is realized at the reception. The fundamental difference between OFDM and CP-SC is the effect of the channel on the transmitted symbols. Indeed, still assuming an LTI model, we have seen that in the case of OFDM, the effect of the channel is represented as a product between the DFT of the channel impulse response and the symbols. However, in CP-SC, the IDFT operation being put at the receiving side, the transmitted symbols are said to live in the delay domain where the effect of the channel is represented by a convolution. It can be shown [14] that the ML detection of the CP-SC scheme does not come down to a symbol by symbol detection. A loss of performance is then to be expected if the decision is still done symbol by symbol compared to the ideal ML detection. However, to keep the detection complexity relatively low, two linear equalizers followed by a symbol by symbol detection are frequently presented with the CP-SC. The first equalizer, which forces the interferences between symbols to zero, is the so called *zero-forcing* (ZF) equalizer. When mobility on the channel is neglected, the input/output relationship of this equalizer is given as

$$\widehat{Y^{ZF}}[k] = \frac{Y[k]}{\lambda[k]}, \tag{3.16}$$

$$= C[k] + \frac{\nu[k]}{\lambda[k]}, \tag{3.17}$$

with the difference compared to OFDM that $C[k]$ is the DFT of the transmitted constellation symbols $c[m]$ evaluated at frequency k and not directly the symbols. This kind of equalizer have the disadvantage of enhancing the noise at frequencies where the channel frequency gain $\lambda[k]$ is small with a limit case where it is zero. Therefore, other equalizers have been developed such as the *minimum mean square error* (MMSE) [15]. This equalizer is optimal with regard to the SINR of the received signal but do not entirely cancel interferences between symbols even in no mobility scenarios. The input/output relationship is given by (still neglecting the mobility)

$$\widehat{Y^{MMSE}}[k] = \frac{Y[k]\lambda[k]^*}{\sigma_\nu^2 + |\lambda[k]|^2}, \tag{3.18}$$

$$= \frac{C[k]|\lambda[k]|^2}{\sigma_\nu^2 + |\lambda[k]|^2} + \frac{\nu[k]\lambda[k]^*}{\sigma_\nu^2 + |\lambda[k]|^2} \tag{3.19}$$

The BER of both equalizers are given in result 3.3.1.

Result 3.3.1: BPSK BER of CP-SC on a given static channel realization for ZF and MMSE equalization

For a given channel scenario without any mobility, the overall BER of a CP-SC system can be derived for the ZF and MMSE equalizers and is given for a BPSK constellation by [14]

$$BER_{ZF}^{CP-SC}(\gamma) = Q\left(\sqrt{\frac{2}{\frac{1}{N}\sum_{k=0}^{N-1}\frac{1}{\gamma|\lambda[k]|^2}}}\right), \tag{3.20}$$

$$BER_{MMSE}^{CP-SC}(\gamma) = Q\left(\sqrt{2\left(\frac{1}{\frac{1}{N}\sum_{k=0}^{N-1}\frac{1}{\gamma|\lambda[k]|^2+1}} - 1\right)}\right). \tag{3.21}$$

It can be shown based on the properties of $Q(x)$ that [14]

$$BER_{MMSE}^{CP-SC}(\gamma) \leq BER^{OFDM}(\gamma) \quad \forall\gamma \in \mathbb{R}, \tag{3.22}$$

$$BER_{MMSE}^{CP-SC}(\gamma) \leq BER_{ZF}^{CP-SC}(\gamma) \quad \forall\gamma \in \mathbb{R}. \tag{3.23}$$

Discussion 3.2: One can see the convolution operation of the channel as adding a certain redundancy in the received signal. Indeed, after the convolution, different copies each with a certain gain and delay of the transmitted signal appears in the output signal. Therefore, a copy of every transmitted symbol will always appear with the highest gain of the channel in the output signal. On the other hand, in OFDM, a symbol transmitted on a frequency over which the channel frequency gain is low leads to a very poor detection at the receiving side which is detrimental for the overall performance of the system.

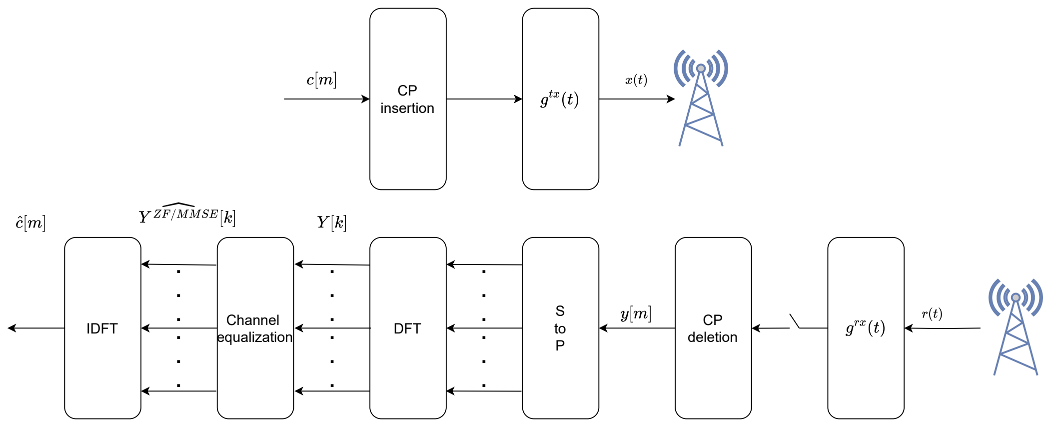

Figure 3.4: Transmission chain of a CP-SC system.

3.4 Simulation result

The comparison between the BER curves of the OFDM and CP-SC chains is presented for two static and one mobile channel scenarios. Then an investigation of the impact of the phase of the propagating path coefficients on the BER curves is proposed. At this point, this investigation might somehow feel like it comes out of the blue, however, it is critical for the following of the thesis. The two static channel realizations are presented in the frequency domain in Figure 3.5. The simulation parameters are given in the following table

Number of subcarriers	$N = 64$
Carrier frequency	$4GHz$
Modulation size	4-QAM
Subcarrier spacing Δ_f	$30kHz$
Number of OFDM blocks simulated	6 400
m_{freeze} (see (3.8))	$\frac{N}{2} = 32$

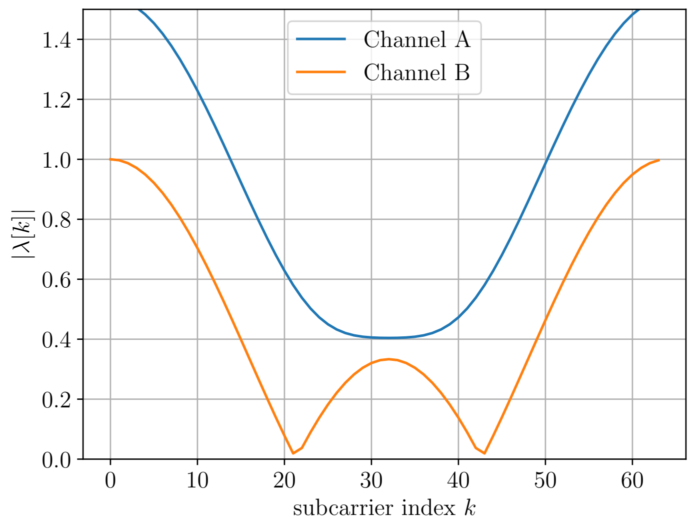

Figure 3.5: Frequency domain representation of the two static channel realizations considered in this section. The channel impulse responses are $h_A[m,n] = \frac{1}{\sqrt{1+0.7^2+0.2^2}}(1\delta[m] + 0.7\delta[m-1] + 0.2\delta[m-2])$ and $h_B[m,n] = \frac{1}{\sqrt{3}}(1\delta[m] + 1\delta[m-1] + 1\delta[m-2])$ for channel A and B respectively.

In Figure 3.6, the CP-SC with MMSE equalization leads to better BER performance for every SNR as predicted in (3.22). On the other hand, for the ZF equalizer, at low SNR the noise enhancement is such that the performance of the CP-SC is worse than the OFDM. When the SNR rises, this phenomenon tends to disappear since the noise in the system is more and more negligible. This noise enhancement is more pronounced in channel B since the frequency gains (i.e., $\lambda[k]$) of this channel are closer to zero (Figure 3.5). At high SNR, ZF and MMSE give the same performance.

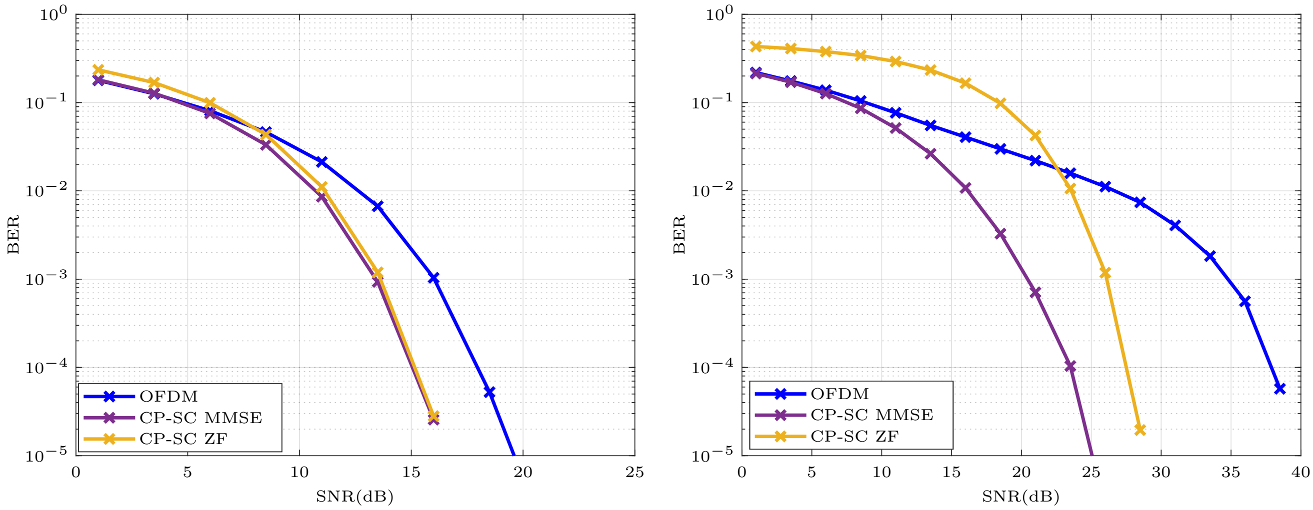

(a) Channel A

(b) Channel B

Figure 3.6: BER comparison between OFDM and CP-SC with ZF and MMSE equalizers in both channel scenarios presented Figure 3.5. There is mobility in neither of the channel scenarios. (The SNR axis is not the same in the two figures)

Impact of mobility

When mobility is added inside the channel, the performance of the three chains drops drastically as shown in Figure 3.7 which is to be compared with Figure 3.6a. This is due to the loss of orthogonality of the subcarriers leading to many interfering term as shown mathematically in (3.7). The channel used for Figure 3.7 is described with the following sets of parameters

$$r_i \in \{0, 1, 2\}, \tag{3.24}$$

$$h_i \in \frac{1}{\sqrt{1 + 0.7^2 + 0.2^2}}\{1, 0.7, 0.2\}, \tag{3.25}$$

$$\nu_i \in \{3.5, 0, 1\}kHz. \tag{3.26}$$

For a carrier frequency of $4Ghz$, the highest Doppler frequency of $3.5kHz$ corresponds to a user moving towards the transmitter at $945km/h$. The phase shift between the reference time m_{freeze} and the end of the OFDM block induced by this Doppler frequency is $2\pi\nu_i(N - m_{freeze})T_s = 0.18 \approx \frac{\pi}{17}$ which can be considered as relatively small. However, the impact on the performance is already critical.

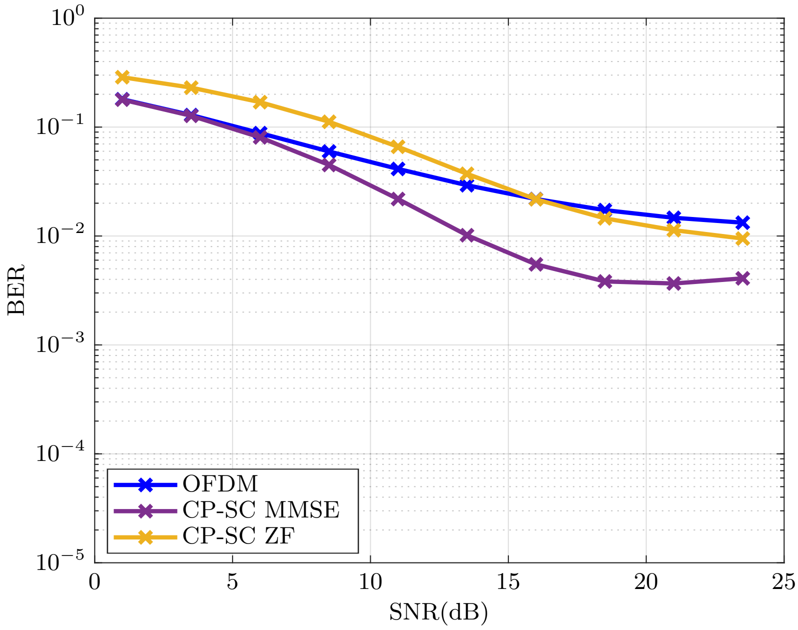

Figure 3.7: BER comparison between OFDM and CP-SC with ZF and MMSE equalizers in a channel with high mobility as described in (3.24). This figure is to be compared with Figure 3.6a. 64 consecutive OFDM blocks of 64 subcarriers are repeatedly simulated.

Impact of the phase of the path coefficients on the CP-SC BER
Channel A is considered here. The impulse response is modified as such

$$h_A[m,n] = \frac{1}{\sqrt{1+0.7^2+0.2^2}}\left(e^{j2\pi x}\delta[m] + 0.7\delta[m-1] + 0.2\delta[m-2]\right), \qquad (3.27)$$

with x that takes five different values, i.e., $x \in \{0.1, 0.2, 0.3, 0.4, 0.5\}$.

It is clear that adding a phase shift on the gain of the first path will impact the BER curves of OFDM due to the impact on the channel frequency response. However, the impact on the BER of CP-SC is less obvious. The sensibility of CP-SC to the channel tap phase shift is highlighted in Figure 3.8. This phase shift might be due to a Doppler frequency. Indeed, the frequency equalization is performed with an impulse response of the channel sampled at m_{freeze} as explained in (3.8). If two blocks of N samples are sent in a row, the gain of the i-th path used for equalization is given by

$$h'_{i,0} = h_i e^{j2\pi\nu_i m_{freeze} T_s}$$
$$h'_{i,1} = h_i e^{j2\pi\nu_i (m_{freeze}+N) T_s}$$

where $h'_{i,j}$ is the gain used for equalization of the i-th path at block j. It is fundamental for the understanding of OTFS to see through Figure 3.8 that, even if the amplitude of the channel taps $|h[m,n]|$ are not fading over time and if we neglect the interfering term caused by the equalization step, the performance of the CP-SC still fluctuates between each consecutive block in presence of Doppler effect due to the different phase shift.

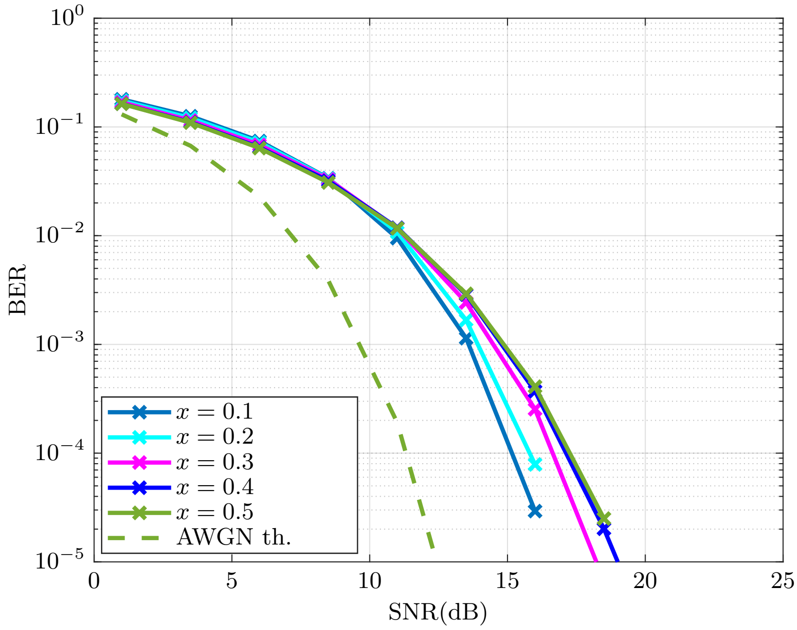

Figure 3.8: BER of the CP-SC system with different phase shift on the first channel tap as described in (3.27)

Finally, only the BER of OFDM and CP-SC has been discussed. However, other performance metrics have favored OFDM over CP-SC in current telecommunication systems. Among other things, the capacity of OFDM is greater than CP-SC [16]. On top of that, the structure of OFDM enables simple resource allocation between users and resource management such as the waterfilling algorithm [17].

Key take-away messages of chapter 3:

- An OFDM system is a block-by-block modulation that modulates the constellation symbols in the frequency domain where the effect of the channel is represented by a product. This modulation is described with the following parameters :
  - Number of subcarriers N
  - Sampling period T_S
  - Bandwidth of the system $B \approx \frac{1}{T_s}$
  - Time duration of an OFDM block (without the CP) $T_{OFDM} = NT_s$

- Thanks to the CP addition the OFDM equalization is easily implemented in frequency domain with the DFT operator.

- The frequency domain equalization perfectly prevents ISI when there is no Doppler effect in the channel.

- Frequency fading is detrimental for the overall BER of the OFDM system. A transceiver scheme analogous to the OFDM one is the CP-SC. The CP-SC system modulates the constellation symbols in delay domain where the effect of the channel across the delay dimension is represented as a convolution. This convolution adds a certain kind of redundancy in the received signal, therefore improving the BER curves of CP-SC compared to OFDM.

- The same frequency equalizer as in OFDM can be used for CP-SC. However, using a variation of this equalizer called MMSE leads to better performance. The computation complexity of both equalizers are the same.

- When the mobility of the channel increases, the performance of both OFDM and CP-SC drops drastically.

- To characterize the importance of the Doppler frequencies of the channel, the key quantity is the maximum phase rotation between the chosen equalization time reference m_{freeze} and the beginning/end of the OFDM block.

- To reduce this phase rotation, the time duration of a block T_{OFDM} can be reduced. However, doing so degrades the performance in terms of datarate because the overhead of the CP is enlarged.

Chapter 4

delay-Doppler modulations

When the mobility inside the channel increases, the performance of the OFDM system in terms of BER drops drastically. Indeed, the equalizer was designed with the assumption of an LTI channel representation. On top of that, each symbol inside an OFDM system experiences a different channel gain due to frequency and time fading. This fading is detrimental for the robustness and performance of the system. On the other hand, the CP-SC modulation is not subject to this issue of frequency fading and we have seen the improvement of BER compared to OFDM in the previous chapter. However, the CP-SC modulation does not deal with time fading and still neglects the mobility in its equalization. Therefore, CP-SC exhibit bad performance in high mobility scenarios. For future generation networks, the mobility inside the channel is expected to rise drastically, this has motivated researchers to think about other kinds of modulations more robust to those highly time-varying channels. In that context, the OTFS modulation was first presented in 2017 by Hadani et *al.* [2]. Since then, OTFS has gained more and more popularity and is the main modulation candidate for 6G. OTFS belongs to the multicarrier class of modulation as OFDM. However, the information that one wishes to transmit is placed in what is called a *delay-Doppler* grid where the constellation symbols are said to live in frequency-Time for OFDM. This delay-Doppler grid directly refers to the delay-Doppler representation of the channel introduced in chapter 2. Compared to the frequency-Time representation of the channel used in OFDM, the delay-Doppler (dD) representation is much more sparse and the notion of fading is lost.

This section derives the OTFS equations from first principles. To do so, the delay-Doppler representation of a signal is introduced in section 4.1. It is shown that this representation leads to a natural set of orthonormal basis functions. Those basis functions are neither time nor bandwidth limited which is problematic for practical telecommunication systems. Therefore, the impact of limiting those functions both in time and frequency is analyzed in section 4.2. Then, the final OTFS equations are given in section 4.3. Some useful properties about a new transformation called *discrete Zak transform* are given in subsection 4.3.1. Those properties are used to derive the input/output relationship for two variants of OTFS which are (RCP-)OTFS (subsection 4.3.2) and (CP-)OTFS (subsection 4.3.3). Two known equalization techniques for OTFS are presented in section 4.4. Finally, a new receiver scheme is also presented in section 4.4.

In OTFS, as in the OFDM modulation, the time signals are divided into blocks. Therefore, two timescales are used to describe the signals. The delay axis is a measure of time inside a block while the term "time" is used to iterate across the blocks. It is clear that the terminology can somehow be misleading as the delay axis is also a physical manifestation of time, however, the choice is made to keep this terminology as such since it is the choice made in all the literature around dD modulations.

4.1 delay-Doppler representation of a time signal

The delay-Doppler representation of a time signal is a representation that tries to mimic the two-dimensional dD representation of the channel. Since a time signal is clearly a one dimensional quantity, in order to construct the dD representation, the signal is arbitrarily divided into blocks. The delay axis refers to the time inside a block while the Doppler axis will shape the structure of the signal observed across the blocks. Let us for now put aside the Doppler axis. To completely describe a continuous time signal divided into blocks, on top of referring to the time inside the block, one also needs an indexing of the blocks. The situation is presented in Figure 4.1. The indexing of the blocks is done via the variable n (unfortunately called "time") while the time inside a block is denoted τ and called delay. The maximum value of the delay is the size of the block τ_{max} which is a parameter of the representation. Note also that in order to completely describe a continuous signal, τ has to be a continuous bounded variable while n is a discrete but unbounded variable. The equivalence between the classical continuous time representation of a signal and its delay-Time representation is expressed as follows

$$\exists! \tau \in [0, \tau_{max}[\text{ and } n \in \mathbb{Z} \text{ such that } x(\tau + n\tau_{max}) = x(t) \quad \forall t \in \mathbb{R}. \tag{4.1}$$

The notation $x_{dT}(\tau, n) = x(\tau + n\tau_{max})$ is introduced to highlight the delay-Time two-dimensional representation of the signal. The delay-Doppler representation of a signal is defined as the one-dimensional discrete time Fourier transform of the variable n in the delay-Time representation of (4.1). The link between the two representation is then given by [18]

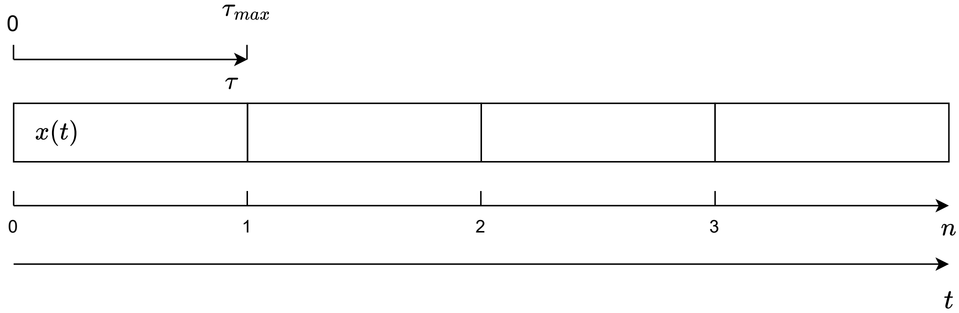

Figure 4.1: Representation of a continuous time signal into blocks of length τ_{max}

$$x_{dD}(\tau,\nu) \triangleq \mathcal{F}_n\{x_{dT}(\tau,n)\}(\nu), \tag{4.2}$$

$$= \sqrt{\tau_{max}} \sum_{n=-\infty}^{\infty} x_{dT}(\tau,n) e^{-j2\pi\nu n\tau_{max}}. \tag{4.3}$$

Due to the uniqueness of the Fourier transform, the dD representation of a signal is also unique. In order to directly jump from the continuous time signal representation $x(t)$ to its dD representation, the Zak transform has been introduced in the literature. Naturally, as the dT and dD representations of a signal always depend on the chosen τ_{max}, the Zak transform of a signal is also always defined with respect to this parameter. However, in the following of this thesis, the parameter is implicitly defined and dropped in the notation.

Définition 4.1: Zak transform

The Zak transform of a signal $x(t)$ is given by

$$\begin{aligned} x_{dD}(\tau,\nu) &= \mathcal{Z}_t\left\{x(t)\right\}(\tau,\nu), \\ &\triangleq \sqrt{\tau_{max}} \sum_{n=-\infty}^{\infty} x(\tau + n\tau_{max}) e^{-j2\pi\nu n\tau_{max}}. \end{aligned} \tag{4.4}$$

Based on this definition, two important characteristic of the delay-Doppler representation are induced. First due to the discrete time Fourier transform, the delay-Doppler representation of a signal is periodic of period $\nu_{max} = \frac{1}{\tau_{max}}$ along the Doppler axis. Then, if the bound on τ is relaxed such that the delay-Doppler representation is defined with $\tau \in]-\infty;\infty]$ we have the following property which is referred to as the quasi-periodicity property [19].

Property 4.1.1: Quasi-periodicity of the delay-Doppler representation

$$
\begin{aligned}
x_{dD}(\tau + m\tau_{max}, \nu) &= \sqrt{\tau_{max}} \sum_{n=-\infty}^{\infty} x(\tau + (n+m)\tau_{max}) e^{-j2\pi\nu n\tau_{max}}, \\
&= \sqrt{\tau_{max}} \sum_{n=-\infty}^{\infty} x(\tau + (n+m)\tau_{max}) e^{-j2\pi\nu(n+m)\tau_{max}} e^{j2\pi\nu m\tau_{max}}, \\
&= e^{j2\pi\nu m\tau_{max}} x_{dD}(\tau, \nu), \qquad \forall m \in \mathbb{Z}.
\end{aligned} \tag{4.5}
$$

We emphasize the fact that the dD representation of any continuous time signal have to respect those two periodicity properties.

At this point, the benefit of using the dD representation of a signal is not that obvious. To highlight the advantage of such a representation and give a glimpse of what is coming, let us look at the effect of a channel made of one path with a given delay τ_0 and Doppler frequency ν_0. If the signal $x(t)$ is sent at the transmission side, the noise-free received signal $r(t)$ then writes as

$$
r(t) = x(t - \tau_0) e^{j2\pi\nu_0 t}. \tag{4.6}
$$

And its dD representation is expressed as

$$
\begin{aligned}
r_{dD}(\tau, \nu) &= \sqrt{\tau_{max}} \sum_{n=-\infty}^{\infty} r(\tau + n\tau_{max}) e^{-j2\pi\nu n\tau_{max}}, \\
&= \sqrt{\tau_{max}} \sum_{n=-\infty}^{\infty} x(\tau + n\tau_{max} - \tau_0) e^{j2\pi\nu_0(\tau + n\tau_{max})} e^{-j2\pi\nu n\tau_{max}}, \\
&= \sqrt{\tau_{max}} \sum_{n=-\infty}^{\infty} x(\tau + n\tau_{max} - \tau_0) e^{-j2\pi(\nu-\nu_0)n\tau_{max}} e^{j2\pi\nu_0\tau}, \\
&= x_{dD}(\tau - \tau_0, \nu - \nu_0) e^{j2\pi\nu_0\tau}.
\end{aligned} \tag{4.7}
$$

Up to a factor $e^{j2\pi\nu_0\tau}$, the dD representation of $r(t)$ is simply a shifted version of $x_{dD}(\tau, \nu)$ in both directions. This property suggests a simple input/output relationship for the doubly dispersive channel presented in chapter 2. Most importantly, the interaction between a dD representation of a signal and a doubly dispersive channel (still putting aside the factor $e^{j2\pi\nu_0\tau}$) is non-fading which is one of the great advantage of dD modulations.

Discussion 4.1: A useful way of representing the Zak transform is to picture it as a discrete time Fourier transform for which the origin of time is shifted with the variable τ. From this perspective, the quasi-periodicity property (4.5) is nothing else than an application of the well known shift property of a Fourier transform

$$\mathcal{F}_t\{x(t-t_0)\}(\nu) = e^{-j\nu t_0}\mathcal{F}_t\{x(t)\}(\nu).$$

Due to the discrete time characteristic of the Fourier transform that appears in the Zak transform t_0 is constrained to an integer multiple of τ_{max} in the delay-Doppler context, i.e., $t_0 = m\tau_{max}, \quad m \in \mathbb{Z}$.
The factor $e^{j2\pi\nu_0\tau}$ in (4.7) is also understood with this picture. Indeed, the Doppler effect in the channel is modeled as having a time origin at $t = 0$. Therefore, when setting the time origin at $\tau \neq 0$ a phase correction is required to indicate that the Doppler has already turned a bit. In fact, this is the translation of the already mentioned shift property applied to an exponential signal

$$\mathcal{F}_t\{e^{j2\pi\nu_0(t+\tau)}\}(\nu) = e^{j2\pi\nu\tau}\delta(\nu-\nu_0) = e^{j2\pi\nu_0\tau}.$$

The dD representation of a signal has been defined from its continuous time representation. Of course one could go the other way around and define a transformation to go from the dD representation to the continuous time representation of a signal. The name given to this transformation is, without surprise, the inverse Zak transform.

Définition 4.2: Inverse Zak transform

The inverse Zak transform of the signal $x_{dD}(\tau,\nu)$ denoted $\mathcal{Z}^{-1}\left\{x_{dD}(\tau,\nu)\right\}$ is defined as [20]

$$x(t) = \mathcal{Z}^{-1}\left\{x_{dD}(\tau,\nu)\right\}, \tag{4.8}$$

$$\triangleq \sqrt{\tau_{max}}\int_0^{\nu_{max}} x_{dD}(t,\nu)d\nu. \tag{4.9}$$

In the last expression, one recognizes an inverse Fourier transform from ν to the output variable evaluated in $t = 0$. Indeed, it is consistent with the picture where the Zak transform is considered as a Fourier transform with a time origin located in τ. The demonstration of (4.9) is straightforward provided that since $\nu_{max} = \frac{1}{\tau_{max}}$ we have

$$\int_0^{\nu_{max}} e^{-j2\pi\nu n\tau_{max}}d\nu = \begin{cases}\frac{1}{\tau_{max}} & , n = 0\\ 0 & , n \neq 0\end{cases} \tag{4.10}$$

Therefore,

$$\sqrt{\tau_{max}} \int_0^{\nu_{max}} x_{dD}(t,\nu)d\nu = \tau_{max} \sum_{n=-\infty}^{\infty} x(\tau + n\tau_{max}) \int_0^{\nu_{max}} e^{-j2\pi\nu n\tau_{max}} d\nu,$$
$$= x(t).$$

An example of a signal localized in the dD domain and its associated continuous time signal is presented in Figure 4.2. The dD representation of such a signal is given by [19]

$$p_{dD,\tau_0,\nu_0}(\tau,\nu) = \sum_{n=-\infty}^{\infty} \sum_{m=-\infty}^{\infty} e^{j2\pi\nu_0 m\tau_{max}} \delta(\tau - \tau_0 - m\tau_{max})\delta(\nu - \nu_0 - n\nu_{max}), \tag{4.11}$$

where the notation $p_{dD,\tau_0,\nu_0}(\tau,\nu)$ is used to denote a signal localized at τ_0 and ν_0 in the dD domain. Indeed, this notation is very useful as those signals will play an essential role in the following. The double summation in (4.11) appears due to the periodicity constraints imposed on the dD representation of a continuous time signal. The time expression of this dD localized signal is given by

$$p_{\tau_0,\nu_0}(t) = \sqrt{\tau_{max}} \sum_{m=-\infty}^{\infty} e^{j2\pi\nu_0 m\tau_{max}} \delta(t - \tau_0 - m\tau_{max}). \tag{4.12}$$

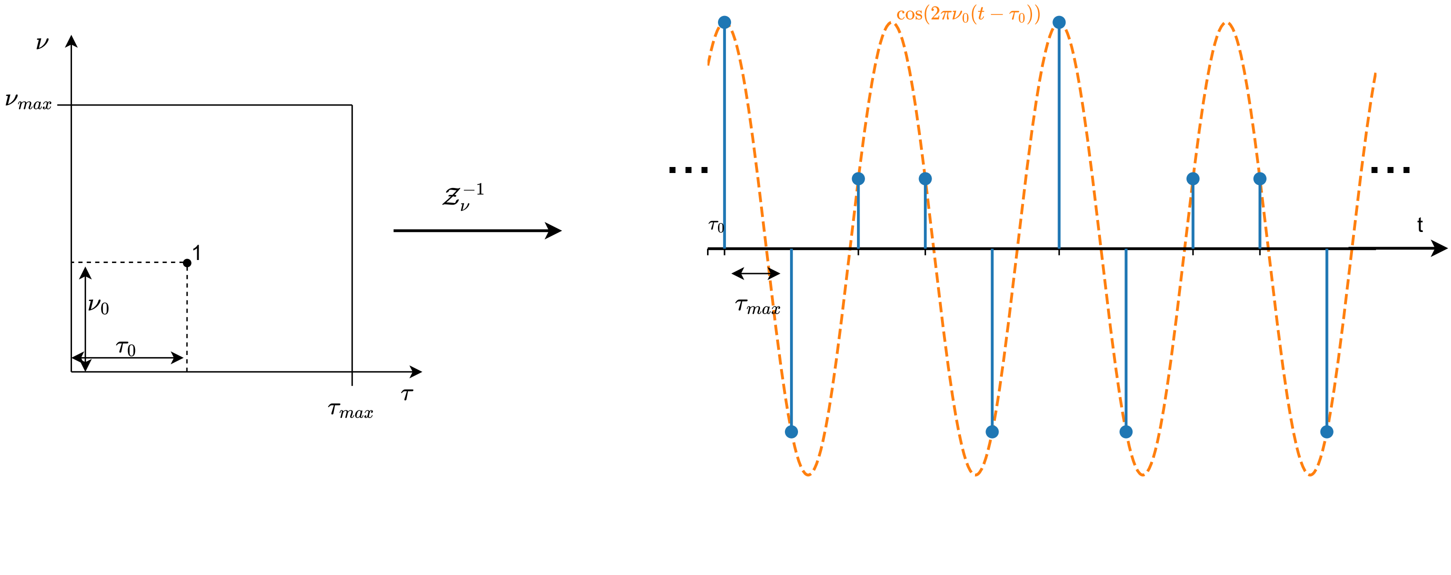

Figure 4.2: Real part of the time representation of a dD basis function, $p_{\tau_0,\nu_0}(t)$. In the dD grid, only the fundamental period (i.e., $\tau \in [0, \tau_{max}[$ and $\nu \in [0, \nu_{max}[$) is shown.

It can be shown that the set of functions $p_{\tau_0,\nu_0}(t), 0 \leq \tau_0 < \tau_{max}, 0 \leq \nu_0 < \nu_{max}$ form an orthonormal basis of the continuous time signal space [19]. Every time continuous signal can then be represented as a linear combination of the basis functions $p_{\tau_0,\nu_0}(t)$. If those functions are to be used as the basis of a multicarrier modulation, their Fourier transforms are of primary importance as the bandwidth is a critical resource in any telecommunication system.

Property 4.1.2: Fourier transform from delay-Doppler representation

The Fourier transform of $x(t)$ can be found via its dD representation as such [19]

$$\mathcal{F}_t(x(t))(f) = \frac{1}{\sqrt{\tau_{max}}} \int_0^{\tau_{max}} x_{dD}(\tau, f) e^{-j2\pi f \tau} d\tau. \tag{4.13}$$

The demonstration is provided in Appendix D.

Applied to $p_{\tau_0,\nu_0}(t)$ this gives

$$\begin{aligned}\mathcal{F}_t(p_{\tau_0,\nu_0}(t))(f) &= \frac{1}{\sqrt{\tau_{max}}} \int_0^{\tau_{max}} \sum_{n=-\infty}^{\infty} \sum_{m=-\infty}^{\infty} e^{j2\pi\nu_0 m\tau_{max}} \delta(\tau - \tau_0 - m\tau_{max}) \delta(f - \nu_0 - n\nu_{max}) e^{-j2\pi f \tau} d\tau, \\ &= \frac{1}{\sqrt{\tau_{max}}} \sum_{n=-\infty}^{\infty} \delta(f - \nu_0 - n\nu_{max}) e^{-j2\pi f \tau_0}. \end{aligned} \tag{4.14}$$

From this last expression, the signal $p_{\tau_0,\nu_0}(t)$ has an infinite bandwidth. At this point, two issues remain to be addressed if one wishes to use the set of basis functions $p_{\tau_0,\nu_0}(t)$ in a multicarrier waveform modulation. Indeed, the basis functions are neither limited in time nor band-limited which is practically not feasible.

4.2 Time and bandwidth limited orthonormal basis for continuous time signals

In order to approximatively limit in time and in frequency the signals $p_{\tau_0,\nu_0}(t)$, one can consider a modified version of the set given by

$$\phi_{\tau_0,\nu_0}(t) \triangleq (p_{\tau_0,\nu_0}(t) q(t)) * g^{tx}(t), \tag{4.15}$$

where $q(t)$ and $g^{tx}(t)$ are approximatively time and bandwidth limited signals respectively[1], i.e., $q(t) \approx 0$ when $t \notin [0, M\tau_{max}[$ and $\mathcal{F}_t(g^{tx}(t))(f) \approx 0$ when

[1] At this point the notation $g^{tx}(t)$ for the bandwidth limited signal seems surprising as the link with a certain pulse shaping filter is not straightforward. It will become clear later why this notation is used

$f \notin [0, N\nu_{max}[$ with a chosen M and N. It remains now to investigate the loss of localization in the dD domain due to this time and bandwidth limitation. Considering a perfect window for $q(t)$

$$q(t) = \begin{cases} 1 & , 0 \leq t < M\tau_{max} \\ 0 & , \text{otherwise} \end{cases} \tag{4.16}$$

the expression of $\phi_{\tau_0,\nu_0}(t)$ simplifies to

$$\phi_{\tau_0,\nu_0}(t) = \sqrt{\tau_{max}} \sum_{n=0}^{M-1} e^{j2\pi\nu_0 n\tau_{max}} g^{tx}(t - \tau_0 - n\tau_{max}). \tag{4.17}$$

And the application of the Zak transform on (4.17) gives for an ideal frequency window $g^{tx}(t)$ [19]

$$|\phi_{dD,\tau_0,\nu_0}(\tau,\nu)| = \frac{\sin\left(\pi(\nu-\nu_0)M\tau_{max}\right)}{\sin\left(\pi(\nu-\nu_0)\tau_{max}\right)} \frac{\sin\left(\pi(\tau-\tau_0)N\nu_{max}\right)}{\sin\left(\pi(\tau-\tau_0)\nu_{max}\right)}. \tag{4.18}$$

The shape of (4.18) is plotted in Figure 4.3. We see that due to the time and bandwidth truncation we loose some degree of localization in the dD domain. This result should not surprise the reader familiar with time limited signals and their associated Fourier transforms.

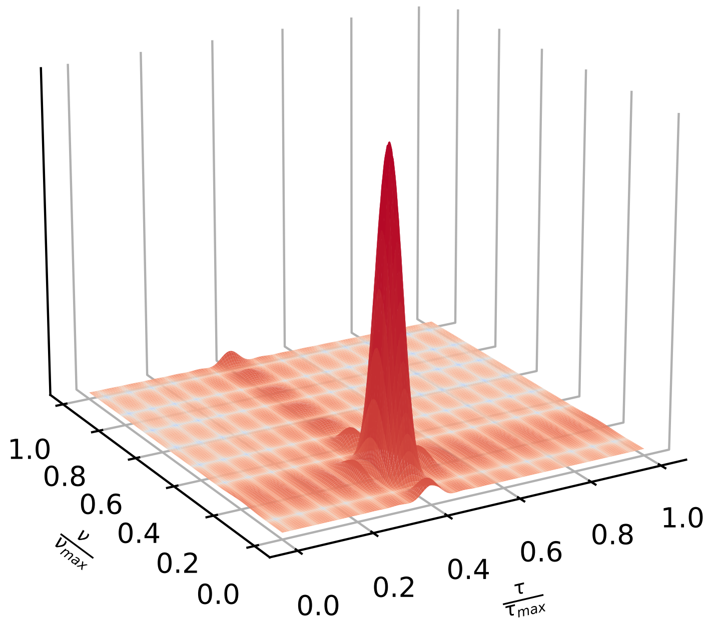

Figure 4.3: Plot of $|\phi_{dD,\tau_0,\nu_0}(\tau,\nu)|^2$. The parameters used for the plot are $M = 8$,$N = 16$, $\frac{\tau_0}{\tau_{max}} = 0.4$ and $\frac{\nu_0}{\nu_{max}} = 0.2$. The width of the main lobe is $\frac{2}{M}$ along the normalized Doppler axis and $\frac{2}{N}$ along the normalized delay axis.

Based on the width of the lobes in (4.18), the set of functions $\phi_{dD,\tau_0,\nu_0}(\tau,\nu)$ can be used to modulated symbols in the delay-Doppler domain without interferences if the basis functions are separated by $\frac{1}{M}$ and $\frac{1}{N}$ along the normalized Doppler and delay axis respectively. Therefore, the set of functions given in result 4.2.1 can be chosen as the orthonormal basis of a multicarrier system.

Result 4.2.1: Set of orthonormal dD basis functions limited in time and frequency

The set of functions given by

$$\alpha_{l,k}(t) = \frac{1}{\sqrt{MN}}\phi_{\tau_0=\frac{l\tau_{max}}{N},\nu_0=\frac{k\nu_{max}}{M}}(t), \tag{4.19}$$

$$= \sqrt{\frac{\tau_{max}}{NM}}\sum_{n=0}^{M-1} e^{j2\pi\frac{kn}{M}} g^{tx}(t - \frac{l\tau_{max}}{N} - n\tau_{max}) \tag{4.20}$$

$$\text{with } l \in \{0, ..., N-1\} \text{ and } k \in \{0, ..., M-1\},$$

can be used to modulate information in the dD domain without interferences. Those functions are limited both in time and frequency. The factor $\frac{1}{\sqrt{MN}}$ ensures a unit energy for the basis functions. An example for a given τ_0 and ν_0 of such a basis function is given in Figure 4.4.

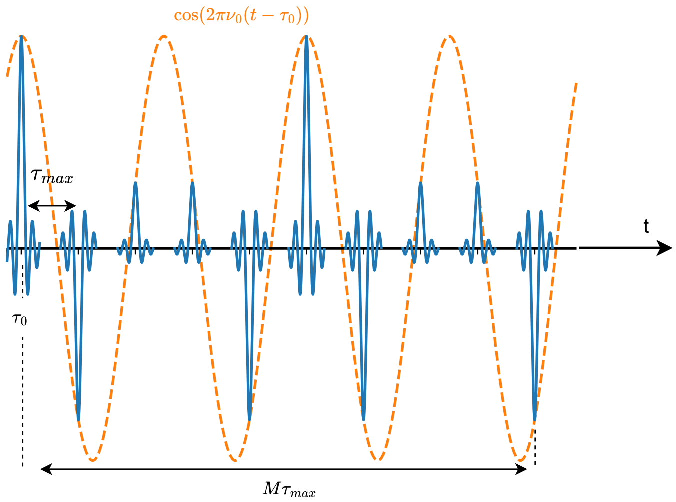

Figure 4.4: Illustration of $\alpha_{l,k}(t)$ for a given l and k. $g^{tx}(t)$ is chosen as $sinc(N\nu_{max}t)$, i.e., a perfect frequency window. Those $g^{tx}(t)$ are truncated in the plot so that it remains understandable. However, theoretically, $g^{tx}(t)$ spans across an infinite time, the reader thus understands the necessity of adding the adjective *approximatively* when talking about time and bandwidth limited signals. The width of the main lobe of those $g^{tx}(t)$ is $\frac{2\tau_{max}}{N}$.

4.3 OTFS modulation

As it has been shown, the set of functions $\alpha_{l,k}(t)$ can be used as the basis of a multicarrier system without creating interferences between the modulated symbols. It is precisely the working principle of OTFS. If the constellation symbols are arranged in a two-dimensional grid and denoted $c[l,k]$, the signal transmitted by such a system is given by

$$
\begin{aligned}
x(t) &= \sum_{k=0}^{M-1}\sum_{l=0}^{N-1} c[l,k]\alpha_{l,k}(t), & (4.21)\\
&= \sum_{k=0}^{M-1}\sum_{l=0}^{N-1} c[l,k]\sqrt{\frac{\tau_{max}}{NM}}\sum_{n=0}^{M-1} e^{j2\pi\frac{kn}{M}} g^{tx}(t-\frac{l\tau_{max}}{N}-n\tau_{max}), & (4.22)\\
&= \sqrt{\frac{\tau_{max}}{NM}}\sum_{n=0}^{M-1}\sum_{l=0}^{N-1} g^{tx}(t-\frac{l\tau_{max}}{N}-n\tau_{max})\sum_{k=0}^{M-1} c[l,k]e^{j2\pi\frac{kn}{M}}. & (4.23)
\end{aligned}
$$

The last expression highlights a very important property of the OTFS modulation. Indeed the last summation $\frac{1}{\sqrt{M}}\sum_{k=0}^{M-1} c[l,k]e^{j2\pi\frac{kn}{M}}$ is exactly the expression of the IDFT of $c[l,k]$ along index k. Consequently, the OTFS modulation is easily implemented with the framework presented in chapter 2 where the constellation symbols are transformed and then brought to continuous time thanks to the pulse shaping filter $g^{tx}(t)$. Therefore, the considered chain of an OTFS system is presented in Figure 4.5. In this figure, a new pair of transformations called Discrete Zak transform and Inverse discrete Zak transform are introduced. Those are discretized versions of the Zak and inverse Zak transform. Two of their most important properties in the context of OTFS are derived in the following section.

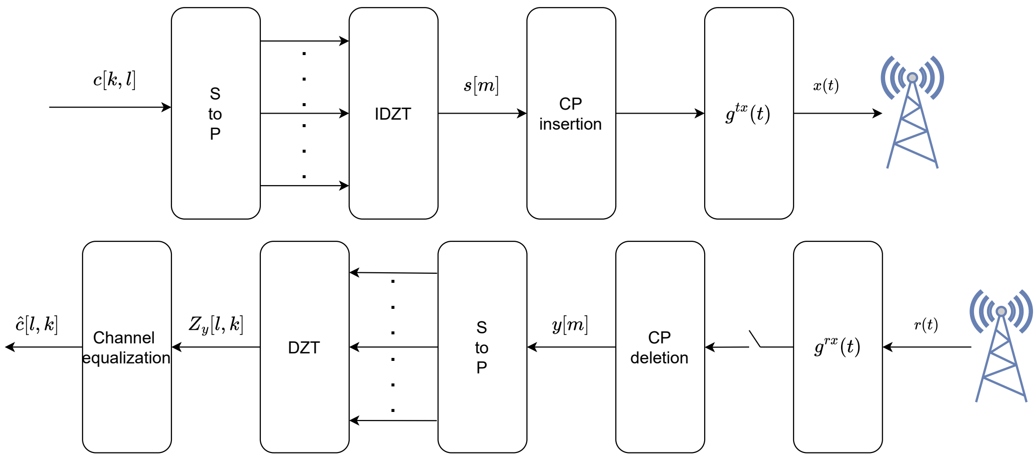

Figure 4.5: Transmission chain of a generic OTFS system.

4.3.1 Useful properties of the discrete Zak transform

The discrete Zak transform (DZT) is defined as the discretization along the Doppler and delay axis of the Zak transform previously defined. The delay axis is discretized into the samples $\frac{l\tau_{max}}{N}$ and the Doppler axis into $\frac{k\nu_{max}}{M}$. This discretization directly echoes the discussion about the time and bandwidth limited basis functions $\alpha_{l,k}(t)$.

Définition 4.3: Discrete Zak transform

The definition of the DZT is given by

$$Z_x[l,k] = DZT\left\{x(t)\right\}[l,k] \triangleq \frac{1}{\sqrt{M}} \sum_{n=0}^{M-1} x[l+nN] e^{-j2\pi\frac{kn}{M}}. \tag{4.24}$$

As the continuous Zak transform, the DZT depends on the chosen τ_{max} but also on the value attributed to N and M. The notation $Z_x[l,k]$ is now used to denote the DZT of the signal $x(t)$.

Définition 4.4: Inverse discrete Zak transform

Its counterpart, the inverse discrete Zak transform, is defined as

$$x[l+nN] = IDZT\left\{Z_x[l,k]\right\}[l+nN] \triangleq \frac{1}{\sqrt{M}} \sum_{k=0}^{M-1} Z_x[l,k] e^{j2\pi\frac{kn}{M}}. \tag{4.25}$$

Note that the DZT is quasi periodic along the delay and periodic along the Doppler just as the continuous Zak transform. Therefore, an equivalent form of the IDZT is also given by

$$x[m] = \frac{1}{\sqrt{M}} \sum_{k=0}^{M-1} Z_x[m,k]. \tag{4.26}$$

The first important property of the DZT is the *modulation* property.

Property 4.3.1: Modulation

Let $z[n] = x[n]y[n]$, then,

$$
\begin{aligned}
Z_z[l,k] &= \frac{1}{\sqrt{M}} \sum_{n=0}^{M-1} x[l+nN]y[l+nN]e^{-j2\pi\frac{kn}{M}}, && (4.27)\\
&= \frac{1}{M} \sum_{n=0}^{M-1} \sum_{k'=0}^{M-1} Z_x[l,k']e^{j2\pi\frac{k'n}{M}} y[l+nN]e^{-j2\pi\frac{kn}{M}}, && (4.28)\\
&= \frac{1}{M} \sum_{k'=0}^{M-1} Z_x[l,k'] \sum_{n=0}^{M-1} y[l+nN]e^{-j2\pi\frac{n}{M}(k-k')}, && (4.29)\\
&= \frac{1}{\sqrt{M}} \sum_{k'=0}^{M-1} Z_x[l,k']Z_y[l,k-k']. && (4.30)
\end{aligned}
$$

The DZT transforms a modulation in the time domain into a convolution along the Doppler axis of the DZTs.

Another important property is the *circular convolution* property.

Property 4.3.2: Circular convolution

Let this time $z[n]$ be the circular convolution between $x[n]$ and $y[n]$, i.e., $z[n] = (x \circledast y)[n]$, their DZT is expressed as

$$
Z_z[l,k] = \sqrt{M} \sum_{l'=0}^{N-1} Z_x[l',k]Z_y[l-l',k]. \tag{4.31}
$$

A circular convolution in time domain is equivalently represented by a convolution along the delay axis of the DZTs. The demonstration of this property is presented in Appendix A.

Two important DZTs are now derived.

Result 4.3.1: DZT of a Dirac delta

The fundamental period of the DZT of a Dirac delta $x[m] = \delta[m - r_i]$ with $0 \leq r_i \leq N - 1$ is given by

$$Z_x[l,k] = \frac{1}{\sqrt{M}} \sum_{n=0}^{M-1} x[l + nN] e^{-j2\pi \frac{kn}{M}}, \tag{4.32}$$

$$= \frac{1}{\sqrt{M}} \sum_{n=0}^{M-1} \delta[l - r_i] \delta\,[n]\, e^{-j2\pi \frac{kn}{M}}, \tag{4.33}$$

$$= \frac{1}{\sqrt{M}} \delta[l - r_i]. \tag{4.34}$$

Result 4.3.2: DZT of a complex exponential

The DZT of $x[m] = e^{j2\pi \frac{k_i}{NM} m}$ is given by

$$Z_x[l,k] = \frac{1}{\sqrt{M}} \sum_{n=0}^{M-1} e^{j2\pi \frac{k_i}{NM}(l+nN)} e^{-j2\pi \frac{kn}{M}}, \tag{4.35}$$

$$= \frac{1}{\sqrt{M}} e^{j2\pi \frac{k_i}{NM} l} \sum_{n=0}^{M-1} e^{-j2\pi \frac{n}{M}(k-k_i)}, \tag{4.36}$$

$$= \frac{1}{\sqrt{M}} e^{j2\pi \frac{k_i}{NM} l} e^{-j\pi \frac{M-1}{M}(k-k_i)} \frac{\sin(\pi(k - k_i))}{\sin\left(\frac{\pi}{M}(k - k_i)\right)}. \tag{4.37}$$

If k_i is an integer, the previous expression degenerates into [1]

$$Z_x[l,k] = e^{j2\pi \frac{k_i}{NM} l} \sqrt{M} \delta[k - k_i]. \tag{4.38}$$

4.3.2 Input/output relationship of the (RCP-)OTFS modulation

Thanks to the two properties of the DZT derived above, the impact of the channel on the OTFS modulation is easily derived.The transmitted signal was written in (4.23), it can be rewritten with the newly introduced IDZT as given in the following result[2].

[1]It is in fact a discretization of the second property presented in Discussion 4.1.

[2]The additional factor $\sqrt{\frac{\tau_{max}}{N}}$ in (4.23) is absorbed in $g^{tx}(t)$.

Result 4.3.3: Transmitted signal of an OTFS system

The transmitted signal of an OTFS system is given by

$$x(t) = \sum_{m=0}^{MN-1} g^{tx}(t - mT_s)s[m], \tag{4.39}$$

where $s[m] = IDZT\left\{c[l,k]\right\}[m]$ and $T_s = \frac{\tau_{max}}{N}$.

In this subsection, we consider that a CP is prepended at the beginning of the whole OTFS frame, i.e., there is a CP every MN samples. Therefore, the system is named (RCP-)OTFS for *reduced cyclic prefix OTFS*. Using the discrete channel (2.28) developed in chapter 2 the received samples after the matched filter write

$$\begin{aligned} y[m] &= \sum_{i=0}^{P-1} h_i e^{j2\pi\nu_i mT_s} s\Big[[m - r_i]_{MN}\Big] + w[m], &(4.40)\\ &= \sum_{i=0}^{P-1} h_i e^{j2\pi\nu_i mT_s} (s \circledast \delta_{r_i})[m] + w[m], &(4.41) \end{aligned}$$

where the modulo MN appears due to the CP, δ_{r_i} denotes the sequence defined as $\delta[m - r_i]$ and $w[m]$ is the AWGN term.

The *circular convolution* and *modulation* properties as well as the expression of the DZT of a Dirac delta (see subsection 4.3.1) are used sequentially to express the DZT of the received sequence as (ommiting the noise term)

$$Z_y[l,k] = \sum_{i=0}^{P-1} h_i \frac{1}{\sqrt{M}} \sum_{k'=0}^{M-1} Z_s[l - r_i, k'] Z_{\nu_i}[l, k - k'], \tag{4.42}$$

where the notation $Z_{\nu_i}[l,k]$ is introduced to describe the DZT of the sequence given by $z[m] = e^{j2\pi\nu_i mT_s}$. The Doppler frequency is now reexpressed as $\nu_i = \frac{k_i}{MNT_s}, \quad k_i \in \mathbb{R}$ which is not an approximation since k_i is defined as a real number. We can finally use (4.37) to develop $Z_{\nu_i}[l, k - k']$

$$Z_y[l,k] = \frac{1}{M} \sum_{i=0}^{P-1} h_i \sum_{k'=0}^{M-1} Z_s[l - r_i, k'] e^{j2\pi \frac{k_i}{NM} l} e^{-j\pi \frac{M-1}{M}(k-k'-k_i)} \frac{\sin(\pi(k - k' - k_i))}{\sin\left(\frac{\pi}{M}(k - k' - k_i)\right)}. \tag{4.43}$$

As we did for the delays τ_i, the previous expression is often simplified by supposing $k_i \in \mathbb{Z}$ leading to

$$Z_y[l,k] = \sum_{i=0}^{P-1} h_i Z_s[l-r_i, k-k_i] e^{j2\pi \frac{k_i}{NM} l}. \tag{4.44}$$

Again the number of paths P might be adapted to better grasp the spreading of the information symbols along the Doppler axis in case $k_i \notin \mathbb{Z}$. Remember that $s[m]$ was first defined as the IDZT of $c[l,k]$. The DZT of $y[n]$ is then a two-dimensional shift of the grid of the transmitted symbols $c[l,k]$.
Finally, since we are using an (approximatively) Nyquist pair of filters, the noise samples are i.i.d. distributed as a centered complex normal $\mathcal{CN}(0, N_0)$. The DZT of those samples is basically a DFT of a downsampled version of those noise samples. Since the distribution of AWGN noise is unchanged through a unitary DFT [21], we conclude that the noise samples have the same distribution before and after the DZT. Those noise samples in the delay-Doppler domain are written as $\nu[l,k]$ leading to the full and final input/output expression given in result 4.3.4.

Result 4.3.4: Received signal in the delay-Dopppler domain of an (RCP-)OTFS system.

The received signal of an (RCP-)OTFS system in the dD domain writes

$$Z_y[l,k] = \sum_{i=0}^{P-1} h_i c[l-r_i, k-k_i] e^{j2\pi \frac{k_i}{NM} l} + \nu[l,k]. \tag{4.45}$$

where $c[l,k]$ are the sent constellation symbols and $\nu[l,k]$ an AWGN term.

The last step in an OTFS system is to recover the information symbols from (4.45). Different algorithm have been proposed to that aim. Before diving into those algorithms, another variant of OTFS where a CP is prepended every N samples is presented in the following section.

4.3.3 Input/output relationship of the (CP-)OTFS modulation

Following the same idea as in the previous section, the input/output relationship of the OTFS system where a CP is added in front of each block of N data symbols in the same way as in OFDM is presented. In this scenario, the received samples after matched filtering and discarding the CP write

$$y[l+nN] = \sum_{i=0}^{P-1} h_i e^{j2\pi\nu_i(l+n(N+L_{cp}))T_s} s\Big[[l-r_i]_N + nN\Big] + w[l+nN], \tag{4.46}$$

where L_{cp} is the number of samples composing the CP. Again we assume $\nu_i = \frac{k_i}{MN}$ and introduce the factor $\gamma = 1 + \frac{L_{cp}}{N}$ so that the Doppler effect can equivalently be represented as $e^{j2\pi\frac{k_i}{MN}l}e^{j2\pi\frac{k_i}{MN}\gamma nN}$. By taking the DZT of (4.46), i.e., a DFT along index n and assuming $k_i\gamma \in \mathbb{Z}$ the resulting quantity is

$$Z_y[l,k] = \sum_{i=0}^{P-1} h_i e^{j2\pi\frac{k_i}{MN}l} Z_s\Big[[l-r_i]_N, k-k_i\gamma\Big] + \nu[l,k]. \tag{4.47}$$

Result 4.3.5: Received signal in the delay-Doppler domain of a (CP-)OTFS system

The received signal of a (CP-)OTFS system in the dD domain writes

$$Z_y[l,k] = \sum_{i=0}^{P-1} h_i e^{j2\pi\frac{k_i}{MN}l} c\Big[[l-r_i]_N, k-k_i\gamma\Big] + \nu[l,k], \tag{4.48}$$

where $c[l,k]$ are the sent constellation symbols, $\nu[l,k]$ is the AWGN term and $\gamma = 1 + \frac{L_{cp}}{N}$.

The difference compared to the (RCP-)OTFS lies in the modulo operator found in (4.45) and (4.48). Consequently, when $l - r_i < 0$ an additional factor appears in (4.45) compared to (4.48) due to the quasi-periodicity property of the DZT.

4.4 Equalization methods for OTFS

The last step in an OTFS system is the recovering of the transmitted information $c[l,k]$ from (4.45) or (4.48). For both (CP-) and (RCP-) the input/output model can be rewritten as

$$\boldsymbol{z_y} = \boldsymbol{H}\boldsymbol{c} + \boldsymbol{w} \quad \boldsymbol{c} \in \mathcal{A}^{MN}, \tag{4.49}$$

where $\mathcal{A}^{MN}$ is the MN dimensional vector space with entries that belong to the constellation alphabet and $\boldsymbol{H}$ is an $MN \times MN$ matrix whose entries depend on the chosen system (RCP or CP). $\boldsymbol{z_y}$ and $\boldsymbol{c}$ denote the vectorization of $Z_y[l,k]$ and $c[l,k]$ respectively. Since the noise samples are assumed i.i.d. Gaussian and that no prior information on the transmitted symbols is available (the symbols are all considered equiprobable) the ML and MAP optimal decision rules are both given by

$$\widehat{\boldsymbol{c}} = \underset{\tilde{\boldsymbol{c}} \in \mathcal{A}^{MN}}{\arg\min} ||\boldsymbol{z_y} - \boldsymbol{H}\tilde{\boldsymbol{c}}||^2. \tag{4.50}$$

The complexity of the detector based on this criteria grows exponentially with MN due to exhaustive search [22]. Therefore, a multitude of algorithms have been proposed to decrease the complexity of the detector while keeping the performance as high as possible [22], [23]. Two algorithms are presented here. The first one is a direct application of the OFDM equalizer to the OTFS structure and the other one was proposed by Hong, Thaj, and Viterbo in [23]. This last algorithm exploits the delay and time diversity provided by the OTFS signaling structure.

4.4.1 Single-tap frequency equalizer

Using the (CP-)OTFS system where a CP is prepended at the beginning of each block of N samples, a single tap equalizer in the frequency-Time domain can be built exactly as in OFDM. This equalizer assumes no or at least limited mobility inside the channel. Indeed, by writing $y_n[l] = y[l + nN]$ and $h'_i = h_i e^{j2\pi \frac{k_i}{MN} n(N+L_{cp})}$, (4.46) simplifies into

$$y_n[l] = \sum_{i=0}^{P-1} h'_i e^{j2\pi\nu_i l} s_n \Big[[l - r_i]_N \Big] + w[n] \tag{4.51}$$

which for a fixed n is exactly the same form as the received signal in an OFDM system (3.2). The ZF or MMSE criterion can then both be used to equalize block by block the received OTFS signal in low mobility channel scenarios as illustrated in Figure 4.6. For each of the M blocks, a pair of N points FFT/IFFT is used leading to an overall complexity of $\mathcal{O}(MNlog_2(N))$.

This single tap frequency equalizer can also be used with the (RCP-)OTFS system on blocks of length NM. The length of the blocks being M times longer than in the (CP-)system, the hypothesis that the mobility of the channel can be neglected is more restrictive. Therefore, the frequency equalizer is primarily used with (CP-)OTFS.

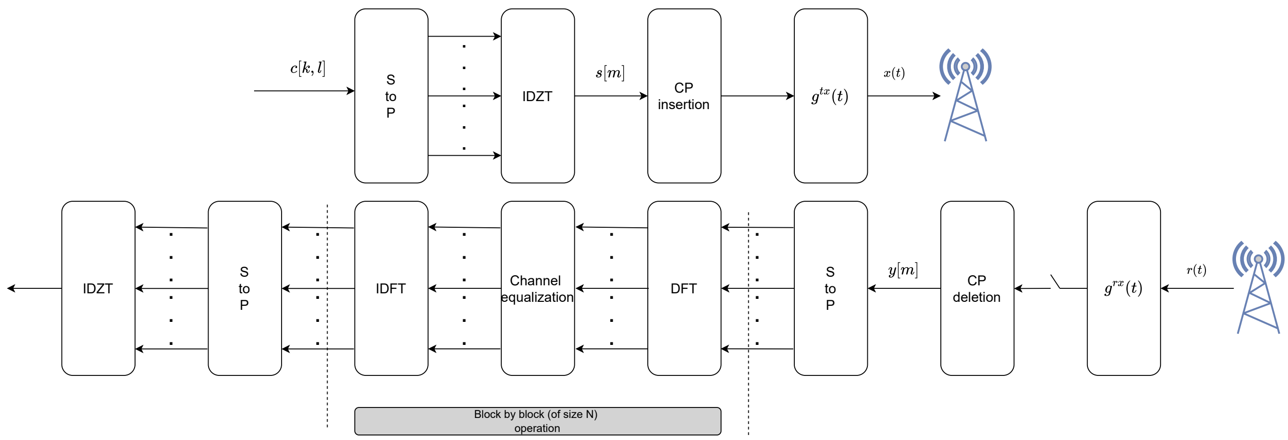

Figure 4.6: Transmission chain of an OTFS system with frequency equalization. Two *S to P* blocks are required at the reception to first group the samples into blocks of N and then to group the M blocks together.

4.4.2 Maximum-ratio combining detection

The Maximum-ratio combining (MRC) detection algorithm presented in [23] will be used in the next sections as a baseline to compare OTFS and OFDM in different scenarios. The main ideas are reminded here and details can be found in [23]. The MRC detection offers similar performance as the message passing algorithm which is an approximate symbol-by-symbol MAP detector while reducing its complexity [22],[23].

The MRC algorithm uses the structure of the received delay-Doppler information. Let us rewrite the (RCP-)OTFS input/output relationship (4.45) in a matrix form as

$$\boldsymbol{Z_y}[\boldsymbol{l}] = \sum_{i=0}^{P-1} h_i e^{j2\pi \frac{k_i l}{NM}} \boldsymbol{\Pi}^{\boldsymbol{k_i}} \boldsymbol{c}[\boldsymbol{l} - \boldsymbol{r_i}] + \boldsymbol{\nu}[\boldsymbol{l}], \tag{4.52}$$

where $\boldsymbol{Z_y}[\boldsymbol{l}]$, $\boldsymbol{c}[\boldsymbol{l}]$ and $\boldsymbol{\nu}[\boldsymbol{l}]$ are the l-th row of $Z_y[l,k]$, $c[l,k]$ and $\nu[l,k]$ respectively. The dimension of those three quantities is therefore $M \times 1$. On the other hand, $\boldsymbol{\Pi}$ is an $M \times M$ circular[1]-shift matrix given by

$$\boldsymbol{\Pi} = \begin{bmatrix} 0 & 0 & 0 & 0 & 0 & ... & 1 \\ 1 & 0 & 0 & 0 & 0 & ... & 0 \\ 0 & 1 & 0 & 0 & 0 & ... & 0 \\ & & . & & & & \\ & & & . & & & \\ & & & & . & & \\ 0 & ... & 0 & 0 & 0 & 1 & 0 \end{bmatrix}. \tag{4.53}$$

We now suppose that there is no redundancy in the set of delays, i.e., there is no i and i' such that $r_i = r_{i'}$ with $i \neq i'$. Finally, the quasi periodicity of $c[l,k]$ along the delay axis is exploited to write the final expression of the received (RCP-)OTFS signal in matrix form as

$$\boldsymbol{Z_y}[\boldsymbol{l}] = \sum_{i=0}^{P-1} \boldsymbol{K_{l,i}} \boldsymbol{c}\Big[[\boldsymbol{l} - \boldsymbol{r_i}]_{\boldsymbol{N}}\Big] + \boldsymbol{\nu}[\boldsymbol{l}]. \tag{4.54}$$

$\boldsymbol{K_{l,i}}$ is an $M \times M$ matrix defined as

$$\boldsymbol{K_{l,i}} \triangleq \begin{cases} h_i e^{j2\pi \frac{k_i l}{NM}} \boldsymbol{\Pi}^{\boldsymbol{k_i}} & , l - r_i \in [0, N-1] \\ h_i e^{j2\pi \frac{k_i l}{NM}} \boldsymbol{\Pi}^{\boldsymbol{k_i}} \ \mathrm{diag}_k \left(e^{j2\pi k \lfloor \frac{l - r_i}{N} \rfloor} \right) & , \text{otherwise} \end{cases}, \tag{4.55}$$

[1]The circularity comes from the periodicity property of the Doppler axis of the DZT

in which $\text{diag}_k\left(e^{j2\pi k\lfloor\frac{l-r_i}{N}\rfloor}\right)$ is a diagonal matrix with on its k-th element the value $e^{j2\pi k\lfloor\frac{l-r_i}{N}\rfloor}$. Please note that having redundancy in the delays does not prevent from writing (4.54) but $\boldsymbol{K}_{l,i}$ would have a more complex form (for the sake of what follows, we want to keep the summation in (4.54) on paths that have distinct delays).

The idea of the MRC algorithm is illustrated for a channel with two paths in Figure 4.7. It is an iterative process where the estimate $\hat{\boldsymbol{c}}[\boldsymbol{l}]$ are iteratively updated until a convergence criterion is met.

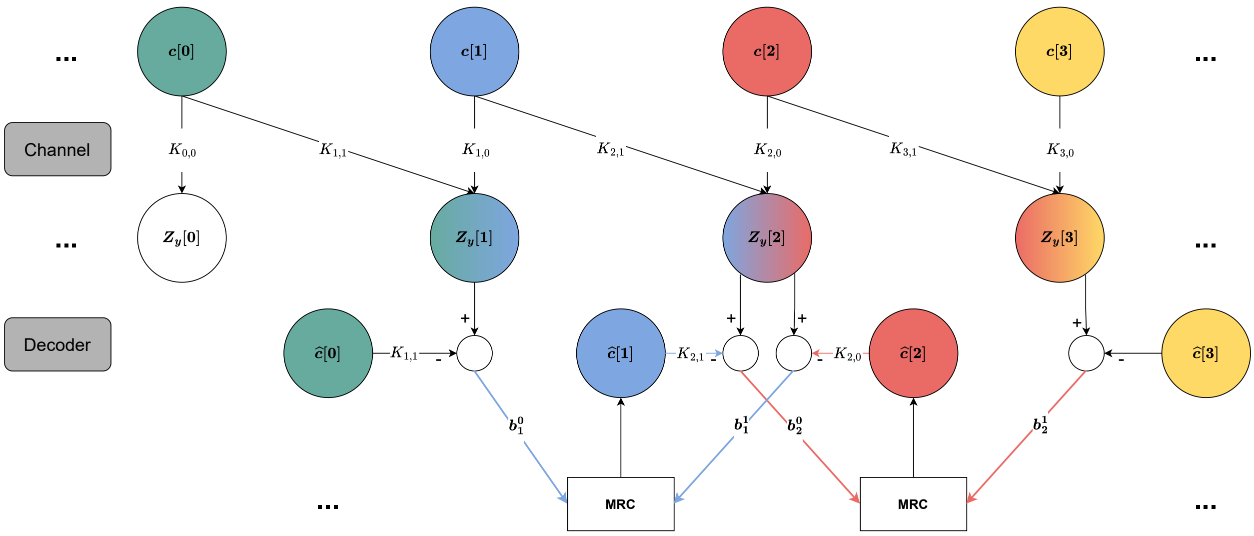

Figure 4.7: Illustration of the MRC algorithm for a channel with two delays given by $r_i \in \{0, 1\}$

For ease of notation the iteration index is omitted. The first step of the algorithm is to isolate the component linked to $\boldsymbol{c}[\boldsymbol{m}]$ from the received information $\boldsymbol{Z_y}[\boldsymbol{m}+\boldsymbol{r_i}]$ by cancelling the interfering terms. The component used to estimate $\boldsymbol{c}[\boldsymbol{m}]$ from $\boldsymbol{Z_y}[\boldsymbol{m}+\boldsymbol{r_i}]$ is denoted as $\boldsymbol{b}_{\boldsymbol{m}}^{\boldsymbol{r_i}}$ and is given by

$$\boldsymbol{b}_{\boldsymbol{m}}^{\boldsymbol{r_i}} = \boldsymbol{Z_y}[\boldsymbol{m}+\boldsymbol{r_i}] - \sum_{i'=0|r_{i'}\neq r_i}^{P-1} \boldsymbol{K}_{\boldsymbol{m}+\boldsymbol{r_i},\boldsymbol{i'}}\hat{\boldsymbol{c}}\Big[[\boldsymbol{m}+\boldsymbol{r_i}-\boldsymbol{r_{i'}}]_{\boldsymbol{N}}\Big], \tag{4.56}$$

where the notation $\sum_{i'=0|r_{i'}\neq r_i}^{P-1}$ is introduced to denote a summation over all the path that have an associated delay different from r_i. In the previous expression, we admitted that a previous estimation of $\hat{\boldsymbol{c}}[\boldsymbol{m}+\boldsymbol{r_i}-\boldsymbol{r_{i'}}]$ was available, be it simply equal to zero or given by the estimate of a frequency equalizer as previously presented. Substituting (4.54) in (4.56), the analytical expression of those $\boldsymbol{b}_{\boldsymbol{m}}^{\boldsymbol{r_i}}$ is given by

$$\boldsymbol{b}_{\boldsymbol{m}}^{\boldsymbol{r_i}} = \boldsymbol{K}_{m+r_i,i}\boldsymbol{c}[\boldsymbol{m}] + \sum_{i'=0|r_{i'}\neq r_i}^{P-1} \boldsymbol{K}_{m+r_i,i'}\left(\boldsymbol{c}\Big[[\boldsymbol{m}+\boldsymbol{r_i}-\boldsymbol{r_{i'}}]_{\boldsymbol{N}}\Big] - \widehat{\boldsymbol{c}}\Big[[\boldsymbol{m}+\boldsymbol{r_i}-\boldsymbol{r_{i'}}]_{\boldsymbol{N}}\Big]\right) + \boldsymbol{\nu}[\boldsymbol{m}+\boldsymbol{r_i}]. \tag{4.57}$$

Finally, an MRC step is performed on (4.56) followed by a symbol-by-symbol ML detection to update the estimate $\widehat{\boldsymbol{c}}[\boldsymbol{m}]$. Those last two steps are given mathematically by

$$\tilde{\boldsymbol{c}}_{\boldsymbol{m}} = \left(\sum_{i=0}^{P-1} \boldsymbol{K}_{m+r_i,i}^{\boldsymbol{H}}\boldsymbol{K}_{m+r_i,i}\right)^{-1}\left(\sum_{i=0}^{P-1} \boldsymbol{K}_{m+r_i,i}^{\boldsymbol{H}}\boldsymbol{b}_{\boldsymbol{m}}^{\boldsymbol{r_i}}\right) \tag{4.58}$$

$$\widehat{c}[m,k] = \arg\min_{a\in\mathcal{A}} |a - \tilde{c}_m[k]| \tag{4.59}$$

where $\mathcal{A}$ is the modulation alphabet.
The core of the MRC algorithm is the computation of the $\boldsymbol{b}_{\boldsymbol{m}}^{\boldsymbol{r_i}}$. The number of paths with distinct delay is denoted $\mathcal{P}$. There are $\mathcal{P}$ $\boldsymbol{b}_{\boldsymbol{m}}^{\boldsymbol{r_i}}$ to compute for each $\tilde{\boldsymbol{c}}_{\boldsymbol{m}}$. To compute a single $\boldsymbol{b}_{\boldsymbol{m}}^{\boldsymbol{r_i}}$, $\mathcal{P}-1$ matrix multiplication between an $M\times M$ matrix and an $M\times 1$ vector are required leading to an overall complexity $\mathcal{O}(M^2\mathcal{P}(\mathcal{P}-1))$. Then the procedure is repeated for each iteration, the total number of iterations is denoted n_{iter}. Finally, at the recombination step $\left(\sum_{i=0}^{\mathcal{P}-1} \boldsymbol{K}_{m+r_i,i}^{\boldsymbol{H}}\boldsymbol{K}_{m+r_i,i}\right)^{-1}$ has to be computed but can be reused at every iteration leading to a complexity of $\mathcal{O}(M^3)$ (inversion of an $M\times M$ matrix [24]). The overall complexity is then found as $\mathcal{O}\left(N(M^3 + n_{iter}M^2\mathcal{P}(\mathcal{P}-1))\right)$. The complexity can be further reduced by exploiting the circulant structure of $\boldsymbol{K}_{\boldsymbol{m},\boldsymbol{i}}$, [23] achieved an overall complexity of $\mathcal{O}(NM\mathcal{P}n_{iter})$ where we see that the complexity per iteration is comparable to the complexity of the single tap equalizer.

We understand that the MRC algorithm coherently combines the copies of the same symbol from every delay and Doppler of the channel which echoes to the working principle of a Rake receiver [25],[26]. Therefore, we propose an adaptation of the rake receiver to this delay-Doppler modulation.

4.4.3 Adaptation of the Rake receiver to delay-Doppler communication

The structure of the receiver discussed here is described in Figure 4.8

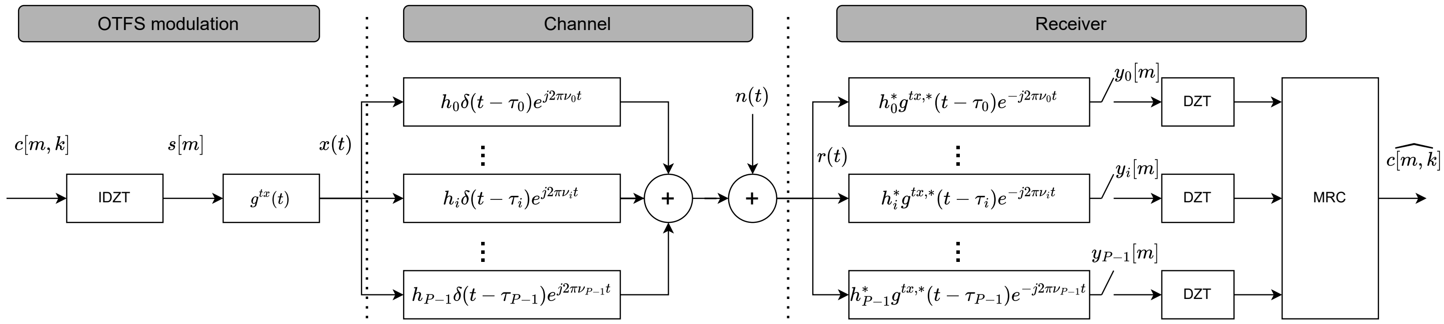

Figure 4.8: Proposed receiver structure inspired by the rake receiver structure

To capture the information carried by every delay and Doppler of the channel, i.e., every path, P filters matched to the cascade of the transmitting filter and the delay Doppler impairments are used at the reception. The output of the filter i is denoted $y_i[l+nN]$ and is given by

$$\begin{aligned}
y_i[l+nN] &= h_i^* \int_{-\infty}^{\infty} r(t) e^{-j2\pi \frac{k_i}{MNT_s} t} g^{tx,*}(t-(l+nN-r_i)T_s) dt, \\
&\approx h_i^* e^{-j2\pi \frac{k_i}{MN}(l+nN-r_i)} \int_{-\infty}^{\infty} r(t) g^{tx,*}\left(t-(l+nN-r_i)T_s\right) dt, \\
&\approx h_i^* \sum_{i'=0}^{P-1} h_{i'} e^{-j2\pi \frac{k_i-k_{i'}}{MN}(l+nN-r_i)} s[l-r_i+r_{i'}+nN] \\
&\qquad + h_i^* e^{-j2\pi \frac{k_i}{MN}(l+nN-r_i)} w[l-r_i+nN],
\end{aligned} \tag{4.60}$$

Applying a DZT on (4.60) leads to the following expression

$$\begin{aligned}
Z_{y_i}[l,k] &= h_i^* \sum_{i'=0}^{P-1} h_{i'} e^{-j2\pi \frac{k_i-k_{i'}}{MN}(l-r_i)} c[l-r_i+r_{i'}, k-k_i+k_{i'}] \\
&\qquad + h_i^* e^{-j2\pi \frac{k_i}{MN}(l-r_i)} \nu[l-r_i, k-k_i] \\
&= |h_i|^2 c[l,k] + h_i^* \sum_{i'=0 | i' \neq i}^{P-1} h_{i'} e^{-j2\pi \frac{k_i-k_{i'}}{MN}(l-r_i)} c[l-r_i+r_{i'}, k-k_i+k_{i'}] \\
&\qquad + h_i^* e^{-j2\pi \frac{k_i}{MN}(l-r_i)} \nu[l-r_i, k-k_i]
\end{aligned}$$

The different output of the matched filters can then be coherently combined to produce the soft estimate given by

$$
\begin{aligned}
\widehat{c}[l,k] &= \frac{\sum_{i=0}^{P-1} Z_{y_i}[l,k]}{\sum_{i=0}^{P-1} |h_i|^2}, \\
&= c[l,k] + \frac{\sum_{i=0}^{P-1} h_i^* \sum_{i'=0|i'\neq i}^{P-1} h_{i'} e^{-j2\pi \frac{k_i - k_{i'}}{MN}(l-r_i)} c[l - r_i + r_{i'}, k - k_i + k_{i'}]}{\sum_{i=0}^{P-1} |h_i|^2} \\
&\quad + \frac{\sum_{i=0}^{P-1} h_i^* e^{-j2\pi \frac{k_i}{MN}(l+nN-r_i)} \nu[l - r_i, k - k_i]}{\sum_{i=0}^{P-1} |h_i|^2}.
\end{aligned}
$$

For a normalized channel, i.e., $\sum_{i=0}^{P-1} |h_i|^2 = 1$, given that the $\nu[l,k]$ are i.i.d, the SNR of this decision variable is the upper bound given by the SNR of an AWGN channel $SNR = \frac{1}{\sigma_\nu^2}$ as shown in Appendix E. This means that the receiving structure is able to extract and combine all the information that provides the channel about every constellation symbol. However, the number of interfering terms grows as $P(P-1)$ which can become detrimental for the overall performance of the receiver. Therefore, one could wonder what happens when an equalization step is added in each finger. We show that a single-tap frequency equalizer as in subsection 4.4.1 on each finger leads to correlated noise across the fingers which prevents the receiver from reaching an SNR given by $\frac{1}{\sigma_\nu^2}$. However, the receiver still provides a diversity source for the interferences. The noise correlation between the fingers is shown analytically for a (CP-)OTFS system. The structure of this new receiver is presented in Figure 4.9.

As usually with equalizers in the frequency domain, the Doppler effect inside each block of N samples is ignored. The equations are derived in a matrix form and make use of the theory of circulant matrices [27]. The subscript n is used to index the block of the delay-Time representation of a signal. Therefore, $\boldsymbol{s_n}$ is the n-th column of $s_{dT}[l,n]$. The received sequence after matched filter i' is, based on (4.60), written as

$$
\boldsymbol{y_{n,i'}} = \sum_{i=0}^{P-1} h_{i'}^* h_i \boldsymbol{\Pi}^{-r'_i + r_i} e^{j2\pi \frac{k_i - k_{i'}}{M} n} \boldsymbol{s_n} + h_{i'}^* \boldsymbol{\Pi}^{-r_{i'}} e^{-j2\pi \frac{k_{i'}}{M} n} \boldsymbol{w_n} \tag{4.61}
$$

$$
= \boldsymbol{W^H} h_{i'}^* \boldsymbol{\Lambda}_{\boldsymbol{r'_i}}^{\boldsymbol{-1}} \sum_{i=0}^{P-1} h_i \boldsymbol{\Lambda}_{\boldsymbol{r_i}} \boldsymbol{W} \boldsymbol{s_n} + \boldsymbol{W^H} h_{i'}^* \boldsymbol{\Lambda}_{\boldsymbol{r'_i}}^{\boldsymbol{-1}} \boldsymbol{W} \boldsymbol{w_n}, \tag{4.62}
$$

where the diagonalization of the circulant matrices $\boldsymbol{\Pi}^{\boldsymbol{r_i}}$ follows from [27]. $\boldsymbol{W}$ is the unitary DFT matrix and $\boldsymbol{\Lambda_{r_i}}$ is the eigenvalue diagonal matrix of $e^{j2\pi \frac{k_i}{M} n} \boldsymbol{\Pi}^{\boldsymbol{r_i}}$. The equalization on finger i' is performed as such

$$\widehat{\boldsymbol{y_{n,i'}}} = \boldsymbol{W^H} \left(h_{i'}^{*} \boldsymbol{\Lambda_{r_i'}^{-1}} \sum_{i=0}^{P-1} h_i \boldsymbol{\Lambda_{r_i}} \right)^{-1} \boldsymbol{W} \boldsymbol{y_{n,i'}} \tag{4.63}$$

$$= \boldsymbol{s_n} + \boldsymbol{W^H} \sum_{i=0}^{P-1} \boldsymbol{\Lambda_{r_i}^{-1}} \boldsymbol{W} \boldsymbol{w_n}. \tag{4.64}$$

From the last expression, we see that the noise on the different fingers is correlated preventing any improvement of SNR by recombining the different matched filters. However, the interfering term on each branch is caused by different Doppler frequencies due to the Doppler compensation in the matched filter. Those interfering terms therefore add up non-coherently at the recombination.

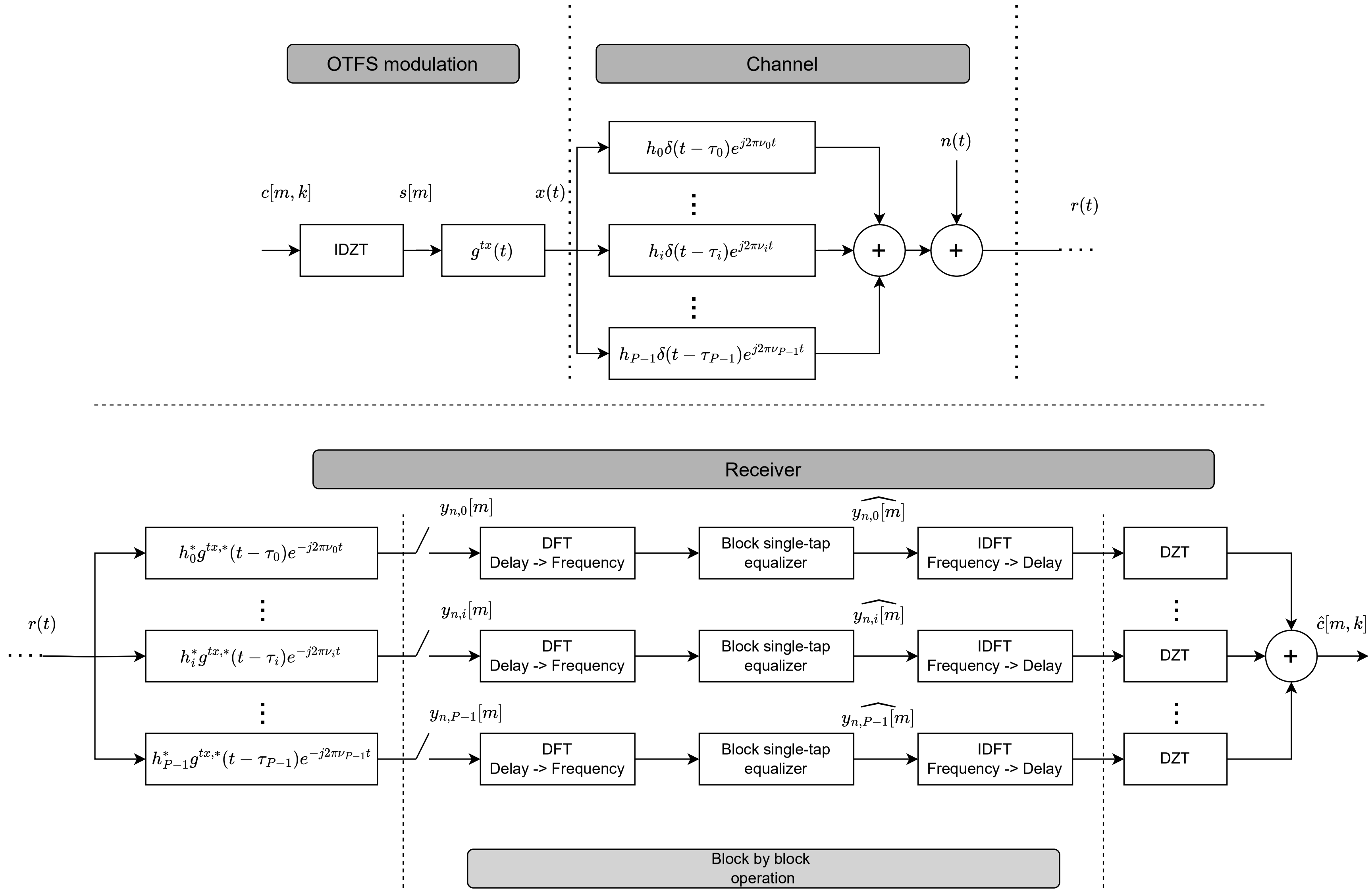

Figure 4.9: Proposed receiver structure inspired by the rake receiver structure with frequency equalization

Key take-away messages of chapter 4:

- The delay-Doppler representation is an equivalent way of representing any continuous time signal. In this representation, the effect of a doubly dispersive channel is, up to a factor $e^{j2\pi\nu_0\tau}$, represented as a 2D convolution. In this delay-Doppler domain, the notion of channel fading is therefore lost. In other words, every information modulated in the delay-Doppler domain is received in the delay-Doppler domain without any loss of energy that could arise from fading. This fundamental difference with, for example, the delay-Time domain where the received energy could fluctuate from symbol to symbol, is the major advantage of dD modulations.

- OTFS is a block by block multicarrier modulation just as OFDM. However, in OTFS, the constellation symbols are modulated in the delay-Doppler domain.

- The OTFS modulation is described with the following parameters :
  - Number of samples along the delay axis N
  - Number of samples along the Doppler axis M
  - Sampling period T_s
  - Bandwith of the system $\frac{1}{T_s}$
  - Time duration of an OTFS grid MNT_s

- Two variants of OTFS have been presented. In one of them, a single CP is prepended every NM samples. This variant is therefore called (RCP-)OTFS. On the other hand, in (CP-)OTFS, a CP is added every N samples.

- The single tap frequency equalizer can be used with both variants. However, with the (RCP-) one, the effect of the Doppler frequencies becomes very detrimental.

- The MRC algorithm is a more complex equalizer that does not neglect the Doppler effect in its conception and combines the information contained in each delay and Doppler frequency of the channel.

- A bank of matched filter can also be used at the reception to coherently combine the constellation symbol carried through every propagating path of the channel. However, the number of interfering terms becomes detrimental if no equalizer is used. If a frequency equalizer is used, the noise realizations are correlated across the fingers.

Chapter 5

Structural comparison between OFDM, CPSC and OTFS

This chapter provides a comparison of the OFDM, CP-SC and OTFS with frequency and MRC equalization transceiver architectures. The block diagram of the four chains are reminded in the following figures.

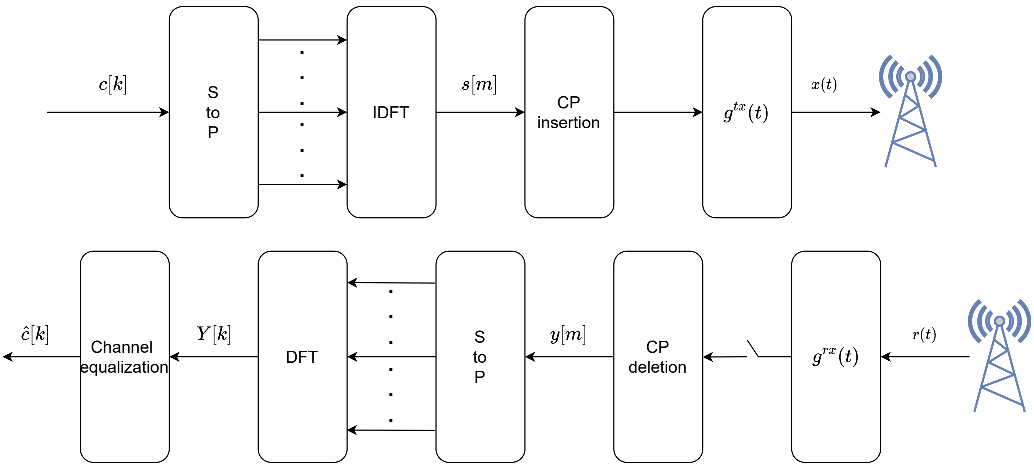

Figure 5.1: Transmission chain of an OFDM system.

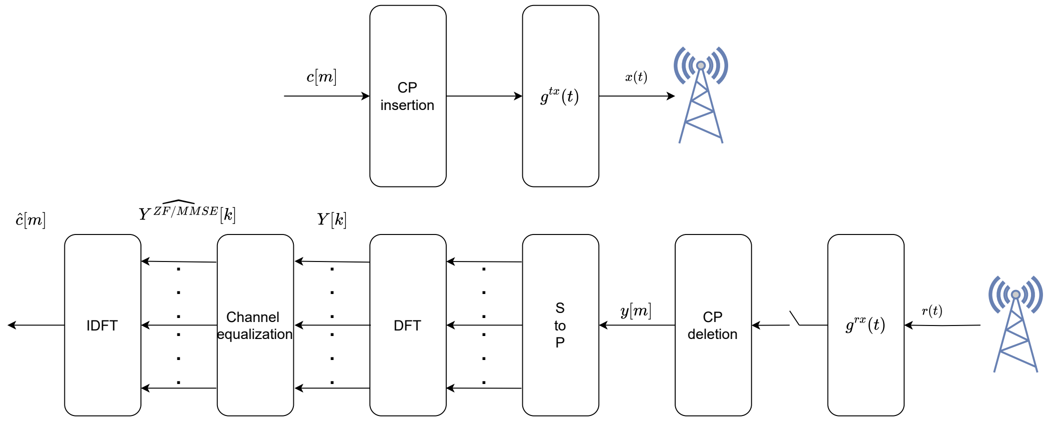

Figure 5.2: Transmission chain of a CP-SC system.

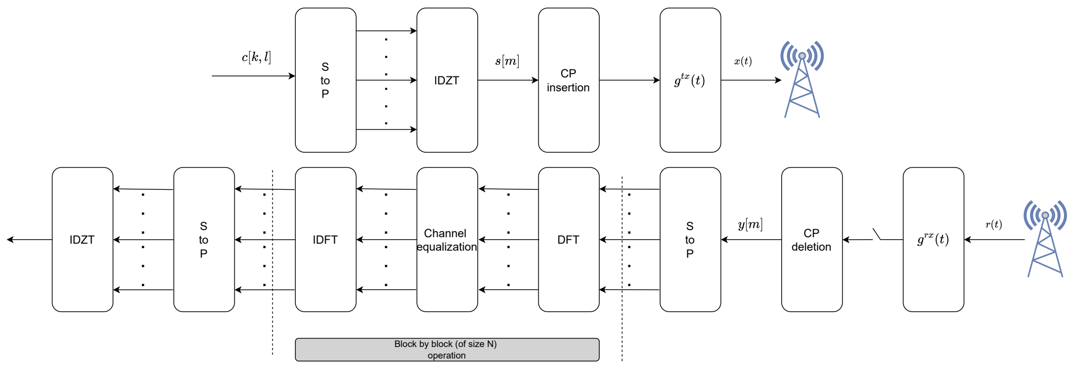

Figure 5.3: Transmission chain of an OTFS system with frequency equalization. Two *S to P* blocks are required at the reception to first group the samples into blocks of N and then to group the M blocks together.

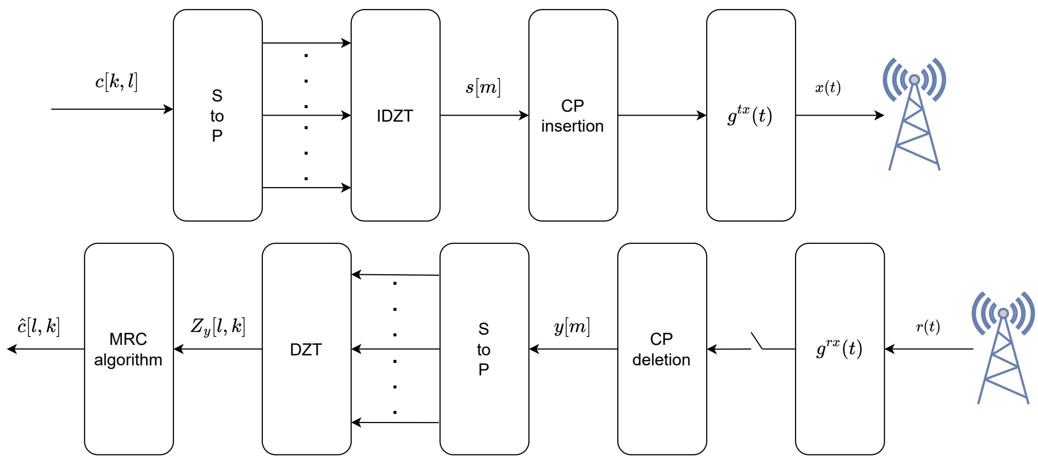

Figure 5.4: Transmission chain of an OTFS system with MRC equalization.

It is clear from those block diagrams that OFDM and OTFS share an intricate link as the only notable difference in the transmitting architecture is the IDFT in OFDM that turns into an IDZT in OTFS. However, the philosophy of both modulations are very different. Both modulations have a block by block principle. Let us look at the transmission of NM constellation symbols in systems where the block size is N. In OFDM, the constellation symbols are grouped into blocks of N symbols that live in the frequency domain. Each block undergoes an IDFT causing a certain **spreading of the constellation symbols across a single block but not over multiple OFDM blocks.** The time fading behavior of the channel can therefore lead to poor performance on certain blocks and consequently degrade the overall performance of the system. On the other hand, OTFS also groups the symbols into blocks of N information, however, **the IDZT spreads the information across the M blocks of the system.** This way, the fading of the channel over time is mitigated as a part of each and every symbol appears in each block. This very important difference is highlighted in Figure 5.5.
Frequency fading also induces a loss of performance on the OFDM system. This frequency fading is not affecting the CP-SC chain. However, as OFDM, this CP-SC chain inherently suffers from time fading. By comparing the different chain diagram, OTFS with frequency equalization can be seen as a precoded version of the CP-SC chain. Consequently, the loss of performance that the CP-SC chain might experience on certain blocks due to time fading is mitigated in OTFS.

Bandwith
The bandwidth of both OFDM and OTFS, for a given T_s, is the same. Indeed, it is given for OFDM as $\frac{1}{T_s}$ (section 3.2) and for OTFS as $\frac{N}{\tau_{max}} = \frac{N}{NT_s} = \frac{1}{T_s}$ (section 4.2). However, the datarate of an OFDM system inevitably suffers from the CP overhead on every OFDM block while in an (RCP-)OTFS system, only a single CP can be used on the whole OTFS grid of NM symbols at the expense of a much more complex equalization algorithm (subsection 4.4.2). The latency of the OTFS system is M times longer than in an OFDM system since it requires the reception of the whole NM symbols before starting the demodulation while OFDM only requires the reception of a single block of N samples.

Doppler resolution
The number of interfering term in an OTFS system is P (see (4.45)) if the Doppler frequencies are all multiple of $\frac{1}{MNT_s}$ [1] while in an OFDM system, in order to contain the number of interfering to P, the Doppler frequencies have to be integer multiple of $\frac{1}{NT_s}$. For a same amount of transmitted information, the Doppler resolution of an OTFS system is M times better than the one of an OFDM system.
The periodization along the Doppler axis of an OTFS system is $\frac{1}{NT_s}$. Therefore, the OTFS system has access to M samples across this dimension to modulate

[1] In a (CP-)OTFS system a factor γ appears in the expression of the Doppler resolution due to the longer time duration of the signal (see 4.48).

information. It is clear on Figure 5.5 that if $M = 1$, OTFS degenerates into the CP-SC chain. The CP-SC can therefore be seen as a particular case of an OTFS scheme. On the other hand, if $N = 1$, OTFS is equivalent to an M subcarrier OFDM system.

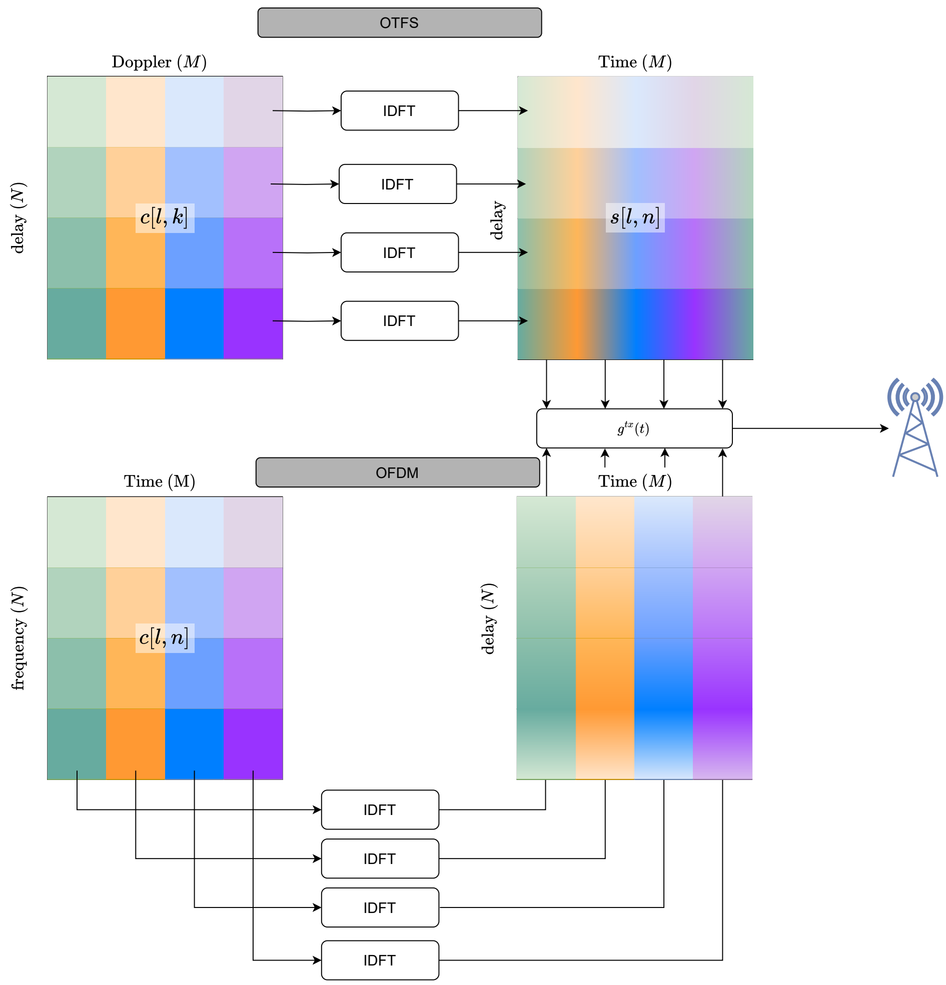

Figure 5.5: Transformation of the constellation symbols in the OFDM and OTFS systems. In OTFS, the constellation symbols are spread across the time dimension while in OFDM, they are spread along the delay dimension. Here the IDZT of OTFS is explicitly developed into a bank of IDFT along the Doppler axis. The gradient of color indicates how the information spreads in the different modulations.

Chapter 6

Simulation results

The simulation results of 5 transceiver structures are presented here for comparison. On one side there are transceiver schemes that neglect the effect of the Doppler in their equalization. Those are the already presented OFDM, CP-SC and (CP-)OTFS with single tap frequency equalization as well as the adaptation of the rake receiver with frequency equalization that is now referred to as *bank of MF* for conciseness. On the other hand, the (CP-)OTFS with MRC combining as presented in subsection 4.4.2 which does not neglect the Doppler in the equalization is also shown. The adaptation of the rake receiver without any equalization as in Figure 4.8 is not presented in the upcoming figures due to really poor performance in terms of BER compared to OFDM as shown in the first simulation (Figure 6.2a).

First, the behavior of the BER curves of every scheme is investigated on fixed and deterministic channels where the gains, delays and Doppler frequencies are fixed and known by the receiver. The choice of those parameters is somehow arbitrary, therefore, the BER curves are averaged on different channel gains and Doppler frequencies to validate and generalize the results inferred from the previous channels. The averaging is done by drawing the channel gains and Doppler frequencies from certain distributions as discussed in the dedicated section. This statistical description appears because the user might find itself in different channel scenarios with different geometries and speeds. It is a completely different origin of randomness from the one described in section 2.4 where Rayleigh and Rice models were discussed. A simulation of the Rayleigh channel model is provided in section 6.4. The Rayleigh model is simulated by using channels with multiple propagating paths that fall on the same channel tap with uniform direction of arrival as described in the dedicated section.

The simulations are performed in discrete time using the discrete channel model (2.28). Therefore, they do not entail the approximation $e^{j2\pi\nu_i t}s(t) \approx s(t)$.

6.1 Simulation parameters

The simulation codes used throughout this chapter are deeply inspired by the ones provided in [23]. The MRC algorithm used for OTFS uses the exact same implementation as the one provided in [23]. Unless mentioned otherwise, the simulation parameters are the following :

Number of subcarriers for OFDM	$N = 64$
Number of consecutive blocks of the delay-Time representation for OFDM and CP-SC	$M = 64$
OTFS variant	CP
Number of samples along Doppler axis for OTFS	$M = 64$
Number of samples along Delay axis for OTFS and CP-SC	$N = 64$
L_{cp} for every scheme	$\frac{N}{16} = 4$
Carrier frequency	$f_c = 4 \quad GHz$
Modulation size	4-QAM
Subcarrier spacing $\Delta_f = \frac{1}{NT_s}$	$30 \quad kHz$
Equalizer type for frequency equalization	MMSE
Maximum number of iterations in MRC equalization for OTFS	25
Initial estimate of MRC equalization for OTFS	OTFS with frequency equalization

Throughout this section, the Doppler frequencies are given as normalized value k_i[1], the equivalence between this notation and the true Doppler frequency is reminded here.

$$\nu_i = \frac{k_i}{MNT_s} \approx k_i \cdot 450Hz \implies \frac{\nu_i}{\Delta_f} = \frac{k_i}{64}$$

The Doppler shift induced between the beginning and the end of an OFDM block or equivalently of a block fed to the frequency equalizer in an OTFS and CP-SC system can be computed for a receiver moving in the direction of the transmitter for different speeds and carrier frequency as $f_c \frac{vT_{OFDM}}{c} = f_c \frac{v}{c\Delta_f}$. This Doppler shift is presented in Figure 6.1. For a given $f_c = 4GHz$ the symbolic Doppler shift of $\frac{\pi}{8}$ limit is reached at roughly $500km/h$ which translates into a normalized Doppler of $k_i \approx 4$[2].

[1] Since we are in a (CP-)OTFS system, the values of k_i are in fact the values of $k_i\gamma$. However, the γ has been omitted in the notation for clarity.

[2] In the upcoming simulations the reference time chosen for the frequency equalization is the middle of an OFDM block, i.e. $m_{freeze} = \frac{N}{2}$ (come back to (3.8) for further explanation).

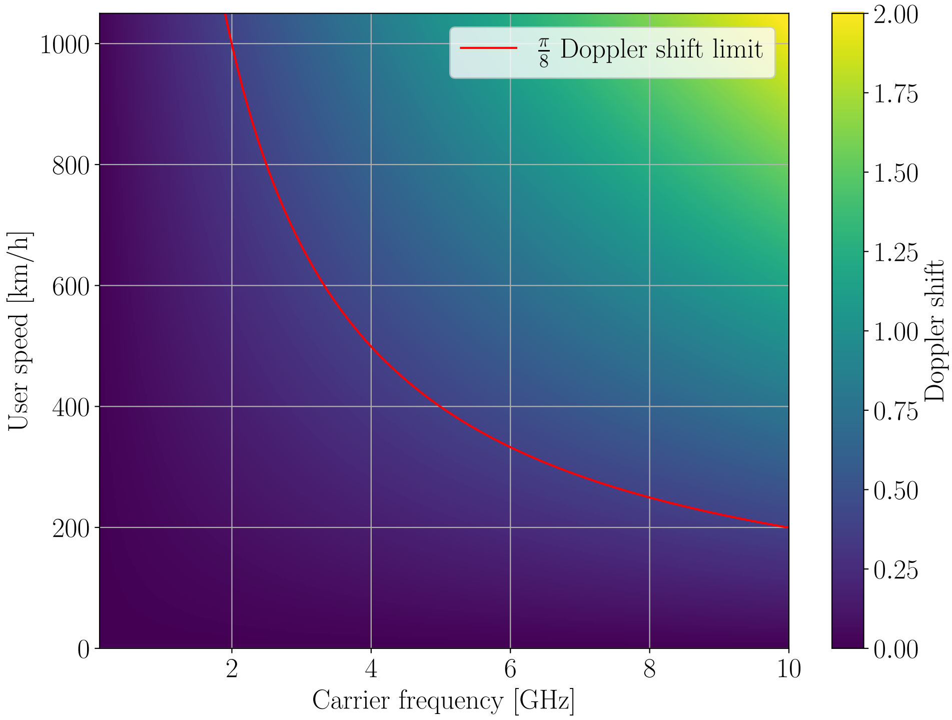

Figure 6.1: Doppler shift across a block of the frequency equalizer in both OFDM and OTFS systems for $\Delta_f = 30kHz$.

6.2 Fixed channel

Fixed and non-fading channels are investigated to have a first understanding of the phenomena at stake. Different scenarios for the Doppler frequencies are considered while the gains and delays of the paths are fixed and given in the following table. Please note that for those considered scenarios the channel taps are made of only one path. Therefore, the channel taps do not fade in time.

$\boldsymbol{h}$	$[1, 0.7, 1]/\sqrt{(2 + 0.7^2)}$
Delays $\boldsymbol{r}$	$[0, 1, 2]$

Impact of mobility

First, the impact of mobility on the different transceiver architectures is analyzed in Figure 6.2. Observations are made in the following.

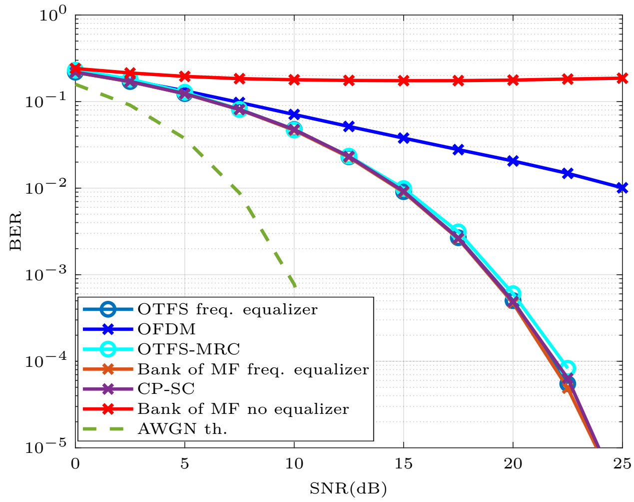

(a) No mobility $k_i \in \{0,0,0\}$. The *Bank of MF frequency equalization*, *OTFS* and *CP-SC* curves are all superposed.

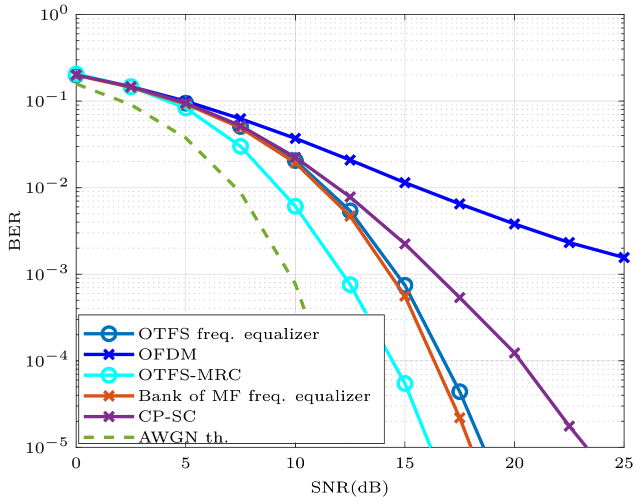

(b) Moderate mobility $k_i \in \{3,0,2\} \Leftrightarrow \nu_i \in \{1.41 \cdot 10^3, 0, 940\}Hz \Leftrightarrow v_i \in \{381,0,254\}km/h$.

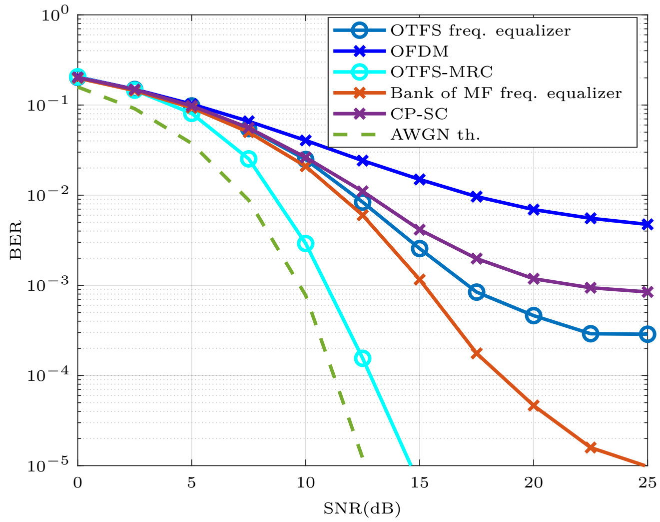

(c) High mobility $k_i \in \{7,0,2\} \Leftrightarrow \nu_i \in \{3.29 \cdot 10^3, 0, 940\}Hz \Leftrightarrow v_i \in \{890,0,254\}km/h$.

Figure 6.2: BER of the different chains in fixed channels

Impact of recombination on the bank of matched filters

The bank of matched filters has a compensation of the Doppler effect at the receiver that the OTFS with frequency equalization does not have. If the performance of the two are to be compared, one has to isolate the effect of the Doppler compensation from the effect of recombination. Therefore, the performance of the individual matched filters before recombination are presented in the following figure.

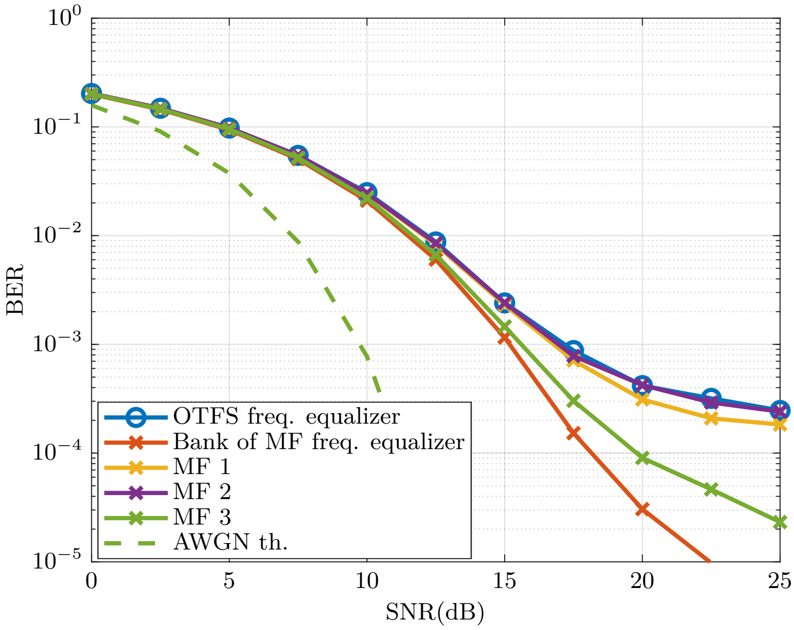

Figure 6.3: BER of the different matched filter $k_i \in \{7, 0, 2\} \Leftrightarrow \nu_i \in \{3.29 \cdot 10^3, 0, 940\}Hz$ (same channel as Figure 6.2c). The second matched filter shows the same performance as the OTFS with frequency equalization which makes sense since on this second path there is no Doppler compensation due to a Doppler frequency which is null.

The following observations are drawn from the presented simulations.

- As expected the bank of matched filters with no equalization leads to very poor performances due to the high amount of interfering terms. Indeed, its BER saturates at ≈ 0.1639 even in no mobility channel scenarios as in Figure 6.2a.
- In a static scenario as in Figure 6.2a, the CP-SC, bank of matched filters, OTFS with frequency equalization and OTFS with the MRC algorithm exhibit roughly the same BER curves. The performance of those schemes is better compared to the OFDM system. This behavior has already been investigated in section 3.4 between OFDM and CP-SC. Since the Doppler axis in static scenarios does not provide any degree of freedom, it makes sense that the delay-Doppler modulations exhibit the same BER as the CP-SC.
- When the mobility is slightly increased ($\nu_{max} = 3/64\Delta_f$) as in Figure 6.2b, the OTFS modulation with the MRC algorithm performs better than every other scheme because the equalization does not neglect the Doppler. The OTFS with frequency equalization achieves a steeper slope than the CP-SC. This behavior points out that even in non-fading scenarios, the DZT in OTFS extracts some sort of diversity from the combination of different CP-SC blocks. Indeed, it had already been pointed out in section 3.4 that even

in non-fading scenarios, the performance of CP-SC could fluctuate in time. On the other hand, the combination of the different CP-SC blocks in OTFS leads to non-fluctuating and improved performance. This phenomenon is very similar as the one that leads CP-SC to exhibit better BER curves than OFDM.
At high SNR, the slope of the OTFS with frequency equalization is the same as the one with MRC equalization. In this high SNR regime, an SNR gap of roughly $2.5dB$ is observed between those two curves.

- When the mobility is pushed even higher ($\nu_{max} = 7/64\Delta_f$) as in Figure 6.2c, every scheme with frequency equalization saturates at high SNR due to important interfering terms. The figure also shows that the OTFS with frequency equalization saturates at a better BER value than CP-SC. This better saturation level is due to the smaller number of interfering term in the delay-Doppler domain. Indeed, in the simulation, the Doppler frequencies in the channel fall perfectly on the Doppler resolution of the OTFS system but not on the OFDM or CP-SC system as explained in chapter 5. The bank of matched filter exhibits a huge BER improvement compared to the OTFS with frequency equalization. However, it is shown in Figure 6.3 that this improvement is mainly due to the usage of the third matched filter over which the Doppler frequency is less severe ($\nu_3 = 2/64\Delta_f$) rather than the effect of the combination of the three matched filters. Still, it is shown that the combination of the three matched filters increases a little bit more the overall performance due to non-coherent interference combination.

6.3 Channel averaging

The number of paths and the associated delays are kept as in the previous section $r_i \in \{0, 1, 2\}$ for Figure 6.4a and Figure 6.4b. However, the gains are drawn from a complex normal distribution $h_i \sim \mathcal{CN}(0, \frac{1}{3})$ where the $\frac{1}{3}$ is to ensure a normalized receive power. The Doppler frequencies are drawn from a uniform distribution and are still assumed to land perfectly on the delay-Doppler grid, i.e. $k_i \in \mathbb{N}$.

Simulation results are provided in Figure 6.4 for two different Doppler distribution. Then, the number of paths is increased in Figure 6.5.
First, in every scenario, OTFS even with frequency equalization is still better than OFDM and CP-SC confirming the observations made before. Then, by comparing Figure 6.4b and Figure 6.5 it is clear that the higher number of paths in Figure 6.5 is beneficial to OTFS with MRC equalization. This impact of the number of paths on the BER of OTFS with MRC is further investigated in the next paragraph.

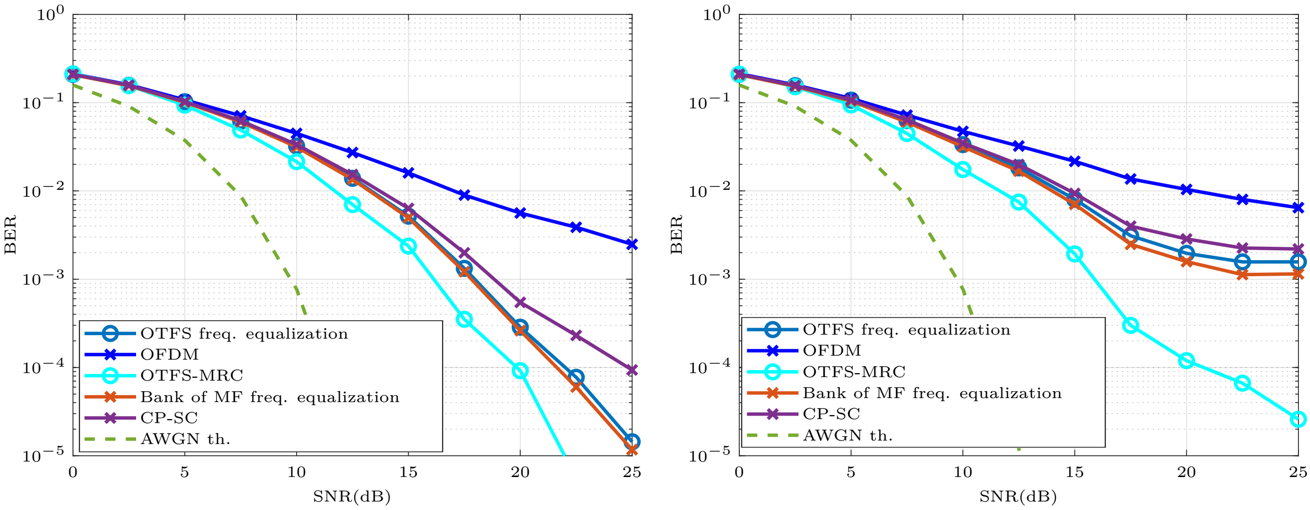

(a) Low mobility $r_i \in \{0, 1, 2\}$, $k_i \sim \mathcal{U}_{[-3,3]\in\mathbb{N}}$. (b) High mobility $r_i \in \{0, 1, 2\}$, $k_i \sim \mathcal{U}_{[-7,7]\in\mathbb{N}}$.

Figure 6.4: BER of the different chains in averaged channels

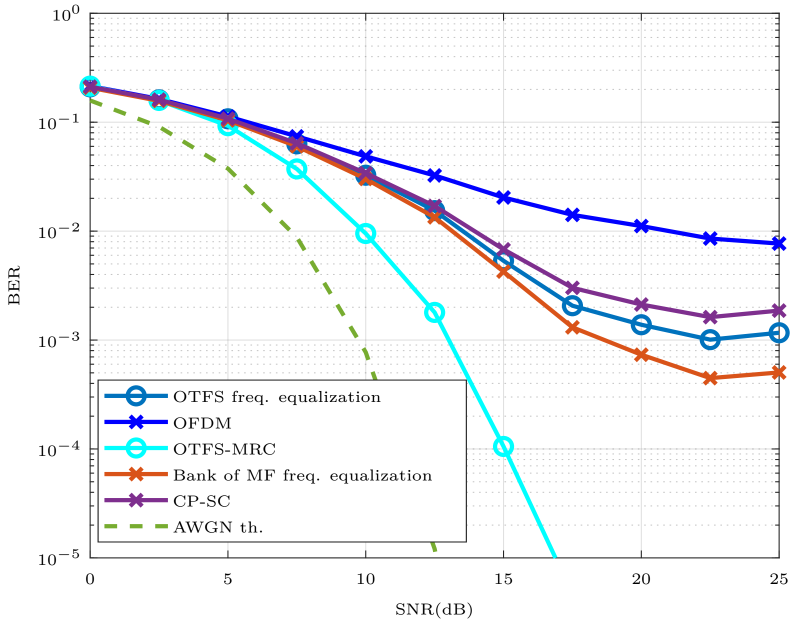

Figure 6.5: BER of the different chains in an averaged channel with $r_i \in [0, 1, 2, 3, 4, 5]$, $h_i \sim \mathcal{CN}(0, \frac{1}{6})$ and $k_i \sim \mathcal{U}_{[-7,7]\in\mathbb{N}}$.

Impact of the number of paths on the performance of OTFS with MRC equalization

It is shown in the following figure that the number of paths even in presence of relatively high Doppler frequencies ($k_i \sim \mathcal{U}_{[-7,7]\in\mathbb{N}}$) is beneficial for the performance of OTFS with MRC equalization due to the higher number of terms used at the recombination step. The slope of the BER increases with the number of paths with a saturation at six propagating paths.

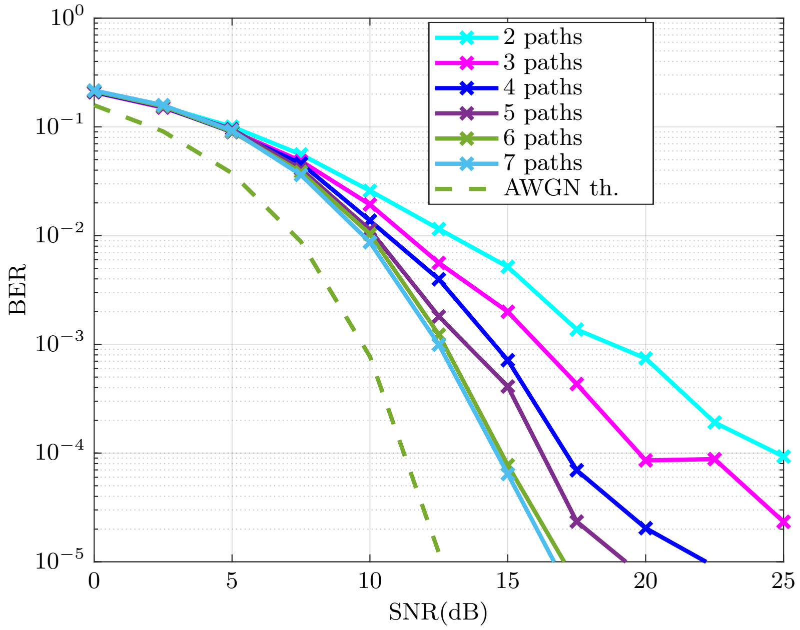

Figure 6.6: BER of OTFS with MRC equalization with different number of paths (still no redundancy in the delays) and $k_i \sim \mathcal{U}_{[-7,7]\in\mathbb{N}}$. The length of the CP has been increased to 8

6.4 Fading channel

In this subsection, channels with redundancy in the set of delays and fractional Doppler frequencies are considered. If not specified otherwise, the speed of the user is fixed and uniform direction of arrivals are considered. The Doppler frequencies are therefore drawn as

$$\nu_i \sim \nu_{max} \cdot \cos(\mathcal{U}_{[0,2\pi]}),$$

where ν_{max} is the maximum Doppler frequency in the system. The power spectral density of the resulting channel taps is the Jake's spectrum [28] presented in Figure 6.7.

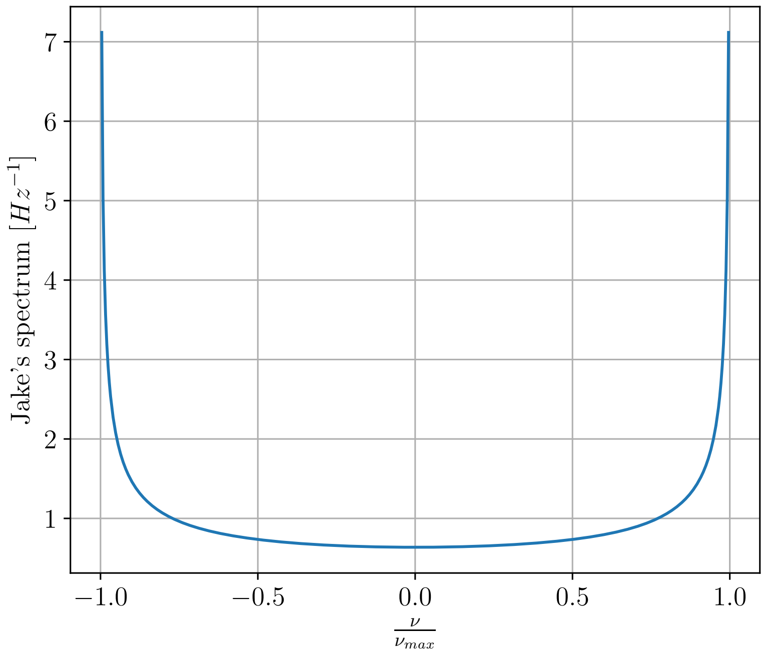

Figure 6.7: Power spectral density of the channel taps with uniformly distributed direction of arrival, i.e., the Jake's spectrum.

Simulations results are given in Figure 6.8. In this figure 5 physical propagating paths fall on the same symbol period. A single channel tap is therefore made of 5 different Doppler frequencies. In those channel, the difference of performance between CP-SC and OTFS with frequency equalization is enhanced compared to Figure 6.4 due to the time fading effect of the channel which is detrimental for CP-SC. This highlights the benefit of using OTFS in scenarios where time fading is important.

It is also shown in Figure 6.8 that OTFS with MRC equalization performs better in the channel made of three channel taps as it was already described in the previous section. It is shown in the next paragraph that not only the number of channel taps matters but also the number of propagating paths constituting each of the channel taps has an impact on the performance.

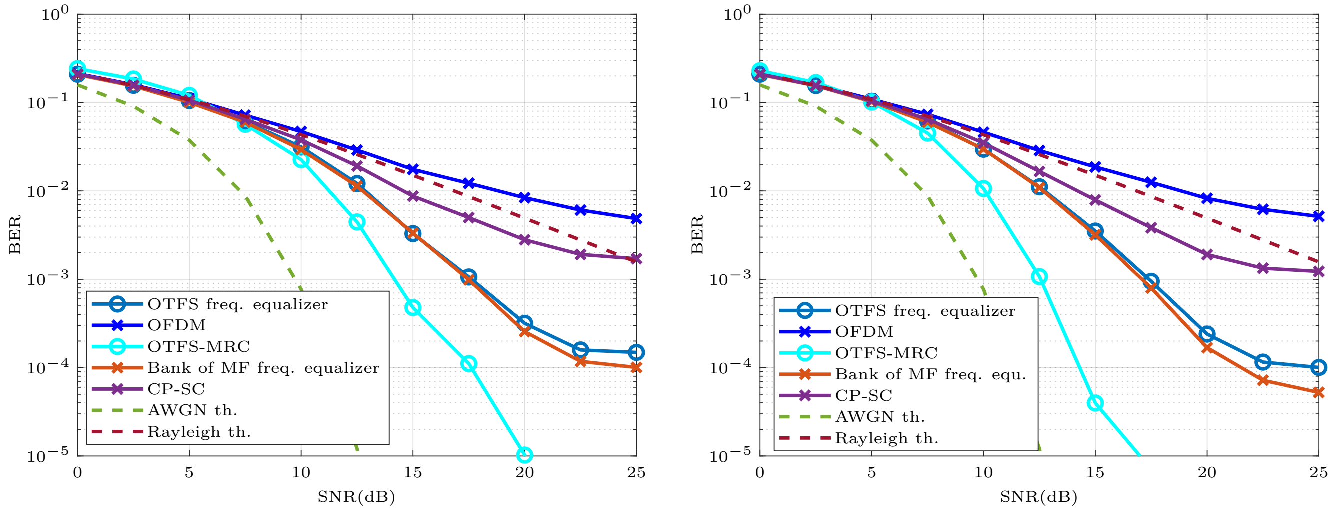

(a) BER of the different chains with 2 aggregates max speed = 550km/h $\implies \nu_{max} \approx 2kHz$.

(b) BER of the different chains with 3 aggregates max speed = 550km/h $\implies \nu_{max} \approx 2kHz$.

Figure 6.8: Each channel tap (=aggregation of paths) is made of 5 physical propagating paths associated with a specific gain and Doppler frequency.[1]

Impact of number of Doppler frequencies

The impact of the number of Doppler frequencies in the channel on the performance of OTFS with MRC is illustrated in Figure 6.9. The number of Doppler frequencies directly impacts the number of terms recombined in the MRC algorithm. Consequently, a higher number of Doppler frequencies improves the performance of the detection algorithm with a saturation in our scenario at 3 Doppler frequencies.

[1]The theoretical Rayleigh curve is obtained with a single delay channel for a single carrier modulation with ML decoding [29], [30]. The OFDM therefore shows worse performance than the Rayleigh theoretical curve due to the Doppler effect and the underlying loss of performance in the equalizer. It is shown in Appendix F that for a block fading Rayleigh channel, i.e a channel that the frequency equalizer compensates perfectly, the OFDM performance matches the theoretical one.

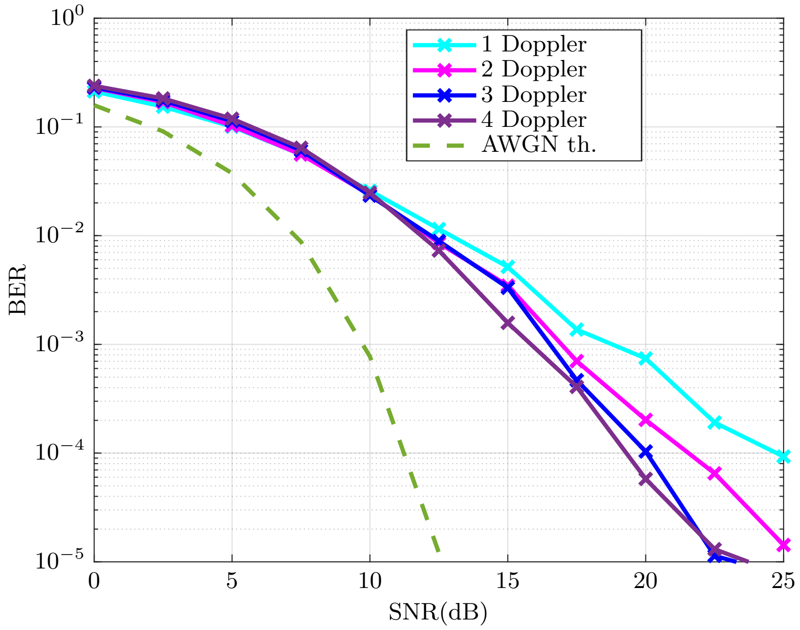

Figure 6.9: BER of OTFS with MRC. In every scenario there is a line of sight of paths $r_0 = 0$ and then depending on the legend there is a certain number of paths arriving at $r_i = 1$ each with its own Doppler frequency $k_i \sim \mathcal{U}_{[-7,7]\in\mathbb{N}}$.

Impact of the number of sample along the Doppler axis M

Finally, the impact of the number of points along the Doppler axis M or equivalently the length of the transmitted signal on the performance of OTFS is now investigated. The Doppler resolution of the system decreases with M which leads more easily to fractional Doppler frequencies, consequently increasing the number of interfering term. This effect is mainly visible at high SNR where the impact of the interferences is predominant. However, the observed impact of going from $M = 64$ to $M = 16$ in Figure 6.10 is not significant for both OTFS with MRC and frequency equalization. For OFDM and CP-SC there is no impact of M on the performance since the performance of those systems is completely independent of the number of transmitted blocks.

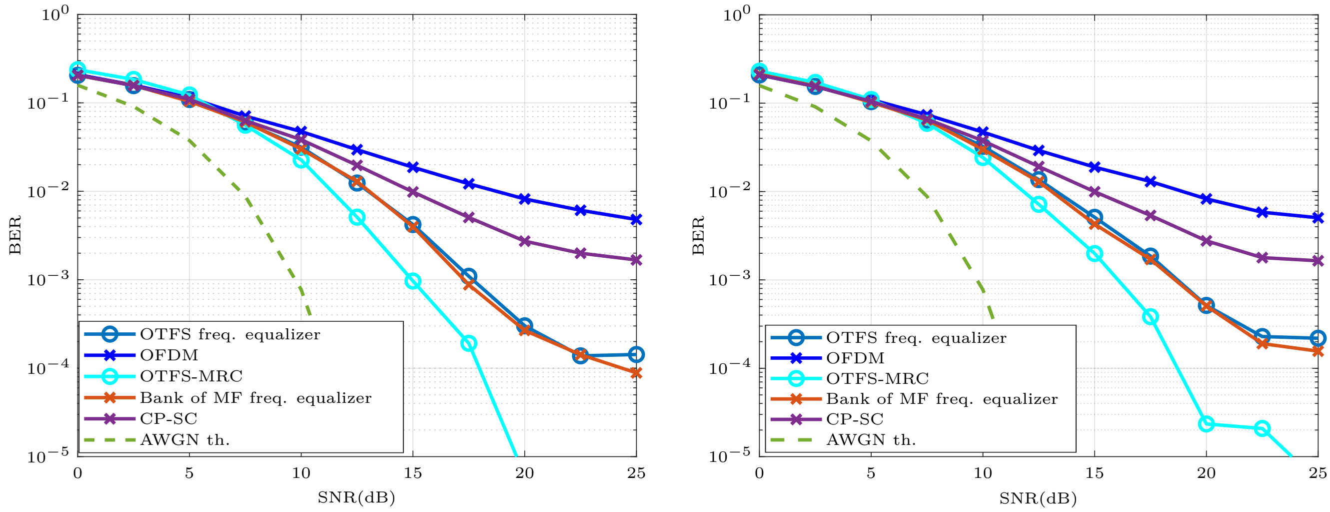

(a) BER of the different chains with 2 aggregates max speed = 550km/h $M = 64$.

(b) BER of the different chains with 2 aggregates max speed = 550km/h. $M = 16$

Figure 6.10

To finally draw conclusions on the relevance of OTFS versus OFDM in practical use cases, a standard channel model is simulated. The chosen standard is the EVA model which is specified in TS 36.101 [31] and given in Appendix G. Three different scenarios are considered. First, a low mobility scenario with a maximum speed of 100km/h is simulated, then the mobility is increased to 500km/h and 1000 km/h. At 100km/h (Figure 6.11a), beyond $15dB$ of SNR, the slope of the OTFS with frequency and MRC equalizations are roughly the same. The observed SNR gap is about $3dB$ which, given the difference of complexity between the algorithm is small. At 500km/h (Figure 6.11b), the difference of performance between the two aforementioned systems is enhanced but the saturation of the different systems with frequency equalization is not that obvious yet at the considered SNR. At 1000km/h (Figure 6.11c), however, every scheme with a frequency equalization saturates around a BER of 10^{-2} while the OTFS with MRC equalization clearly do not saturate in our range of SNR and reach a BER of 10^{-5} at an SNR$\approx 18dB$. The advantage of OTFS with MRC equalization is clear in those very high mobility scenario. However, up to 500km/h the benefit of using the MRC algorithm over the frequency equalization for the OTFS is not evident. The very interesting property of the (CP-)OTFS is that both equalizers can be used at the reception without requiring any modification on the transmitting side. Therefore, adaptative systems that tune their equalization on the receiving side based on the channel topology are easily imagined.

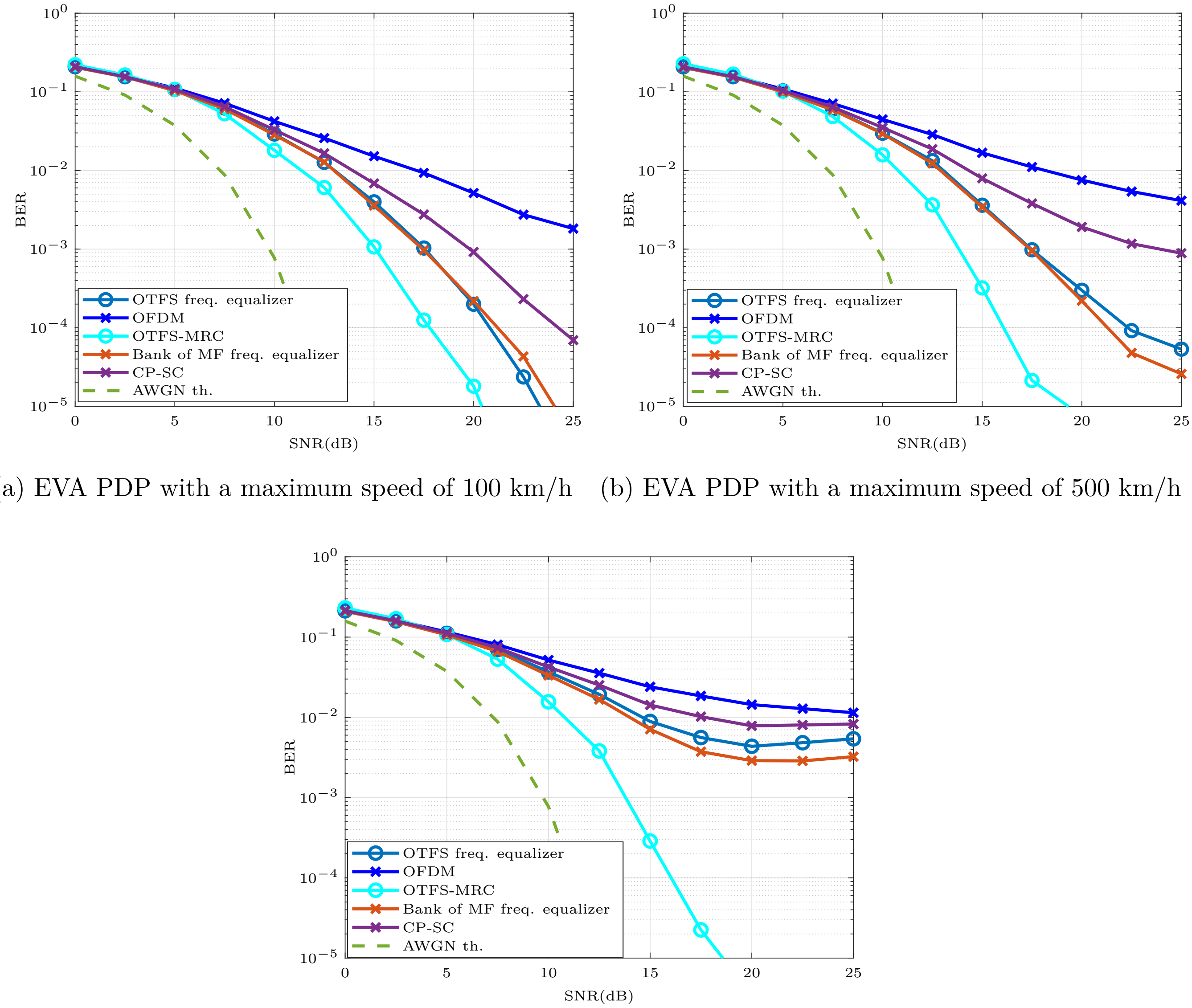

(a) EVA PDP with a maximum speed of 100 km/h (b) EVA PDP with a maximum speed of 500 km/h

(c) EVA PDP with a maximum speed of 1000 km/h

Figure 6.11: BER of the different chains in a channel with an EVA PDP and a Jake's spectrum for the Doppler frequencies

Chapter 7

Conclusion

In this thesis, provided the small approximation that the Doppler frequency is negligible compared to the pulse shaping filter bandwidth, we have presented a framework in which both OFDM and OTFS systems are implemented based on a common architecture.

We have presented a common model for the wireless channel in highly mobile scenarios. In this context, the channel is represented as a two-dimensional quantity. We have presented the equivalent delay-Doppler representation of this channel and the sparsity of this representation was highlighted. We then spent some time clarifying the statistical representation of the channel model that is often used in the OFDM context and its link with the delay-Doppler representation.

Then, the impact of frequency fading in OFDM has been highlighted. We have shown how the CP-SC chain is able to get around this issue of frequency fading. Simulation results have been provided to confirm the BER improvement of CP-SC over OFDM. However, we showed that CP-SC performance still fluctuates in time with mobile channel scenarios. Therefore, the OTFS equations have been derived. The OTFS system presents better BER performance than CP-SC. We have explained in which sense the mechanism that is responsible for the improvement between OTFS and CP-SC is very similar to the one that differentiates CP-SC and OFDM. Three equalization techniques for OTFS have been presented. Two of them were already derived in [23]. Those are the single tap frequency and MRC equalization. A novel equalization technique inspired by the rake receiver has been introduced and we have shown that the performance of the MRC algorithm cannot be reached with this kind of receiver structure.

The main messages of this thesis can be summarized as follows

- Simulation results were conducted for common 5G system parameters. In the EVA channel model with a maximal speed of 100km/h, OFDM systems already show a significant loss of performance compared to OTFS no matter what choice of equalization technique is used for OTFS.

- We have shown that in this same channel model, the OTFS single tap frequency equalizer, even when the maximal speed in the channel is pushed to 500km/h, already provides a huge BER improvement compared to OFDM. The performance of the MRC algorithm for OTFS still improves the BER of OTFS. However, the complexity of such an equalizer is much higher. Indeed, we have shown that the complexity of a single iteration of this algorithm is equivalent to the overall complexity of a frequency equalizer.
- When the maximal speed is increased, the OTFS with single tap equalizer system saturates. This level of saturation is found to be BER= 10^{-2} at 1000km/h with the simulation parameters used. The MRC on the other hand, has not shown any sign of saturation up to an SNR of $25dB$. In those highly mobile scenarios OTFS with MRC equalization would be the chosen architecture.
- However, in moderate mobility scenarios, there is a trade-off between the OTFS with frequency and MRC equalization. This trade-off highlights the need of having highly reconfigurable systems where the number of iterations or equalization techniques can be adapted. The (CP-)OTFS modulation has the advantage that the choice of the equalization technique does not depend on the transmitting architecture and therefore only depends on the receiver choices.
- The latency of the OTFS system is M times higher than in OFDM, where M is the number of points along the Doppler axis of the delay-Doppler grid of the OTFS system.
- Simulation results have also pointed out that the OTFS performance is highly sensible to the channel topology, therefore, reinforcing the need of having solid standard channel models to assess the performance. Quite counterintuitively, the performance of OTFS with MRC equalization is improved when the number of paths in the channel increases with a limit in our scenario at 6 channel taps.

Future work
Current telecommunication systems extensively rely on error correcting code which have not been considered here. Clearly, the performance of OTFS has to be assessed when those codes are used to truly characterize the potential improvement brought by OTFS over OFDM. The channel estimation question has also not been tackled here. The OTFS modulation has the advantage from this point of view to rely on the dD representation of the channel which is a clear image of the physical geometry around the base station and the user. Therefore, it can have interesting properties in the context of joint communication and sensing.

Appendix A

Proof of the circular convolution property

Let $z[n]$ be the circular convolution between $x[n]$ and $y[n]$, i.e. $z[n] = (x \circledast y)[n]$. We want to prove that the DZT of $z[n]$ is expressed as

$$Z_z[l,k] = \sqrt{M} \sum_{l'=0}^{N-1} Z_x[l',k] Z_x[l-l',k]. \tag{A.1}$$

The demonstration is based on the DFT of the sequences. Indeed, it is well known that a circular convolution is equivalently represented as a product of the DFTs [12]. Let us denote by $Z[k]$,$X[k]$ and $Y[k]$ the MN points DFT of $z[n]$, $x[n]$ and $y[n]$ respectively. Therefore, $Z[k]$ is expressed as

$$Z[k] = \sqrt{MN} X[k] Y[k]. \tag{A.2}$$

And using appendix B

$$\begin{aligned}
Z_z[l,k] &= \sqrt{M} \sum_{p=0}^{N-1} X[k+pM] Y[k+pM] e^{j2\pi \frac{k+pM}{NM} l}, & \text{(A.3)}\\
&= \frac{\sqrt{M}}{N} \sum_{p=0}^{N-1} \sum_{l'=0}^{N-1} \sum_{l''=0}^{N-1} Z_x[l',k] e^{-j2\pi \frac{k+pM}{MN} l'} Z_y[l'',k] e^{-j2\pi \frac{k+pM}{MN} l''} e^{j2\pi \frac{k+pM}{NM} l}, & \text{(A.4)}\\
&= \frac{\sqrt{M}}{N} \sum_{l'=0}^{N-1} \sum_{l''=0}^{N-1} Z_x[l',k] Z_y[l'',k] \sum_{p=0}^{N-1} e^{-j2\pi \frac{k+pM}{MN} (l'+l''-l)}, & \text{(A.5)}\\
&= \sqrt{M} \sum_{l'=0}^{N-1} Z_x[l',k] Z_y[l-l',k]. & \text{(A.6)}
\end{aligned}$$

Appendix B

DFT from DZT

Let us denote by $X[k]$ the MN points DFT of $x[n]$. The link between the DZT and DFT is now provided

$$
\begin{aligned}
X[k] &= \frac{1}{\sqrt{MN}} \sum_{l=0}^{N-1} \sum_{n=0}^{M-1} x[l+nN] e^{-j2\pi \frac{k}{MN}(l+nM)}, && \text{(B.1)}\\
&\overset{(a)}{=} \frac{1}{M\sqrt{N}} \sum_{l=0}^{N-1} \sum_{n=0}^{M-1} \sum_{k'=0}^{M-1} Z_x[l,k'] e^{j2\pi \frac{k'n}{M}} e^{-j2\pi \frac{k}{MN}(l+nM)}, && \text{(B.2)}\\
&= \frac{1}{M\sqrt{N}} \sum_{l=0}^{N-1} \sum_{k'=0}^{M-1} Z_x[l,k'] e^{-j2\pi \frac{k}{MN} l} \sum_{n=0}^{M-1} e^{-j2\pi \frac{(k-k')}{M} n}, && \text{(B.3)}\\
&= \frac{1}{\sqrt{N}} \sum_{l=0}^{N-1} \sum_{k'=0}^{M-1} Z_x[l,k'] e^{-j2\pi \frac{k}{MN} l} \sum_{m=-\infty}^{\infty} \delta[k-k'+mM], && \text{(B.4)}\\
&= \frac{1}{\sqrt{N}} \sum_{l=0}^{N-1} Z_x[l,k] e^{-j2\pi \frac{k}{MN} l} && \text{(B.5)}
\end{aligned}
$$

where step (a) is the application of the definition of the IDZT

Appendix C

DZT from DFT

Let us denote by $X[k]$ the MN points DFT of $x[n]$. The link between the DZT and DFT is now provided

$$
\begin{aligned}
Z_x[l,k] &\triangleq \frac{1}{\sqrt{M}} \sum_{n=0}^{M-1} x[l+nN] e^{-j2\pi \frac{kn}{M}}, \\
&= \frac{1}{M\sqrt{N}} \sum_{n=0}^{M-1} \sum_{k'=0}^{NM-1} X[k'] e^{j2\pi \frac{k'}{NM}(l+nN)} e^{-j2\pi \frac{kn}{M}}, \\
&= \frac{1}{M\sqrt{N}} \sum_{k'=0}^{MN-1} X[k'] e^{j2\pi \frac{k'}{NM} l} \sum_{n=0}^{M-1} e^{-j2\pi \frac{k-k'}{M} n}, \\
&= \frac{1}{\sqrt{N}} \sum_{k'=0}^{MN-1} X[k'] e^{j2\pi \frac{k'}{NM} l} \sum_{m=-\infty}^{\infty} \delta[k-k'+mM] \\
&= \frac{1}{\sqrt{N}} \sum_{m=0}^{N-1} X[k+mM] e^{j2\pi \frac{k+mM}{NM} l}
\end{aligned}
$$

Appendix D

Fourier transform from delay-Doppler representation

The Fourier transform of $x(t)$ can be found via its dD representation as such

$$\mathcal{F}_t(x(t))(f) = \frac{1}{\sqrt{\tau_{max}}} \int_0^{\tau_{max}} x_{dD}(\tau, f) e^{-j2\pi f\tau} d\tau. \tag{D.1}$$

Indeed, by expanding the expression of the dD representation we have

$$\frac{1}{\sqrt{\tau_{max}}} \int_0^{\tau_{max}} x_{dD}(\tau, f) e^{-j2\pi f\tau} d\tau = \sum_{m=-\infty}^{\infty} \int_0^{\tau_{max}} x(\tau + m\tau_{max}) e^{-j2\pi f(\tau + m\tau_{max})} d\tau, \tag{D.2}$$

$$\overset{t=\tau+m\tau_{max}}{=} \sum_{m=-\infty}^{\infty} \int_{m\tau_{max}}^{(m+1)\tau_{max}} x(t) e^{-j2\pi ft} dt, \tag{D.3}$$

$$= \int_{-\infty}^{\infty} x(t) e^{-j2\pi ft} dt. \tag{D.4}$$

Appendix E

SNR of the adapted rake receiver

The SNR of the decision variable given by

$$\hat{c}[l,k] = c[l,k] + \frac{\sum_{i=0}^{P-1} h_i^* \sum_{i'=0|i'\neq i}^{P-1} h_{i'} e^{-j2\pi \frac{k_i - k_{i'}}{MN}(l-r_i)} c[l - r_i + r_{i'}, k - k_i + k_{i'}]}{\sum_{i=0}^{P-1} |h_i|^2} + \frac{\sum_{i=0}^{P-1} h_i^* e^{-j2\pi \frac{k_i}{MN}(l-r_i)} \nu[l-r_i, k-k_i]}{\sum_{i=0}^{P-1} |h_i|^2},$$

is derived as follows. Given that the noise realizations $\nu[l,k]$ are i.i.d, the variance of the noisy term is written as

$$\begin{aligned}
&\frac{1}{\left(\sum_{i=0}^{P-1} |h_i|^2\right)^2} \mathbb{E}\Bigg\{ \left(\sum_{i=0}^{P-1} h_i^* e^{-j2\pi \frac{k_i}{MN}(l-r_i)} \nu[l-r_i, k-k_i] \right) \\
&\qquad \left(\sum_{i'=0}^{P-1} h_{i'}^* e^{-j2\pi \frac{k_{i'}}{MN}(l-r_{i'})} \nu[l-r_{i'}, k-k_{i'}] \right)^* \Bigg\} \\
&\overset{(a)}{=} \frac{\sigma_\nu^2}{\left(\sum_{i=0}^{P-1} |h_i|^2\right)^2} \sum_{i=0}^{P-1} \sum_{i'=0}^{P-1} h_i^* e^{-j2\pi \frac{k_i}{MN}(l-r_i)} h_{i'} e^{j2\pi \frac{k_{i'}}{MN}(l-r_{i'})} \delta[i-i']. \\
&= \frac{\sigma_\nu^2}{\left(\sum_{i=0}^{P-1} |h_i|^2\right)^2} \sum_{i=0}^{P-1} |h_i|^2 \\
&= \frac{\sigma_\nu^2}{\sum_{i=0}^{P-1} |h_i|^2}
\end{aligned}$$

where step (a) assumes that no paths have the same associated delay and Doppler frequency. The SNR is therefore given as

$$\text{SNR} = \frac{\sum_{i=0}^{P-1} |h_i|^2}{\sigma_\nu^2} \tag{E.1}$$

Appendix F

Performance of the different chains of chapter 6 in a Rayleigh channel without mobility

The performance of the different chains presented throughout the thesis are presented in a block fading Rayleigh scenario with 2 aggregates. That is

$$\begin{aligned} h[m,n] &= a\delta[m] + b\delta[m-1], \\ a &\sim \mathcal{CN}(0,1), \\ b &\sim \mathcal{CN}(0,1), \end{aligned}$$

with a and b that are redrawn for every OTFS grid, i.e every NM samples.

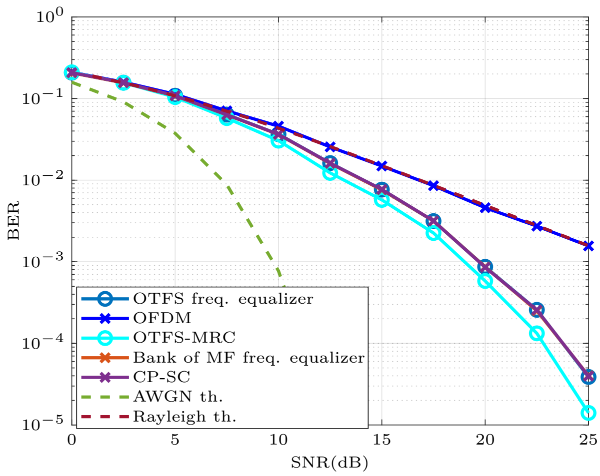

Figure F.1: BER of the different chains with 2 aggregates and max speed = 0km/h. (OFDM and Rayleigh th. match perfectly)

Appendix G

EVA channel model

The eva channel model is parametrized with a set of delays given by

$$\tau_i \in \{0, 30, 150, 310, 370, 710, 1090, 1730, 2510\} * 10^{-9}[s].$$

The associated power delay profile is given in dB by

$$\{0, -1.5, -1.4, -3.6, -0.6, -9.1, -7.0, -12.0, -16.9\}.$$

The Doppler frequencies are drawn from a Jake's spectrum.

Bibliography

[1] Raghavendra Ganiga and Yadav Ramroop. “OFDM and its application in 4G”. In: *SindhuYuva 2012* (Jan. 2012).

[2] R. Hadani et al. “Orthogonal Time Frequency Space Modulation”. In: *2017 IEEE Wireless Communications and Networking Conference (WCNC)*. 2017, pp. 1–6. DOI: 10.1109/WCNC.2017.7925924.

[3] David Tse and Pramod Viswanath. “The wireless channel”. In: *Fundamentals of Wireless Communication*. Cambridge University Press, 2005, pp. 10–48.

[4] D. Slepian. “On bandwidth”. In: *Proceedings of the IEEE* 64.3 (1976), pp. 292–300. DOI: 10.1109/PROC.1976.10110.

[5] Hai Lin et al. *Multi-Carrier Modulation: An Evolution from Time-Frequency Domain to Delay-Doppler Domain*. 2023. arXiv: 2308.01802 [cs.IT]. URL: https://arxiv.org/abs/2308.01802.

[6] Devopedia. *5G NR Transmission Time Interval*. URL: https://devopedia.org/5g-nr-transmission-time-interval.

[7] Yaniv Azar et al. “28 GHz propagation measurements for outdoor cellular communications using steerable beam antennas in New York city”. In: *2013 IEEE International Conference on Communications (ICC)*. 2013, pp. 5143–5147. DOI: 10.1109/ICC.2013.6655399.

[8] S. S. Haykin. *Digital Communication Systems - First Edition*. 1st edition. Hoboken, N.J: John Wiley & Sons Inc, Apr. 5, 2013. 800 pp. ISBN: 978-0-471-64735-5.

[9] Ramjee Prasad Richard Van Nee. *Ofdm for Wireless Multimedia Communications*. Boston London: Artech House Publishers, 2000. 284 pp. ISBN: 978-0-89006-530-3.

[10] Hermann Rohling, ed. *OFDM: Concepts for Future Communication Systems*. Signals and Communication Technology. Berlin, Heidelberg: Springer, 2011. ISBN: 978-3-642-17495-7 978-3-642-17496-4. DOI: 10.1007/978-3-642-17496-4. URL: https://link.springer.com/10.1007/978-3-642-17496-4 (visited on 05/20/2025).

[11] *9.6: The Convolution Operation*. Mathematics LibreTexts. Nov. 14, 2021. URL: https://math.libretexts.org/Bookshelves/Differential_Equations/Introduction_to_Partial_Differential_Equations_(Herman)/09%3A_Transform_Techniques_in_Physics/9.06%3A_The_Convolution_Operation (visited on 05/12/2025).

[12] Bassam Bamieh. *Discovering Transforms: A Tutorial on Circulant Matrices, Circular Convolution, and the Discrete Fourier Transform*. 2022. arXiv: 1805.05533 [eess.SP]. URL: https://arxiv.org/abs/1805.05533.

[13] Bertrand Devillers and Luc Vandendorpe. "Bit rate comparison of adaptive OFDM and cyclic prefixed single-carrier with DFE". In: *IEEE Communications Letters* 13.11 (2009), pp. 838–840. DOI: 10.1109/LCOMM.2009.091008.

[14] Yuan-Pei Lin and See-May Phoong. "MMSE OFDM and prefixed single carrier systems: BER analysis". In: *2003 IEEE International Conference on Acoustics, Speech, and Signal Processing, 2003. Proceedings. (ICASSP '03)*. Vol. 4. 2003, pp. IV–229. DOI: 10.1109/ICASSP.2003.1202602.

[15] A. Czylwik. "Comparison between adaptive OFDM and single carrier modulation with frequency domain equalization". In: *1997 IEEE 47th Vehicular Technology Conference. Technology in Motion*. Vol. 2. 1997, 865–869 vol.2. DOI: 10.1109/VETEC.1997.600452.

[16] Tingting Shi, Shidong Zhou, and Yan Yao. "Capacity of single carrier systems with frequency-domain equalization". In: *Proceedings of the IEEE 6th Circuits and Systems Symposium on Emerging Technologies: Frontiers of Mobile and Wireless Communication (IEEE Cat. No.04EX710)*. Vol. 2. 2004, 429–432 Vol.2. DOI: 10.1109/CASSET.2004.1321915.

[17] G. Munz, S. Pfletschinger, and J. Speidel. "An efficient waterfilling algorithm for multiple access OFDM". In: *Global Telecommunications Conference, 2002. GLOBECOM '02. IEEE*. Vol. 1. 2002, 681–685 vol.1. DOI: 10.1109/GLOCOM.2002.1188165.

[18] Saif Khan Mohammed et al. "OTFS—A Mathematical Foundation for Communication and Radar Sensing in the Delay-Doppler Domain". In: *IEEE BITS the Information Theory Magazine* 2.2 (Nov. 2022), pp. 36–55. ISSN: 2692-4080. DOI: 10.1109/mbits.2022.3216536. URL: http://dx.doi.org/10.1109/MBITS.2022.3216536.

[19] Saif Khan Mohammed. "Derivation of OTFS Modulation From First Principles". In: *IEEE Transactions on Vehicular Technology* 70.8 (2021), pp. 7619–7636. DOI: 10.1109/TVT.2021.3069913.

[20] Saif Khan Mohammed. "Time-Domain to Delay-Doppler Domain Conversion of OTFS Signals in Very High Mobility Scenarios". In: *IEEE Transactions on Vehicular Technology* 70.6 (2021), pp. 6178–6183. DOI: 10.1109/TVT.2021.3071942.

[21] J. Schoukens and J. Renneboog. "Modeling the noise influence on the Fourier coefficients after a discrete Fourier transform". In: *IEEE Transactions on Instrumentation and Measurement* IM-35.3 (1986), pp. 278–286. DOI: 10.1109/TIM.1986.6499210.

[22] CHOCKALINGAM Ananthanarayanan NAIKOTI Ashwitha. "Signal Detection and Channel Estimation in OTFS". In: *ZTE Communications* 19.4, 16 (2021), pp. 16–33.

[23] Yi Hong, Tharaj Thaj, and Emanuele Viterbo. *Delay-Doppler Communications: Principles and Applications*. English. Publisher Copyright: © 2022 Elsevier Inc. All rights reserved. Netherlands: Elsevier, 2022. ISBN: 9780323859660. DOI: 10.1016/C2020-0-01791-3.

[24] *Computational complexity of mathematical operations*. In: *Wikipedia*. Page Version ID: 1289129796. May 6, 2025. URL: https://en.wikipedia.org/w/index.php?title=Computational_complexity_of_mathematical_operations&oldid=1289129796#Matrix_algebra (visited on 05/17/2025).

[25] Tommi Heikkilä. "RAKE Receiver". In: (Jan. 2004).

[26] Konstantinos Baltzis. "The Rake Receiver Principle: Past, Present and Future". In: *Recent Patents on Electrical Engineering* 5 (Apr. 2012), pp. 55–71. DOI: 10.2174/1874476111205010055.

[27] Robert M. Gray. 2006. DOI: 10.1561/0100000006.

[28] M. Pätzold. *Mobile Fading Channels*. Wiley, 2002. ISBN: 978-0-471-49549-9. URL: https://books.google.be/books?id=ffIyrlCyf5cC.

[29] *Analytical Expressions Used in berfading Function and Bit Error Rate Analysis App - MATLAB & Simulink*. URL: https://nl.mathworks.com/help/comm/ug/analytical-expressions-used-in-berfading-function-and-bit-error-rate-analysis-app.html (visited on 05/27/2025).

[30] "Performance of Multichannel Receivers". In: *Digital Communication Over Fading Channels*. John Wiley and Sons, Ltd. Chap. 9, pp. 259–433. ISBN: 9780471200697. DOI: https://doi.org/10.1002/0471200697.ch9. eprint: https://onlinelibrary.wiley.com/doi/pdf/10.1002/0471200697.ch9. URL: https://onlinelibrary.wiley.com/doi/abs/10.1002/0471200697.ch9.

[31] *3GPP – The Mobile Broadband Standard*. 3GPP. URL: https://www.3gpp.org/ (visited on 05/12/2025).

UNIVERSITÉ CATHOLIQUE DE LOUVAIN
École polytechnique de Louvain
Rue Archimède, 1 bte L6.11.01, 1348 Louvain-la-Neuve, Belgique | **www.uclouvain.be/epl**